Stress Analysis of Finned Tubes Subjected to Die Expansion

by

Zijian ZHAO

MANUSCRIPT-BASED THESIS PRESENTED TO ÉCOLE DE TECHNOLOGIE SUPÉRIEURE IN PARTIAL FULFILLMENT FOR THE DEGREE OF DOCTOR OF PHILOSOPHY
PH.D.

MONTREAL, SEPTEMBER, 12, 2023

ÉCOLE DE TECHNOLOGIE SUPÉRIEURE
UNIVERSITÉ DU QUÉBEC

Zijian Zhao, 2023

This Creative Commons licence allows readers to download this work and share it with others as long as the author is credited. The content of this work can't be modified in any way or used commercially.

BOARD OF EXAMINERS

THIS THESIS HAS BEEN EVALUATED

BY THE FOLLOWING BOARD OF EXAMINERS

Mr. Abdel-Hakim Bouzid, Thesis Supervisor
Department of Mechanical Engineering at École de Technologie Supérieure

Mr. Wahid Maref, President of the Board of Examiners
Department of Construction Engineering at École de Technologie Supérieure

Mr. Anh Dung Ngo, Member of the jury
Department of Mechanical Engineering at École de Technologie Supérieure

Mr. Pierre Mertiny, External Evaluator
Department of Mechanical Engineering at University of Alberta

THIS THESIS WAS PRENSENTED AND DEFENDED

IN THE PRESENCE OF A BOARD OF EXAMINERS AND PUBLIC

AUGUEST,14,2023

AT ÉCOLE DE TECHNOLOGIE SUPÉRIEURE

ACKNOWLEDGMENT

I would like to thank my director, Hakim A. Bouzid, for sharing his knowledge and experience without restriction. M. Bouzid has been a driving force and a great mentor from the beginning of this long quest.

I would like to thank the team of technicians, engineers, and teachers at the Ecole de Technologie Superieure for their support in this project

I would like to thank my friends and colleagues, Rashique and Linbo, for their friendship and advice.

Finally, I would like to thank my wife, Mingxia Wang, and my parents, for their invaluable support during my studies. Without their contribution, there is no possible to finish my work.

Analyse des contraintes des tube à ailettes soumis à l'extrusion avec filière

Zijian ZHAO

RESUMÉ

Dans cette étude, une approche analytique est développée pour estimer la force nécessaire pour extruder les tubes avec différentes formes de filières. La répartition des contraintes dans les zones de contact et de transition est estimée à l'aide d'une approche analytique basée sur une combinaison de la loi d'évolution de Prandtl Reuss et de l'auto-adaptation de la courbe contrainte-déformation. La force d'extrusion est prédite sur la base des informations des zones de transition et de contact. Cette nouvelle approche réduit considérablement la difficulté de l'analyse et simplifie le calcul.

L'approche est validée à l'aide de quatre modèles numériques d'éléments finis axisymétriques de différentes tailles, matériaux et formes de filières soumis à une extrusion par poussée et traction. De plus, des tubes en acier inoxydable et en cuivre de 3/8 po de diamètre ont été extrudés avec une filière ovale dans un banc d'essai expérimental dans les deux conditions de poussée et de traction. Les déformations circonférentielles et longitudinales et la force d'extrusion sont surveillées et enregistrées pendant le processus d'expansion. Les résultats des trois approches montrent un très bon accord.

Ce travail de recherche étudie également le comportement élasto-plastique et estime l'état des contraintes résiduelles des tubes soumis au processus d'expansion de la filière. Les contraintes et les déformations des tubes en inox et en cuivre expansés sont analysées numériquement à l'aide de la méthode des éléments finis. Le processus d'expansion et de contraction est modélisé en tenant compte du comportement du matériau élasto-plastique des tubes de différentes grandeur. Les contraintes longitudinales, tangentielles et de contact maximales sont évaluées pour vérifier l'état de contrainte critique des tubes à ailettes pendant le processus d'expansion. L'importance du comportement du matériau dans l'évaluation des contraintes résiduelles par écrouissage cinématique et isotrope est abordée. Enfin, une expérience a été menée pour

évaluer les déformations tangentielles et longitudinales d'un acier inoxydable de diamètre 3/8 soumis à une expansion avec une filière de forme ovale.

Enfin, la qualité de l'assemblage tube à ailettes est étudiée car il s'agit d'un type de connexion courant dans les échangeurs de chaleur. Pendant le processus d'assemblage, une filière ou un mandrin est utilisé pour élargir le tube et fermer l'espace entre le tube et le collier d'ailette pour un meilleur transfert de chaleur. Le niveau d'interférence et la zone de contact créées dépendent à la fois de l'expansion radiale de la filière et du jeu initial, ainsi que de la forme de la zone de contact de l'ailette avec le tube avant l'expansion. Cependant, des recherches récentes ont révélé que le contact entre les surfaces n'est pas constant sur toute la largeur. Il en résulte un transfert de chaleur réduit par conduction et un compromis sur l'efficacité de l'échangeur de chaleur.
L'objectif de cette dernière partie du travail de recherche est d'établir une relation entre la forme du profil du trou d'ailette et la qualité du contact et de fournir des suggestions pour améliorer la connexion tube-ailette. Les simulations impliqueront des tubes faits de divers matériaux, des matrices de différentes tailles et des ailettes avec des colliers en forme de sablier, qui seront évalués à l'aide de modèles d'éléments finis. La taille des micro-espaces générés à l'interface tube-ailette sera utilisée pour déterminer la qualité de la surface de contact, tandis qu'un modèle FEA de contact thermique transitoire local sera utilisé pour évaluer les performances de conduction thermique du contact en présence de ces micro-espaces.

Mots-clés : méthode d'auto-adaptation du matériau, fondation élastique de la poutre, comportement du matériau élasto-plastique, plastification inverse, contact ailette-tube, micro-espace, analyse thermique transitoire

Stress analysis of finned tubes subjected to die expansion

Zijian ZHAO

ABSTRACT

In this study, an analytical approach is developed to estimate the force required to expand tubes for different die shapes. The stress distribution in the contact and transition zones is estimated using the analytical approach based on a combined Prandtl Reuss flow rule and self-adaption of the stress strain curve. The driving force is predicted based on the transition and contact zone information. This new approach greatly reduces the difficulty of the analysis and simplifies the calculation.

The approach is validated using four different numerical axisymmetric finite element models of different sizes, materials, and die shapes subjected to push and pull of the die. Additionally, stainless steel and copper 3/8 in. diameter tubes are expanded with an oval die in an experimental test bench under both push and pull conditions. The tangential and longitudinal strains and driving force are monitored and recorded during the expansion process. The results from the three approaches show a very good agreement.

This research work also investigates the elastics-plastic behavior and estimates the residual stress state of tubes subjected to the die expansion process. The stresses and deformations of the expanded SS316L tube are analyzed numerically using the finite element method. The expansion and contraction processes are modeled considering elastic-plastic material behavior for different die sizes. The maximum longitudinal, tangential and contact stresses are evaluated to verify the critical stress state of the joint during the expansion process. The importance of the material behavior in evaluating the residual stresses using kinematic and isotropic hardening is addressed. Finally, an experiment is conducted to assess the tangential and longitudinal strains of a 3/8 stainless steel subjected to expansion with an oval shape die.

Last, the quality of the fin-to-tube assembly is investigated as it is a common type of connection in heat exchangers. During the assembly process, a die or an expander is used to expand the tube and close the gap between the tube and the fin collar for improved heat transfer. The

amounts of interference and contact area created depend on both the radial expansion from the die and initial gap, as well as the shape of the fin contact area with the tube before expansion. However, recent research has revealed that the contact adhesion between the surfaces is not consistent across the width. This results in a reduction of heat transfer through conduction and a compromise of the heat exchanger efficiency.

The objective of this last part of the research work is to establish a relationship between the fin hole profile shape and contact quality and to provide suggestions for enhancing the tube-to-fin connection. The simulations involve tubes made of various materials, dies of different sizes, and fins with hourglass-shaped collars, all of which are assessed using finite element models. The size of the micro gaps at the tube-to-fin interface is used to determine the quality of the contact surface, while a local transient thermal contact FEA model are used to assess the contact thermal conductive performance in the presence of micro-gaps.

Keywords: Self-adaption material method, beam elastic foundation, elastic-plastic material behavior, reverse yielding, Fin-to-tube contact, micro gap, transient thermal analysis

TABLE OF CONTENTS

Page

LIST OF TABLES

Page

LIST OF FIGURES

Page

LIST OF ABREVIATIONS

ANSI	American National Standard Institute
API	American Petroleum Institute
ASME	American Society of Mechanical Engineering
CFD	Computational Fluid Dynamics
FEM	Finite Element Method
PVP	Pressure Vessel and Piping
PVT	Pressure Vessel Technology
OD	Outer diameter

INTRODUCTION

The motivation behind this study on the integrity and leakage tightness of tube joints stems from their significance in piping systems, where reliability and performance greatly impact industrial equipment such as gas coolers, heat exchangers, steam generators, condensers, and boilers. Finned tubes, crimped tubes, and tube-to-tubesheet joints are widely utilized in the production of the aforementioned equipment Bouzid (2018). Consequently, it is crucial to implement tubular joint design procedures that incorporate analytical methods to accurately predict the stress state and behavior in expanded tube joints.

Typically, these types of joints are formed by expanding the tube, allowing its outer diameter to exceed the inner diameter of the fins or tubesheet hole, thereby creating an interface between the tube and fin or tubesheet. In these expansion processes, the tube can be expanded using a die, mechanical rolling, or hydraulic fluid to expand the tube and form a joint.

However, such expansion processes may not only generate high residual stresses when combined with those created during operation but also lead to leakage failure, as illustrated in Figure 0.1. Micro-cracks, which can occur during expansions even when the process is well-controlled, are also responsible for these issues. This research focuses on examining the elastic-plastic behavior of tubular joints and estimating the residual and operating stress states by modeling the die expansion process. The stresses and deformations of the joint can be analyzed both analytically and numerically using finite element analysis. The expansion and contraction process can be modeled, taking into account an elastic-plastic material behavior.

Figure 0.1 Tube failure

As an example of expanded tubing is the normal die expansion. The die expansion process is illustrated in Figure 0.2, the diameter of die is larger than the inner diameter of the tube, and the die is pushed inside the tube to expand the latter and produce a permanent contact with the fins. Therefore, an interference between the tube and the fin collar is generated because the outer diameter of the expanded tube is larger than the inner diameter of the fin holes. This interference allows the fin collar to adhere to the tube to ensure a good heat transfer.

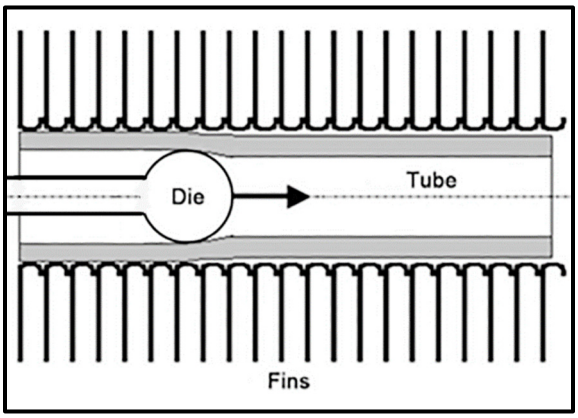

Figure 0.1 Tube expansion with ball die

During operation, the heat from the tube is transferred to the fins through the interface (Hing, Raghavan, & Meng, 2012; M.-H. Kim & Shin, 2005). According to recent research, the contact at the interface is not continuous over the entire mating surfaces.

Global warming is currently one of the biggest universal challenges. Hydrochlorofluorocarbon (CFC) like Hydrofluorocarbons (HCFC) refrigerants have been the subject of a lot of criticism as they represent a major source of atmosphere pollutants. In an effort to reduce fugitive emissions, the Canadian Environment Protection Act encourages the development of green equipment. Using natural refrigerants like carbon dioxide and propane has been proposed. In order for the Canadian manufacturers to offer high performance CO_2-based ACR (air conditioning and refrigeration) products, it is essential to have state-of-the-art tube work qualification tools. Parts made of copper used in low side heat exchangers have been designed and certified. Since copper strength drops drastically with temperature, making a gas cooler

with copper is not feasible. Hence, gas coolers working at high-pressure and high temperature must be made of stainless steel tubes. Replacing copper with stainless steel requires re-evaluation all the design and fabrication processes including size of fins and die, tube expansion, crimping and welding. The tube crimping method is preferred to welding if satisfactory results are obtained during comparison testing of both methods. Therefore, one of the objectives of this research is to investigate the structural integrity and quality of stainless steel tube-to-fin joints.

Problem definition

Previous studies in the literature have shown that the residual stresses in expanded tubes, combined with operational loads, can be high enough to cause micro cracks and failure. In other applications, such as tube-to-tubesheet joints, insufficient expansion led to joint integrity failure as revealed by pull-out tests. Furthermore, in the die expansion of tubes and fins, the full contact of mating surfaces is not achieved, resulting in suboptimal heat transfer efficiency. Thus, accurate prediction of deformation and residual stresses in tubes is crucial for the integrity, adhesion, and leak-tightness of tubular joint designs. The current research program will focus on the following challenges:

- There is no standard procedure for calculating residual stresses in tube transition zones after expansion.
- There is a lack of consensus on the location of the maximum residual stress along the tube and across its thickness, and limited research on tube thinning due to expansion.
- Most previous experimental studies on the tube expansion process focus on indirect assessments of expansion quality through pull-out tests, with limited available data on the tube stress state during the expansion process

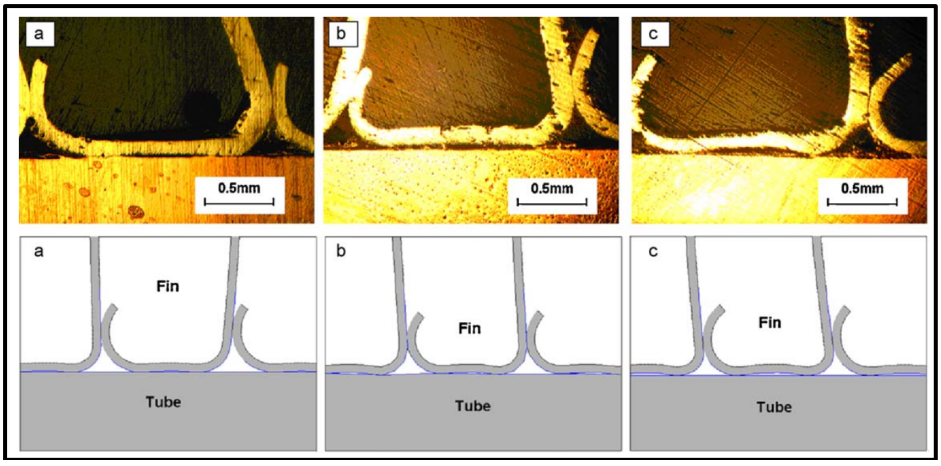

Figure 0.2 Experimental result of the contact status
Taken form Tang et al.(2010, p.1991)

The interface between the fins and the tube is also investigated here which is usually considered continuous and perfectly in contact, however, recent studies (Tang, Li, & Peng, 2011) show that it is not that shown in Figure 0.3. There are gaps at the interface that are inherent to the expansion process. The efficiency of the heat transfer between the tube and the fins depends on the quality of the contact interface and the adhesion of the mating surfaces. Therefore, the efficiency of the heat transfer between the exchange parts can be significantly increased by improving the contact quality between the tubes and the fins. The challenges that the current project faces are as follows.

- Study the die expansion of stainless steel tubing and compare the process with current expansion with copper tubes
- Perform accurate prediction of the deformation of different fin shapes, especially under the ununiform expansion process.
- Develop guidelines to achieve an optimum design of tube-to-fin die expansion.
- Estimate the residual stresses in the tube and conduct experimental validation and verification.

Thesis structure

This thesis is presented in six chapters. The first chapter presents a elaborate literature review on tube expansion and tube to fin assemblies. Also included in this chapter are reviews on analytical experimental and numerical studies on the tube expansion process including detailed investigations and analysis of finned tube assemblies. The second chapter describes the test rig used to produce the results to validate the developed analytical models and the FEM simulations.

The third chapter presents a study on the analysis of stresses in Stainless Steel 316 L tubes subjected to die expansion with special focus on the effect of material reverse yielding. The stresses and strains of tubes during and after expansion are also discussed in this study. This chapter is a copy of the journal paper entitled “Analysis of stresses in stainless steel 316l tubes subjected to die expansion”, which was published in the ASME Journal of *Pressure Vessel Technology*.

The fourth chapter presents an analytical model with a self-adaption method that can estimate the stress distribution in the transition zone of expanded tubes for different die shapes and tube sizes. The force required to expand the tubes is also evaluated. This new approach greatly reduces the difficulty of the stress analysis and simplifies the calculation. This chapter is a copy of the paper entitled “A method of evaluating the driving force and stresses during tube die expansion” which was also published in the ASME Journal of *Pressure Vessel Technology*.

In the fifth chapter, an analytical model is presented that can be used to estimate the stress distribution in the contact and transition zones during tube expansion. The method allows for the determination of the distribution of stresses and strains in the expanded tube during and after expansion. The validity of the method was achieved by confronting its results with those obtained experimentally and numerically using FEM. This chapter is a condensed version of the paper titled 'Stress Analysis of Tubes During Die Expansion Process,' which was submitted to the *International Journal of Thin-Walled Structures*.

The sixth chapter presents a numerical study on the contact quality improvement of the fin to tube. In this study, several factors which may impact the contact quality were investigated such as die size, the material tube, constraint type, and the shape of the fins. After a series of analyses, few recommendations were provided to increase the quality of the contact between the fins and the tube. The study was enriched with a steady state heat transfer analysis to support the methodology. This chapter is a copy of the paper entitled "A study on the contact quality improvement of fin to tube assemblies" which was also submitted for *The Transaction of the Canadian Society of Mechanical Engineers.*

This thesis concludes with a summary of the major findings and by provides recommendations for future work on tube expansion and tube to fin analysis.

CHAPTER 1

LITERATURE REVIEW

1.1 Introduction

A considerable amount of research has been carried out in relation to the development of tube joints and their associated tube expansion/compression techniques. These studies predominantly concentrate on three core aspects: analytical approaches, numerical methods (such as Finite Element Analysis), and experimental investigations. This chapter presents a concise overview of prior research on this topic, taking into account each of these three distinct perspectives.

1.2 Analytical approach

Existing analytical methods primarily rely on two concepts: momentum equations and energy consumption. The majority of these models utilize momentum equations in conjunction with various geometric shapes, while only a few studies estimate the driving force of the die during the expansion process using the energy method. However, numerical methods are employed to obtain the deformations necessary as input for these analytical approaches.

1.2.1 Momentum equations

Tube expansion forming is a traditional process used in the early century and therefore,a large body of research has been conducted in this filed. In 1960 Antoni and Philip (1960) conducted a comparative theoretical study on the yield conditions of circular cylindrical shells subjected to axisymmetric loading, based on the free body diagram shown in Figure 1.1 and several yield criteria were used to treat sandwich and shell tube structures discussed in this study. In particular, both structures were analyzed with Tresca and Von Mises yield criteria. This work provides a method to not only calculate the stress distribution but also the length of the yield

zone. They also introduced nondimensional parameters into the calculation and many posterior tube expansion analytical studies are inspired by this work.

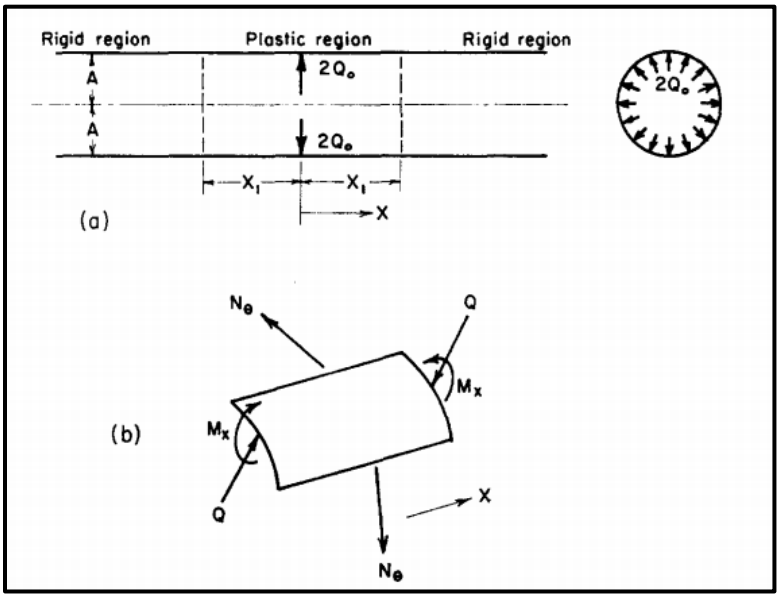

Figure 1.1 Cylinder shell model (Sawczuk & Hodge, 1960)

In this work, the plastic region length x_1 is given as follows

$$x_1 = \left[\int_{p_0}^{p_1} \frac{1}{q} \left(\frac{dm}{dp} \right) dp \right]^{\frac{1}{2}} \tag{1.1}$$

Since the weaknesses of rolling expansion process cannot be countered easily, an alternative method known as hydraulic expansion was proposed by Krip and Podosky (1976) during the 1970s. According to this work, tube expansion with fluid pressure will produce uniform contact between at the tube and tubesheet interface. Scoot et al.(1984) also shows that hydraulic expansion can reduce the residual stress compared with mechanical rolling expansion through tests.

In 1988, Updike et al.(1992) developed an analytical solution of the stresses in the transition zone based on an elastic-plastic material behavior for the tube. The author proposed simplified

formulas based on a numerical method that uses Prandtl Reuss flow rule implemented in the KSHEL-P program. During unloading, the beam on elastic foundation is used to treat the tube with an external pressure applied on its outer surface. The stress distribution in transient zone is calculated with following equations.

$$\frac{\overline{\sigma_x}}{Y} = \pm 1.816 \left(\frac{E\varpi}{YR}\right) e^{-\beta x}(\cos \beta x - \sin \beta x)$$
$$\frac{\overline{\sigma_\theta}}{Y} = \frac{0.3\overline{\sigma_x}}{Y} + \left(\frac{E\varpi}{YR}\right) e^{-\beta x}(\cos \beta x + \sin \beta x) \quad (1.2)$$

It is shown in a parameter study that, for expansions that ensure a leak-tight joint, the maximum residual tensile axial stress at the inside surface of the tube reaches 80-95 percent of the yield stress of the tube, regardless of the geometrical and material parameters of the tube and tube sheet. The analytical model developed in this paper provides a good estimate of residual stresses in the transition zone.

In 1992 Yokell.S (1992) developed an analytical model of the tube-to-tube sheet joint strength, in which he assumed that the tube is uniformly expanded into an infinitely large tubesheet and the axial stress is zero. Taking into account the tube and tubesheet yield strength, he analyzed the variations of the stresses in both tube and tubesheet. He found that the optimum contact pressure occurred when the ratio (outer radius/inner radius) = 1.45, as shown in Figure 1.2.

$$\sigma = P\frac{a^2}{r^2} \quad (1.3)$$

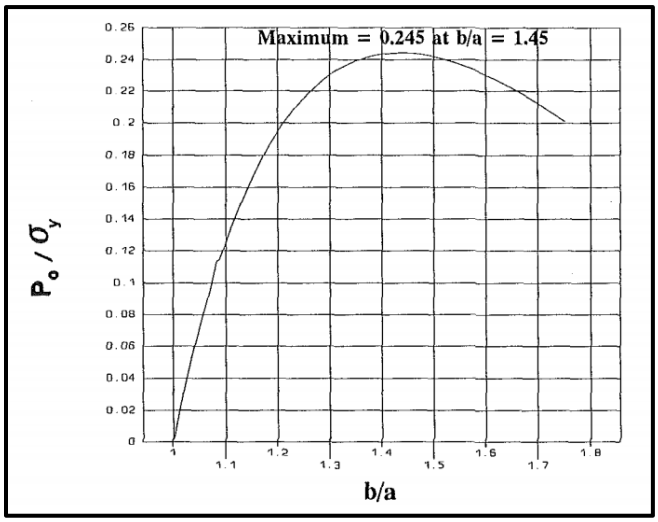

Figure 1.2 Optimized contact pressure conditions
(Yokell,1992)

Allam et al. (1998) developed a theoretical method to calculate the maximum residual stresses in the transition zone of an expanded tube-to-tubesheet joint. The higher positive values of tensile residual stresses and their corresponding axial locations are determined by using a standard deviation analysis. Finite element analysis of some arbitrary cases are conducted in order to validate the developed analytical model. The resulting stresses, when normalized to the yield stress of the tube material show that the tube is mainly affected by the dimensional parameters and the expansion pressure level. Furthermore, the maximum tensile residual stress occurs at the end of the transition zone. The elastic hoop and radial stresses in the expanded zone are given by

$$\frac{\sigma_\theta}{P} = \frac{r_i^2}{r_0^2 - r_i^2}\left(1 + \left(\frac{r_0}{r}\right)^2\right)$$

$$\frac{\sigma_r}{P} = \frac{r_i^2}{r_0^2 - r_i^2}\left(1 - \left(\frac{r_0}{r}\right)^2\right) \qquad (1.4)$$

Normally the expansion affected area in the tube is divided into three zones: expanded, transition and unexpanded zones. Part of the transition zone can be calculated using the discontinuity stress analysis of the thin elastic shell (Harvey, 1985)

$$\frac{s_{u\theta}}{s_{yt}} = 2\frac{\bar{E}_t}{1-\bar{t}}\bar{U}_z \pm \frac{6\upsilon}{\bar{t}^2}\bar{M}_z$$

$$\frac{s_{uz}}{s_{yt}} = \pm\frac{6\upsilon}{\bar{t}^2}\bar{M}_z \tag{1.5}$$

The stresses in the first two zones reach the yield stress, therefore these zones should be paid more attention. Bouzid et al. (2015) propose a methodology that divides the expansion process into two phases: loading and unloading. The model is used to assess the stresses in the expended zone produced during the process of expansion. The accurate residual stress estimation is a critical step in evaluating the mechanical integrity of tube-to-tubesheets during service. Bouzid et al. (2016) indicates that the combined stress of residual and operation pressure could exceed the yield stress of the tube and make it vulnerable to stress corrosion cracking which will lead to a dramatical decrease of reliability and service life of the tube.

In 2018, Avalle et al. (2018) developed an analytical model, as show in Figure 1.3, based on his pervious research (Allam et al., 1998) to predict the push force of an expansion tube with die. The results with linear and rigid with linear hardening behaviors are also provided in this work.

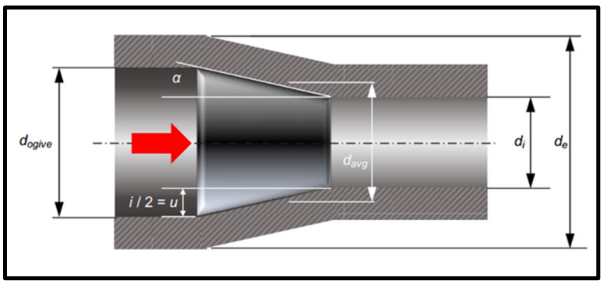

Figure 1.3 The expansion model for
the analysis model (Avalle et al., 2018)

The contact pressure between the die and tube is given by the following equation:

$$P_a = P_r \tan(\alpha + \varphi) = P_r \frac{f + \tan\alpha}{1 - f\tan\alpha} \tag{1.7}$$

The push force is therefore given by the following equation:

$$F = P_a A \approx P_r \tan(\alpha + \varphi)\frac{\pi}{2} i d_{avg} \approx P_r \frac{f + \tan\alpha}{1 - f\tan\alpha}\frac{\pi}{2} i d_{avg} \tag{1.8}$$

1.2.2 Energy method

Different from the previous theoretical analysis, Yuzhe Liu et al. (2016) developed a tube expansion theoretical mode based on the energy dissipation theory, in lieu of the momentum equations. This model estimates the tube radius change after expansion and the push force required for tube expansion with rigid and elastic perfectly plastic material behaviors.

The energy conservation c is W is the summation of the energy dissipation rate for three components as equation 1.9, plastic bending along meridional direction $\dot{E}_l$, plastic stretching along the circumferential direction $\dot{E}_\emptyset$ and friction at the contact area $\dot{E}_f$

$$\dot{\mathcal{W}} = F v_0 = \dot{E}_\emptyset + \dot{E}_l + \dot{E}_f \tag{1.9}$$

The energy dissipation model provides better results than previous analytical study. A study presented by Luo et al. (2019) confirmed this finding. They provided a theoretical model based on energy absorption theory with three geometrical configuration models (tube tip-conical surface contact model, tube wall-conical surface contact model and tube wall-conical and cylindrical surface contact model) and conducted numerical simulation to compare the driving force in the steady-state, the free body diagram shown in Figure 1.4.

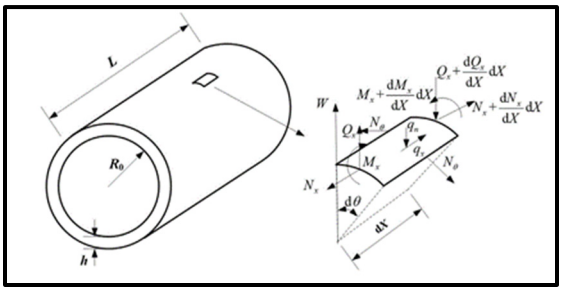

Figure 1.4 The cylindrical shell and
a small element (Luo et al., 2019)

The circumferential membrane force and the axial bending moment in this study are given by following equations:

$$N_\theta = N_s + \frac{E_p h}{R_0} W \quad (if\ N_\theta \geq N_s)$$
$$M_x = M_s + D_P \kappa \quad (if\ M_x \geq M_s) \tag{1.10}$$

1.3 Numerical approach

The numerical approach as an attractive method to solve physical problems that do not have analytical solution and have widely been used in the pressure vessel and piping research field. In 2005 Almeida et al. (2006) conducted serval tests with different die shapes and evaluated the tube thickness reduction in tube expansion forming. Theoretical and experimental investigations were used to establish the tube formability principles benefiting the tubular design work. The finite element method was utilized to validate the theoretical analysis.

Later 2006 Alves et al. (2006) conducted a similar study in which 2D and 3D numerical finite models were developed to analyse expansion and reduction of thin-walled tubes using a die. The results from the numerical models were compared with the experimental results to support and validate the overall investigation.

Die expansion is not only applied to the metallic tube but also the plastic pipe. Alves et al. 2016 investigate the cold expansion of thin-walled PVC tubes using a die. They addresses the limits of pressure-sensitive polymers with cold expansion and propose a flow formulation that can model polymers cold plastic deformation different from the Prandtl flow rule. This work is supported by experimental data obtained under laboratory conditions.

The work by Liu et al. (2016) mentioned previously contains a numerical approach used to validate an analytical model developed to study stresses and deformations of expansion metal tubes. The FE model shown in the Figure 1.5.

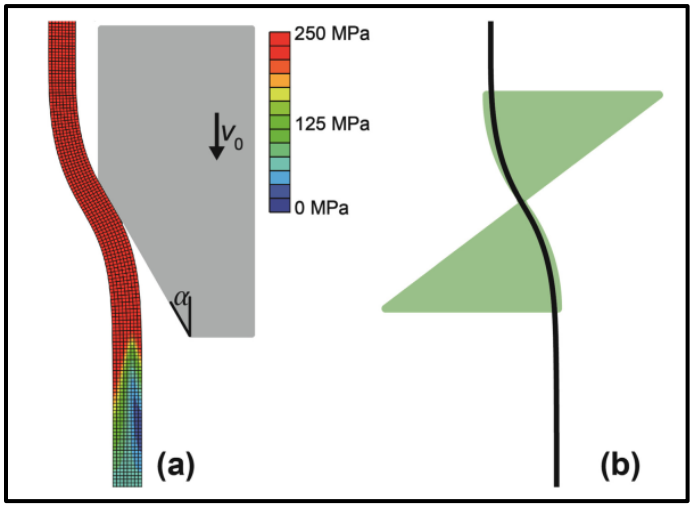

Figure 1.5 2D deformation model (Yuzhe, 2016)

In recent years, inner grooved tubes have attracted more attention due to their thermally efficient geometry. The tube expansion technique is the key process in joining the fins to the tubes. Tang et al. (2009) studied the influence of key parameters of geometry such as the height of the groove, the helix angle and the size of the tube. The result of the push force from the experiment is also assessed using the finite element method in order to complete the investigation. The 3D model used in study shown in Figure 1.6 and the friction coefficients between the tube and die and the fin and tube are determined experimentally.

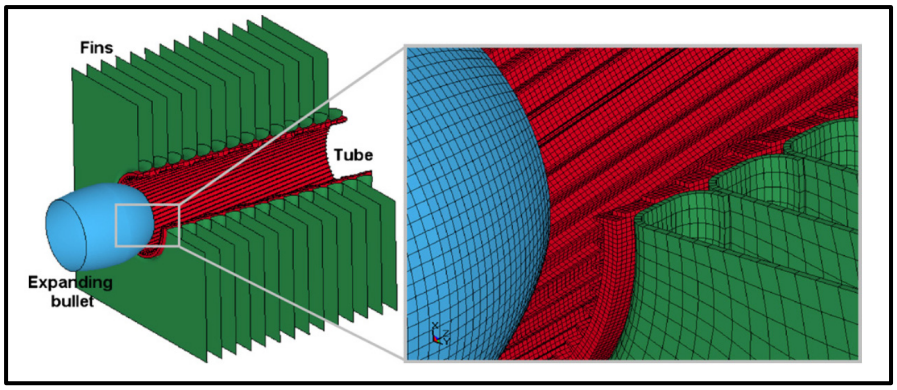

Figure 1.6 Grooved tube expansion FEM model (Ding et al.,2011)

Inner grooved tubes contribute to increasing thermal transform efficiency, however, the tube expansion process reduce the groove size due to die compression stress. In 2019, Kang et al. (2019) conducted a study on groove height reduction and developed a new die to prevent this effect in the tube expansion process. The new die (Figure 1.7) consists of two parts: spiral expanding ball and the conical screw front. The experimental results show that the new die improve the reduction of groove height by 10.3% compared to conventional ball die.

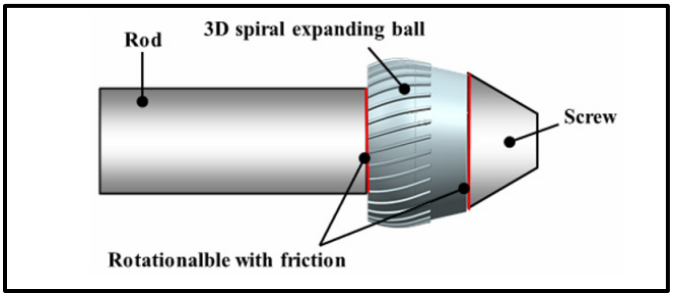

Figure 1.7 Spiral expand die (Kang, 2019)

The three geometrical models used by Luo et al. (2019) are basically finite elements simulation to study the effect of material properties and geometries.

The contact quality between the fins and the tube highly influences the thermal conduction efficiency of finned tube heat exchangers. This together with defects due mechanical tube expansion are the subject of recent research work. The reduction of cracks and improvement

of thermal efficiency are the new challenges of gas-cooled exchangers. Tang et al. (2011) simulated die expansion using 3D finite element models with different geometry parameters to determine an optimized fin shape that maximize fins to tube contact interface.

1.4 Experimental approach

The experiments related to the subject described in the literature can be categorized into three types: push-pull force measurements, strain deformation measurements, and residual stress measurements.

1.4.1 Push-pull force measurement

In 2006 Alves et al. (2006) conducted a series of aluminum tube expansion tests under the push or pull conditions as Figure 1.8. They measured a wide range of measured parameters related to the expansion of thin-walled tube ends using a conical die.

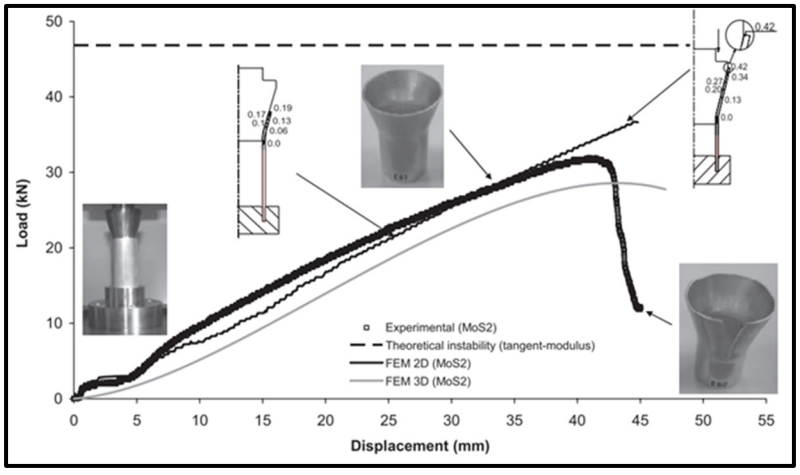

Figure 1.8 The numerical and experimental results for the expansion of thin-walled tubes (Alves, 2005)

Also in 2006, Almeida et al. (2006) conducted a series of tube expansion experiments to study the influence of interface friction. It can easily alter a successful mode of deformation into an inadmissible mode by simply changing the lubrication.

In 2009, Tang et al. (2009) conducted tests on the expansion of grooved tubes using a die. To measure the deformation of the tube and groove, the samples were cut at the center. The test workbench and cut samples are shown in Figure 1.9. The researchers also determined the friction coefficients for FEM simulations using separate tests.

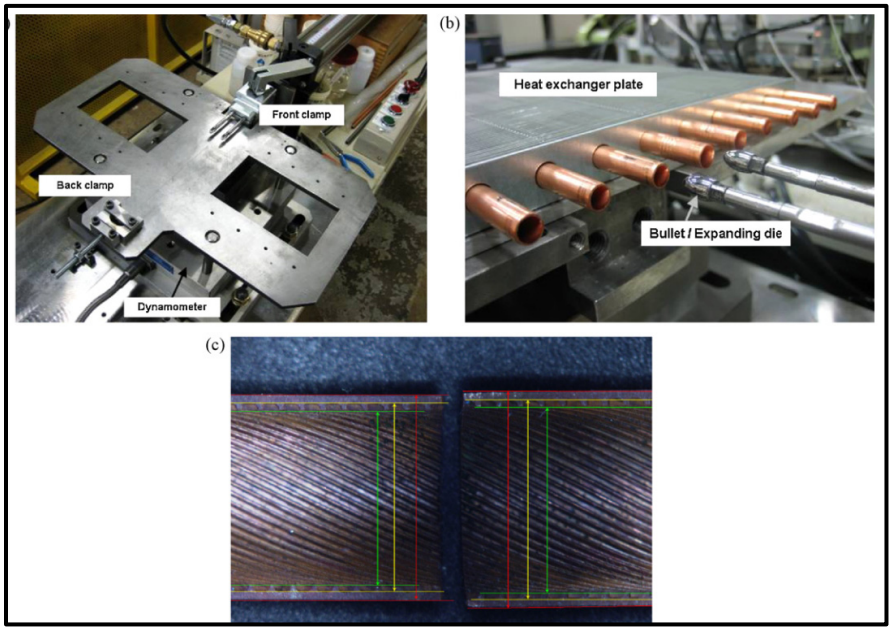

Figure 1.9 The grooved tube expansion test set-up Ding Tang (2009)

The results were used in a future study by Tang et al. (2010). to investigate the effect of fin geometry on contact surface quality. The study presents the experimental and numerical results of fin-to-tube contact, which are shown in Figure 1.10.

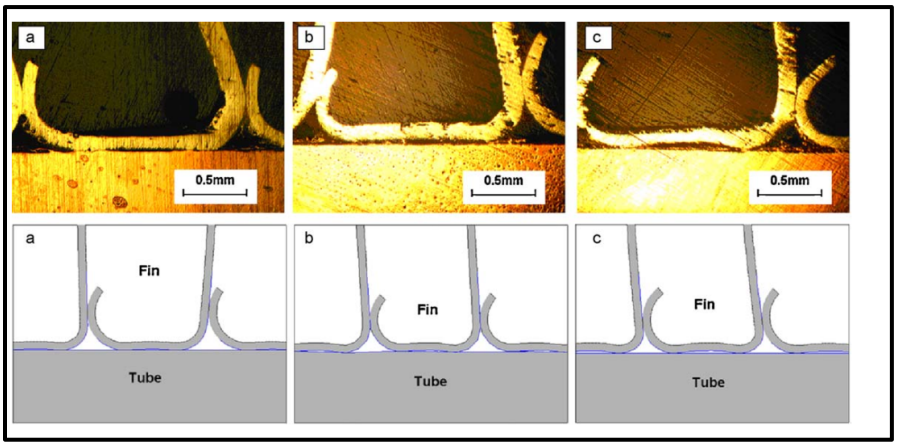

Figure 1.10 Experimental and numerical determination of contact quality (Tang et al., 2010)

In 2014, Avalle et al. (2014) conducted a series of tube expansion experiments to study the effect of die speed on the required driving force. During the test, the die movement inside the tube was kept constant.

In 2018 Avalle and Scattina (2018) published a research study on tube expansion using different materials. Unfortunately, the details of the experiment are not available in the paper. However, the study did reveal that it took approximately 6000 N to expand an AISI 316 steel tube with an outer diameter of 15.88 mm and thickness of 1.65 mm.
The test rig and die shown in Figure 1.11.

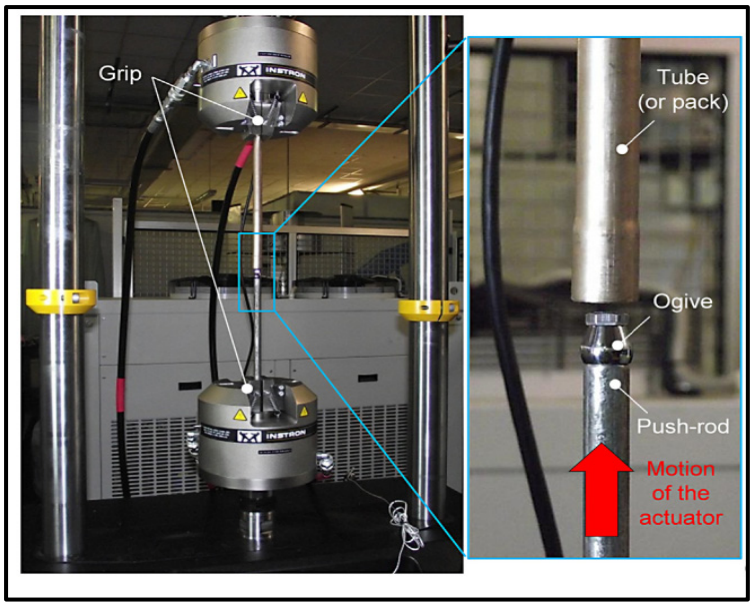

Figure 1.11 Tube expansion test rig (Avalle et al.,2018)

In 2019 Kang et al. (2019) presented a work related to groove tube expansion as shown in Figure 1.12. The die in this study is manufactured with the groove to prevent tube groove height reduction during the expansion process. The die grooves overlap with the tube grooves to increase the contact area and limit groove height by compression.

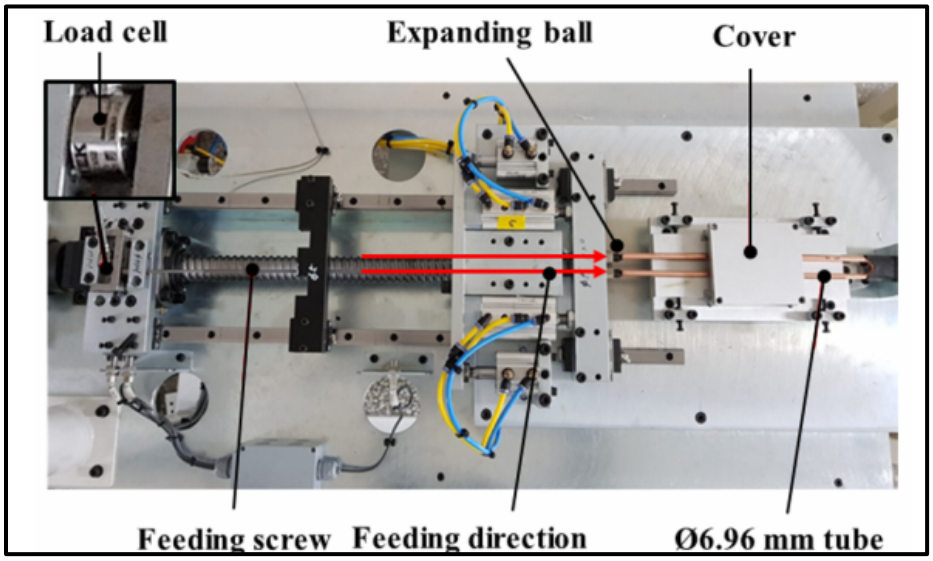

Figure 1.12 Tube expansion test rig with grooved die (Kang et al.,2019)

1.4.2 Residual stress measurement

Residual stresses are the main contributing factor to stress corrosion cracking in heat-exchanger tube joints. Japanese researcher Toba (1966) published a work on residual stress in expanded joints in 1966, investigating their role in stress corrosion cracking through experimental study. This work highlighted the crucial role of residual stress in joint failure in the transition zone.

Residual stresses are difficult to measure directly. J. Druez and A. Bazergui (1983) proposed a method to evaluate residual stresses experimentally by installing strain gauges on inner and outer tube walls and removing the opposite tube wall material by chemical etching. The strain changes were recorded and used to estimate residual stresses in tubes. The stress distribution across the thickness is presented in Figure 1.13.

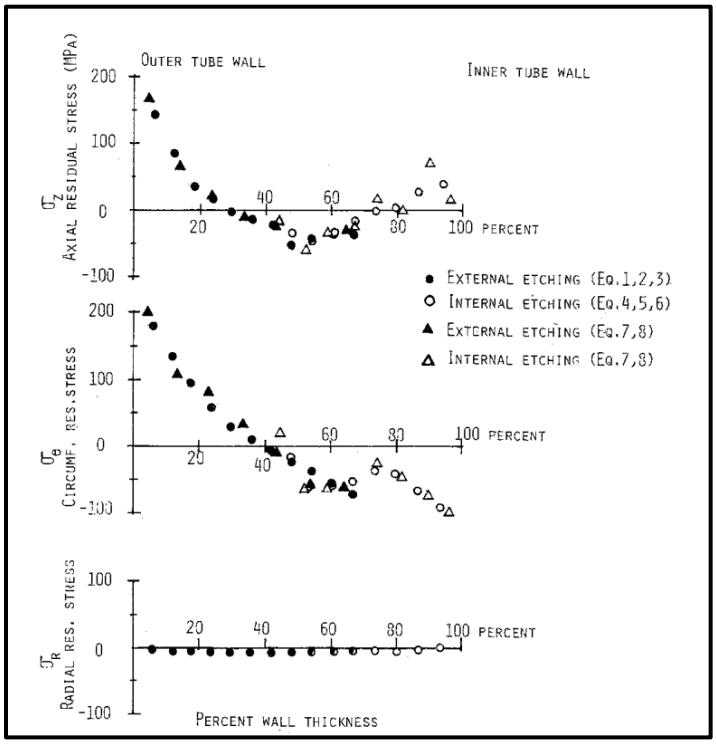

Figure 1.13 The stress distribution across the thickness (J.Druez,1983)

In 1985, Druez et al. (1985) applied the chemical etching method to a roller expanded tube to measure residual stresses. The residual stress distribution through the thickness in the expanded zone is therefore estimated with this experimental technique (see Figure 1.14).

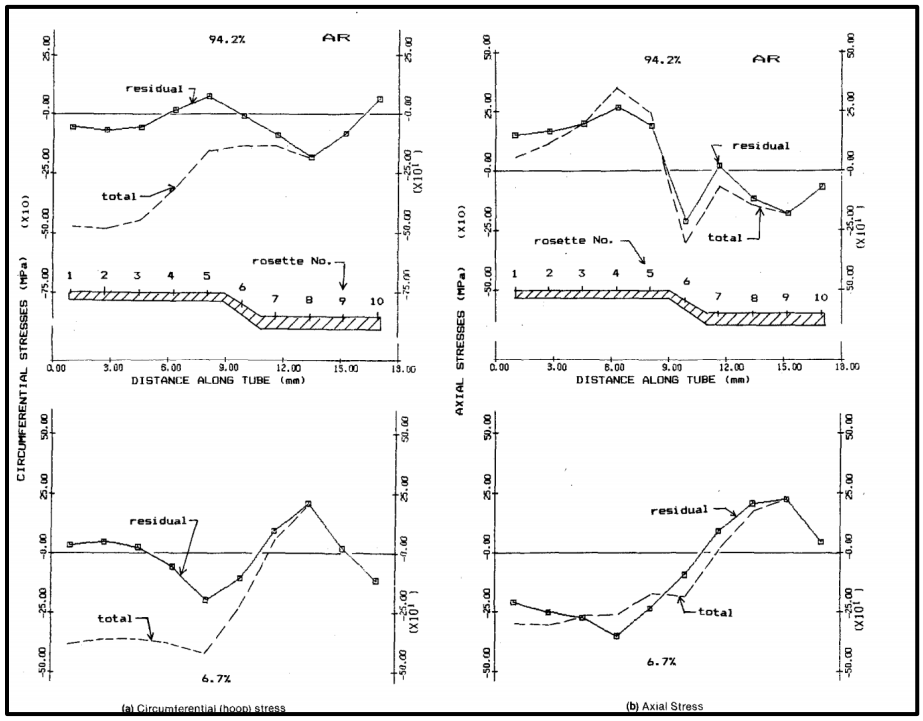

Figure 1.14 The stress distribution in the expansion zone

1.5 Objective of the study

The main objective of this study is to develop a new analytical method for analyzing the nonlinear plastic deformation process of tube expansion. Currently, thin-wall theory only applies to plastic deformation of the expansion zone, while the actual expansion of the tube often involves the three deformation zones; the expanded plastic zone, the elasto-plastic transition zone and the elastic zone. Therefore, if analytical methods can be used to solve complex plastic problems, it will provide great convenience for future theoretical research and engineering analysis, in addition to quickly evaluate the magnitude and distribution of the stresses and strains during finned tube expansion, as well as determine the magnitude of driving force required to move the die inside the tube.

A first secondary objective of the study is to investigate which plastic deformation theory, kinematic or isotropic, is more suitable for analyzing tube expansion through numerical and experimental methods. The study also examines the effect of these different theories on the analysis of residual stress in metal tubes under expansion, as well as the magnitude and distribution of residual stress. This provides a reliable reference for evaluating residual stress in future production and research.

Another secondary objective of the study is to investigate how to improve the thermal conductivity efficiency between tubes and fins. One important factor affecting heat transfer is the contact quality between tubes and fins. Through numerical methods, this study analyzes the contact quality of different collar shapes of the fins after tube-to-fin forming, establishes the relationship between fin shape and contact quality, and develops an optimization scheme to improve contact quality and thus enhance the heat transfer efficiency between tubes and fins.

CHAPTER 2

FINNED TUBE EXPANSION EXPERIMENTAL SETUP

2.1 Introduction

The tube expansion process studied in this research involves not only elastic and plastic deformation, but also loading and unloading behaviors, as well as the interaction between the tube and die. However, both current analytical and numerical approaches have limitations and cannot accurately analyze these complex phenomena. One of the main limiting factors is the loading and unloading plastic behavior of the material. Currently, various theories of plastic deformation have been proposed, with kinematic and isotropic being the most common. Experimental verification is necessary to determine which theory is more suitable for tube expansion analysis. Additionally, the analysis results of the level and distribution of residual stresses in the expanded tube are directly related to the applied plastic deformation theory. Moreover, the magnitude of the driving force during the tube expansion process and the friction coefficient of different materials also need to be determined directly and indirectly through experiments. Therefore, conducting corresponding experiments is essential for this research.

To carry out the experiments that meet the above purposes, a dedicated test fixture consisting of two components and a custom-made expander were manufactured and used for this study. More detailed information will be presented in the corresponding chapters later.

Figure 2.1 Hydraulic tensile compression machine
used for the die expansion tests

The expansion tests are conducted on steel and copper tubes. The tubes are 3/8 inch in diameter and gaged. They are expanded with an oval die on a test workbench that uses a hydraulic tensile/compression machine of the MTS brand as shown in Figure 2.1. The die with the rod shown in Figure 2.2 is fixed to the upper grip while the tube guide is fixed to the lower grip of the MTS machine. The tube guide is specially designed to hold the tube in place without interfering to the expansion allows for the pull test but also prevents buckling during the push test. As shown in
Figure 2.4, the tube is restrained by this guide at the top or the bottom during the process of expansion while letting the die moves inside the tube.

2.2 Expansion dies

The die or expander shown in Figure 2.2 is designed to expand 3/8 tubes. There are different radii on its two sides (4.32mm and 15.24mm), and it can be utilized to conduct the expansion tests for the same maximum outer diameter but different contact radius.

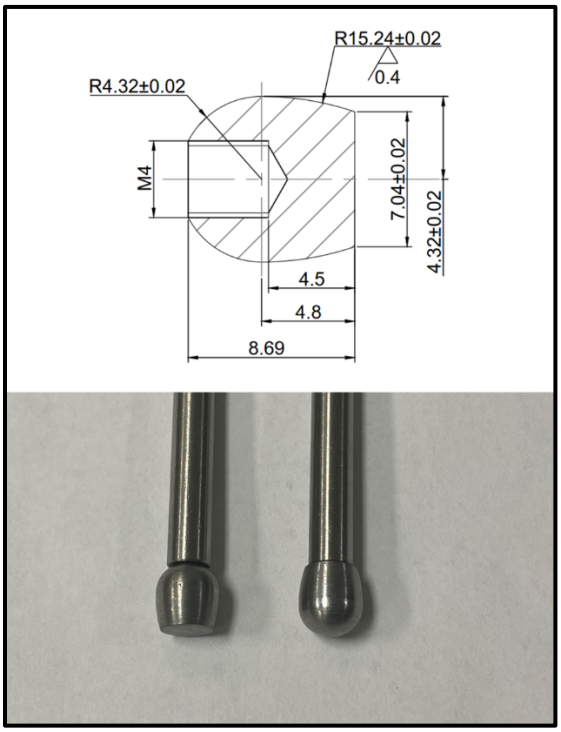

Figure 2.2 Oval dies

The die is manufactured with wear-resistant high-speed M4 tool steel the mechanical properties of which are shown in Table 2.1.

Table 2.1 Material property of die

Yield Strength:	60,000 psi
Hardness:	Rockwell C30 (Hard)
Heat Treatable:	Yes
Max. Hardness After Heat Treatment:	Rockwell C65

2.3 Tube guide

The tube guide consists of two parts, an upper sleeve, and lower guide showed in Figure 2.3 and
Figure 2.4. The lower guide is fixed at the bottom side by the lower grip of the MTS machine. The upper sleeve on the top of the lower guide holds the tube and prevent it from buckling during the test. There are two holes in the mid of the sleeve to let the wires of strain gauge of the tube directly throughout without interfering with small necks on top or bottom of the tube guide. The tube guide is made out of M4 steel material also.

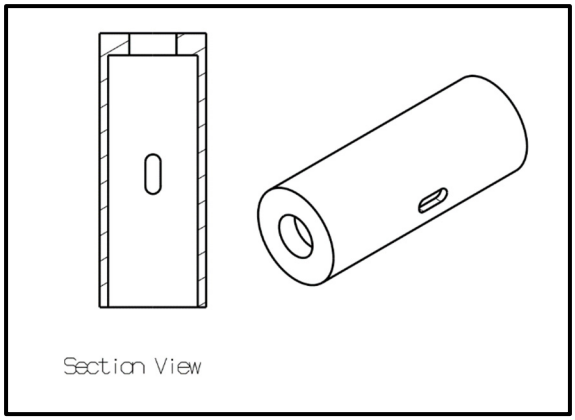

Figure 2.3 Upper sleeve

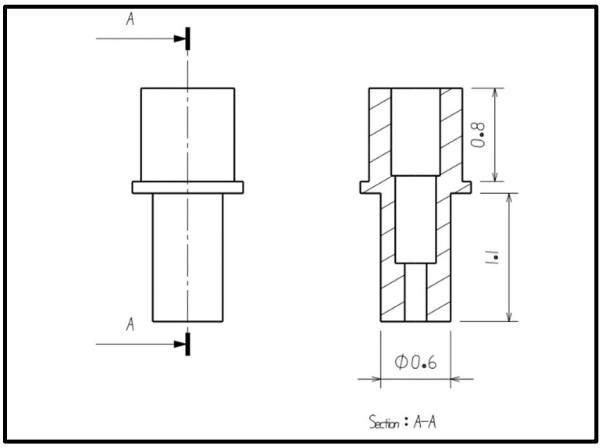

Figure 2.4 Tube lower guide

2.4 Tubes

The tube samples used in the study shown in Figure 2.5 were sourced from Kool-Air Inc., a manufacturer of a full range of heat transfer products for commercial, industrial, and institutional applications. Two types of materials were tested: copper and stainless steel. Table 2.2 provides details on the size and general properties of the tubes, with a tolerance for the outer diameter of less than 0.06 mm.

Table 2.2 Material properties of tubes

Properties	**Materials**	
	SS316L 3/8 x 0.035 in	Copper (C122)
Diameter, mm	9.52	9.52
Thickness, mm	0.89	0.89
Ultimate tensile strength, MPa	483	275
Ultimate compressive strength, MPa	175	69
Modulus of elasticity, GPa	206	112
Poisson's ratio	0.25	0.3

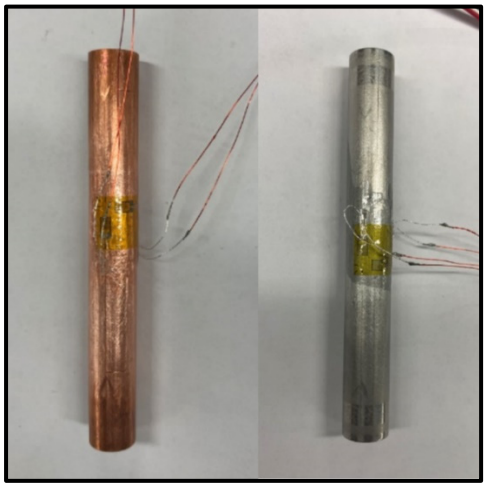

Figure 2.5 Strain gauged tubes

It should be noted that two different tube boundary conditions, pull and push, were tested in this study. These corresponded to the fixed constraints position of tube at the start and end of the die's movement. To achieve these conditions, the tubes were manufactured with two types of ends: flared or straight. Flared tubes were used for pull, while straight tubes were used for push. Flared tubes have an expanded edge produced by pre-expanding, which can hold the tube only in place at the top of the upper sleeve without contact with lower guide during the testing process, as shown in Figure 2.6. All of the axial force on the tube is take by the top of the tube.

Figure 2.6 Flare tube

For the push test, straight tubes were placed in the tube guide and supported by the inside shoulder of the lower guide, as shown in Figure 2.7. In this state, all of the axial force on the tube is borne by the bottom of the tube.

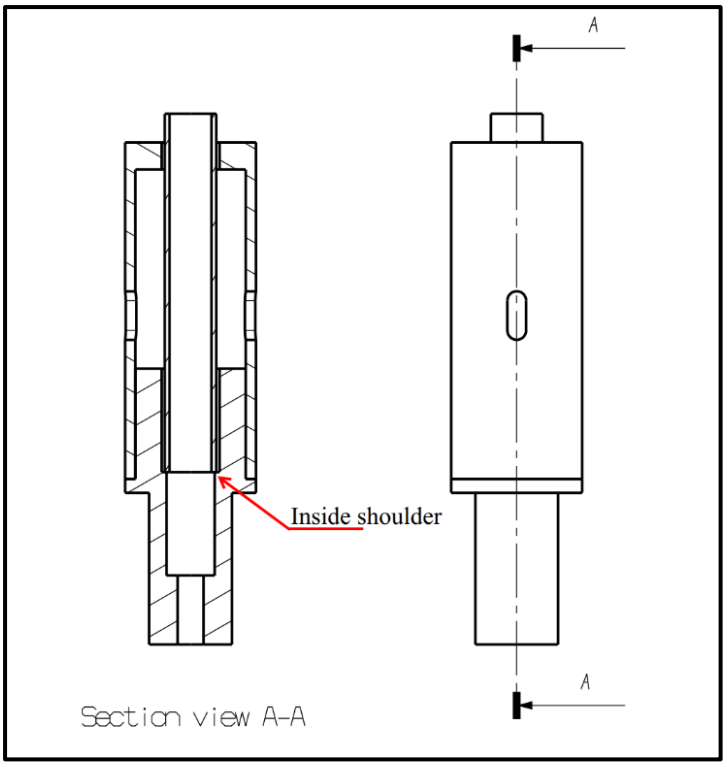

Figure 2.7 Push configuration

2.5 Strain gages

The 2 mm wide tee rosette KYOWA high elongation foil strain gage shown in Figure 2.8 is bonded to the outside wall of the tube and allows up to 15% strain measurement. The operating temperature range is -10 to 80 °C. The biaxial strain is bonded to wall at the middle of the tube and aligned to measure the axial and circumferential strains. The strain gaged copper and steel tubes are shown in Figure 2.5.

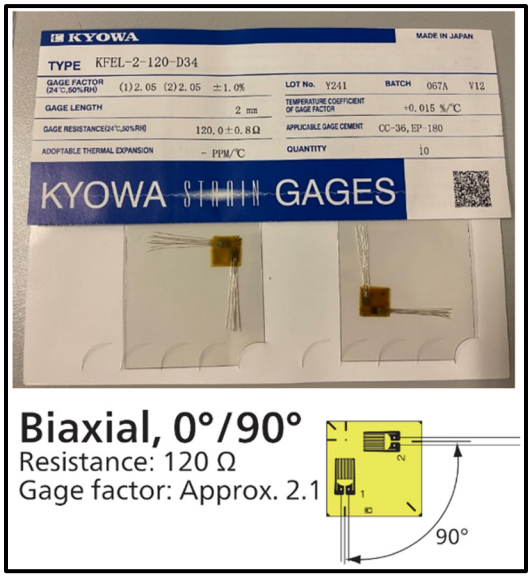

Figure 2.8 Biaxial strain gage

2.6 Data acquisition system

The MTS machine used in this experiment is equipped with a data acquisition system that can record and monitor relevant data in real-time during the test, as shown in Figure 2.9. In this experiment, the axial strain and hoop strain of the strain gauge, as well as the driving force and movement distance of the die, and the duration time of the experiment, were all recorded simultaneously. The data acquisition system can record data at a frequency of 1, 10, or 100 times per second. Since the movement speed of the die in this experiment is relatively slow at 2mm/s, a recording frequency of 10 times per second is sufficient to meet the analysis requirements. Therefore, this recording frequency was used for this study.

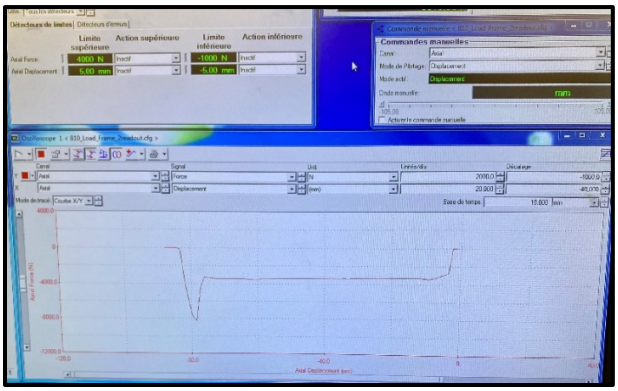

Figure 2.9 The data acquisition system

2.7 Test procedure

Before expansion, the strain-gauged tube sample should be placed in the tube guide. The two sets of wires on the strain gauges should be threaded out separately from the holes on both sides of the sleeve and connected to the data acquisition system. Ensure that the wire position is appropriate and well-insulated to prevent short circuits caused by tube deformation during the experiment.

As previously mentioned, there are two types of tests: pull condition and push condition. For pull condition, the length of the tube sample should be measured in advance, and the flared tube should be fixed to the top of the sleeve by its flared edge. The bottom of the tube should not allowed to contact with the inside shoulder of the lower guide. Then, the die fixed on the upper part of the MTS will be lowered close to the top of the tube, then the experimental settings should be initialized. During the experiment, the driving force and strain gauge readings should be monitored throughout on the data acquisition system. When the driving force drops to zero, it indicates that the die has completely passed through the tube, completing the entire expansion process. At this point, the die movement should be promptly stopped to prevent it from hitting the bottom of the tube guide.

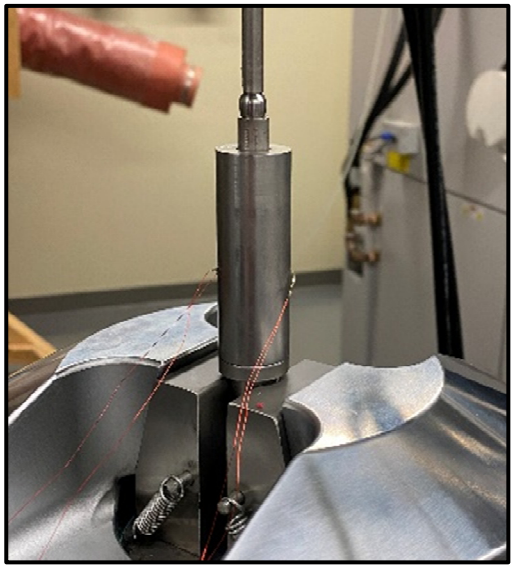

Figure 2.10 Expansion test workbench

The experimental process of the push condition is similar to the pull condition, except that a straight tube is used instead of the flared tube. The straight tube needs to be placed on the inside shoulder of the lower guide, with no axial constraint on the top of the tube, as shown in Figure 2.10. After full expansion, the die can be removed from the bottom by rotating it due to the thread connection with the rod, and the expanded tube can be removed from the test bench without removing the rod.

The experimental process for copper and steel tubes is similar. It should be noted that the inside of the tube must be sufficiently lubricated before the experiment to prevent the die from getting stuck in the tube during the expansion process.

CHAPTER 3

ANALYSIS OF STRESSES IN STAINLESS STEEL 316L TUBES SUBJECTED TO DIE EXPANSION

Zijian Zhao [a], Abdel-Hakim Bouzid [b], Nor-Eddine Laghzale [c]

[a] Ph. D. student, Mechanical Engineering Department, École de technologie supérieure, 1100 Notre-Dame St. West, Montreal, Quebec, H3C 1K3

[b] ASME Fellow, Professor, Mechanical Engineering Department, École de technologie supérieure, 1100 Notre-Dame St. West, Montreal, Quebec, H3C 1K3

[c] Professor, Université Mohammed V, Avenue de l'Armée Royale, Madinat Al Irfane, Rabat, Morocco 10100

Paper published in the Journal of Pressure Vessel Technology, October 2022.
(144(5): 051509 (7 pages))

3.1 Abstract

SS316L finned tubes are becoming very popular in high-pressure gas exchangers and particularly in CO2 cooler applications. Due to the high-pressure requirement during operation, these tubes require an accurate residual stress evaluation during the die expansion process. Die expansion of gas coolers finned tubes creates not only high stresses that can surpass the UTS when combined with operation stresses but also micro-cracks during expansion when the process is not very well controlled.

This research work aims to study the elastics-plastic behavior and estimate the residual stress state of tubes subjected to the die expansion process. The stresses and deformations of the expanded SS316L tube are analyzed numerically using the finite element method. The expansion and contraction process is modeled considering elastic-plastic material behavior for different die sizes. The maximum longitudinal, tangential and contact stresses are evaluated to

verify the critical stress state of the joint during the expansion process. The importance of the material behavior in evaluating the residual stresses using kinematic and isotropic hardening is addressed. Finally, an experiment was conducted to assess the tangential and longitudinal strains of a 3/8 stainless steel subjected to expansion with an oval shape die.

3.2 Introduction

Tube expansion is widely used in the equipment of the petrochemical and nuclear industries. This process is used in the fabrication of boilers, steam generators, and heat exchangers. It has different applications in the latter and is particularly used to produce tube-to-tube sheet joints and finned tube assemblies (Bouzid, 2018; Hing et al., 2012; Ding Tang et al., 2009). The majority of the tubes used in the ACR equipment (air conditioning and refrigeration) are made of copper and nickel alloys. Along with the increasing environmental protection requirements, the once thought traditional environmentally-friendly Hydrochlorofluorocarbon (CFC) like Hydrofluorocarbons (HCFC) refrigerants have recently been the subject of a lot of criticism as they represent a major source of atmospheric pollutants.

According to international agreements on global warming, governments must encourage their local industries to reduce consumption of high GPW (global warming potential) gases and replace them with lesser pollutants. Using natural refrigerants like carbon dioxide, CO_2 and propane have been proposed (Pearson, 2005; Pettersen et al., 1998; R. Wang et al., 2007) as the best alternatives. As propane is a flammable gas, it did not receive the attention that it deserves and was rejected by many industries and safety agencies. CO_2 was the preferred option and therefore is being used as a refrigerant for specific applications. Using such refrigerant leads to higher operating pressures and temperatures; as a consequence, all pressure parts of the system have to be redesigned to meet standard requirements (Pettersen et al., 1998; Ding Tang et al., 2009). CO_2 maximum allowable working pressure is 120 bars at 300°F and 48 bars at 100°F in the high- and low-pressure sides respectively; which is much higher than regular refrigerants. This has a major impact on the design and manufacturing of newly developed stainless-steel heat exchangers because of the different requirements needed on the

material, thicknesses, die geometry, fin whole tolerances and so on. Tubes made of soft materials like copper and nickel alloys have less capability for such high-pressure CO_2 application requirements and therefore the recommendation to replace them with more rigidity tubes such as stainless steel is justified.

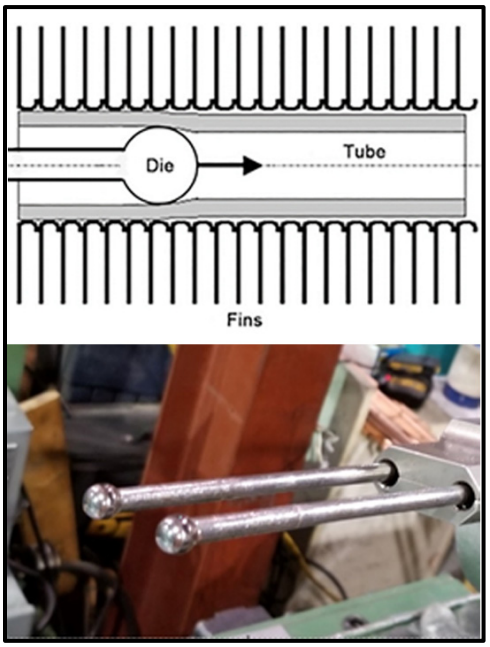

Figure 3.1 Die expansion process

The analysis of tube expansion with the die shown in Figure 3.1 is different from tube-to-tubesheet expansion which leads to a more rigid joint. Unfortunately, the former has drawn less attention and consequently, there is less research on ACR steel tubing. Although die expansion of copper tubes is similar to steel tubes, the related studies on the latter only begin recently. In 2005, Almeida et al. (2006) conducted serval tests with different shapes of die and evaluated the tube thickness reduction in the expansion forming. Theoretical and experimental investigations were used to establish the tube formability principles benefiting the tubular design work. The finite element method was utilized to validate the theoretical analysis. Later in 2006, Alves et al. (2006) studied a similar topic numerically using 2D and 3D finite models using 6060 aluminum alloy. The results on the formability limits from the numerical

simulations were compared to the experimental data to support and validate the overall investigation.

Die expansion is not only applied to the metallic tubes but also the plastic pipes. Alves investigated the cold expansion of thin-walled PVC tubes using a die (L. Alves et al., 2016). He addresses the limits of pressure-sensitive polymers subjected to cold expansion and innovated by implementing a flow formulation that can model polymers cold plastic deformation under a non-associated flow rule. This work is assessed with experimental data obtained under laboratory-controlled conditions. An analytical model based on the Hoop stress reaching yield to predict the push force for the expansion of a tube with a die using a rigid-linearly hardening result is provided (Avalle & Scattina, 2018).

In recent years, internally helical grooved tubes have attracted more attention due to their thermally efficient geometries (L. Alves et al., 2016). The tube expansion forming is the key process in the fabrication of finned tubes. Tang D. et al. (2009) studied the influences of key geometry parameters such as the height of the groove, the angle of the helix and the size of the tube using FEM. The push force obtained from the experiment is compared to that of the finite element to support the whole investigation. The friction coefficients used in FEA between the tube and die and between the fins and tubes are determined experimentally on a specially designed rig. To increase thermal transform efficiency, helical grooves are machined inside the tubes; however, the tube expansion process reduces the groove size due to compression. Kang S.Y. et al. (2019) conducted a study to prevent groove height reduction by implementing a newly designed die consisting of two parts, a spiral expanding ball and the screw.

The experimental results show that the new die can improve the reduction of groove height by 10.3 % as compared to the conventional ball die. In addition to their previous theoretical work on tube expansion based on the momentum equations, Liu Y. et al. (2016) developed an analytical model based on the energy dissipation theory. The new model can estimate the tube radius change after expansion and the push force required for tube compression expansion based on a rigid-perfectly plastic material behavior. The steady compression force determined

by the analytical model is found to be consistent with numerical and experimental results. Since the energy dissipation model provides accurate results, Luo M. et al. (2019) took the analytical model a step further to treat tube wall-conical expansion to predict the driving force under steady-state conditions. The results from the theoretical model are consistent with the experimental data. The contact surface state between fins and tube highly influence the efficiency of thermal conduction of the tube-fin heat exchanger. In addition, failures and defects of tubes subjected to mechanical expansion have been reported in recent research studies. How to eliminate or reduce the impact of those defects is a challenging task. Tang D et al., (2011) simulates die expansion using 3D finite element modeling to study the effects of geometry to determine an optimized fin shape. They suggested a better fin to tube contact interface that improved thermal conduction efficiency.

This paper provides a comprehensive study on the stress state of tubes subjected to die expansion. It provides general guidelines on how to optimize and control the expansion process and helps the design engineer to predict accurately the residual stresses that are the major source of stress corrosion cracking and leakage failure. The methodology consists of conducting a FEM simulation of different die sizes expansion processes of a stainless steel 316L tube with an emphasis on reverse yielding. Such a study will have a major impact on the reliability and durability of equipment such as gas coolers, boilers, heat exchangers and steam generators.

3.3 Finite element model

In this study, the finite element analysis is conducted on Ansys workbench 2019R1, and the plastic models are simulated with multilinear kinematic Harding and multilinear isotropic Harding separately.

Table 3.1 Material properties of tube and die

Properties	**Materials (Ref. 15,16)**	
	Tube SS316L 3/8 x 0.035 in	Die SAE-AISI Steel M4
Diameter, mm	9.52	8.6
Thickness, mm	0.89	
Ultimate tensile strength, MPa	483	-
Ultimate compressive strength, MPa	175	770
Modulus of elasticity, GPa	200	200
Poisson's ratio	0.25	0.29

Material properties

Since the traditional copper tube is not suitable for high pressure CO_2 cooling systems, steel tubing produced with austenitic stainless steel 316L was chosen for this study. The SS 316L geometry and material properties shown in Table 3.1 are introduced to the model based on the ASTM standard, previous research (Desu et al., 2016), and industrial manuals. The SS 316L true stress and strain curve is shown in Figure 3.2. The multilinear kinematic hardening and multilinear isotropic hardening options are both used to describe the plastic hardening behavior of SS316L. These two plastic hardening models share the same material data during the loading part of the curve and are defined by the user. However, the different paths during unloading that define the kinematic and isotropic hardening, are all deduced by the Ansys software and are not required as input. The die is made of M4 steel (Roberts, Krauss, & Kennedy, 1998), the properties of which are listed in Table 3.1.

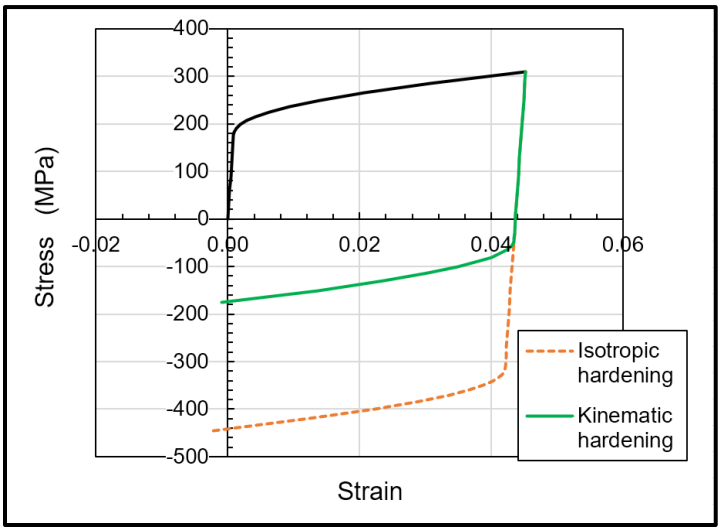

Figure 3.2 Stainless steel 316L stress-strain curves

Meshing and boundary conditions

Since the tube expansion process is a problem where the geometry and loading do not vary with the angle, 2D axisymmetric modeling is utilized for the analysis. Also, 2D modeling reduces the CPU time considerably without altering the accuracy of the results. The dimensions of the die and tube are detailed in Figure 3.3 and Table 3.1. To observe the stress and deformation variations produced by the die movement inside the tube, the nodes located at the tube mid-length position are selected for analysis. Given that the tube was sufficiently long, there was no end effect at this position when the die started traveling inside the tube or when it reached its end. A tube length of 30 mm was found to be sufficient. The mesh of the tube and the area around the ball in contact with the tube was highly refined to obtain accurate stress results. Isoperimetric axisymmetric 8-node elements of around 0.05 mm length were adopted using a mesh refinement criterion of 1% based on the maximum contact stress change of the die to tube interface. Interface and target elements for the axisymmetric case were used to model the contact surface between the tube and die. Several coefficients of friction were considered.

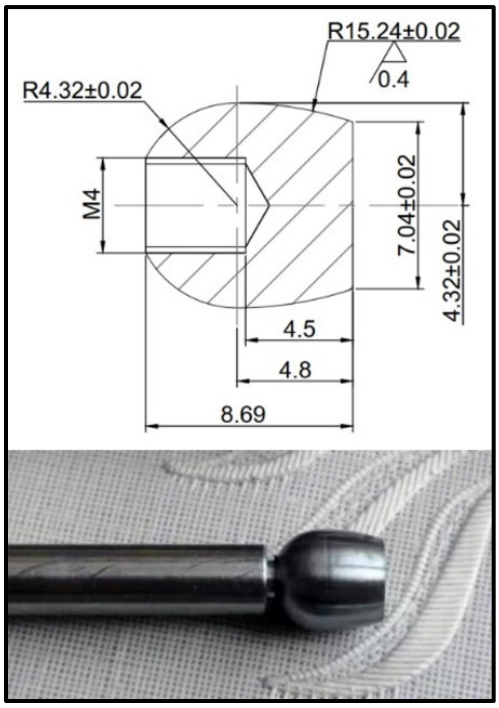

Figure 3.3 Oval die details

The die was pushed inside the tube from one end. The end was constrained axially to generate a longitudinal stretch in the expanded portion of the tube. The die moved at an almost constant speed during the simulation. As the traveling distance of 30 mm was covered in 15 seconds, the average speed of the die was 2 mm/s, which is reasonable according to the literature The radial, longitudinal and tangential stresses through the thickness at the mid-length location during the expansion process were measured at different die positions inside the tube. Since the die speed was low and the interface had been well lubricated, the heat generated at the contact zone was low. Generally, the tube expansion process is conducted in a well-ventilated location and the metallic tube is lubricated, ensuring that contact surfaces remain at a low temperature. Therefore, the simulation of the expansion process was considered as being at room temperature.

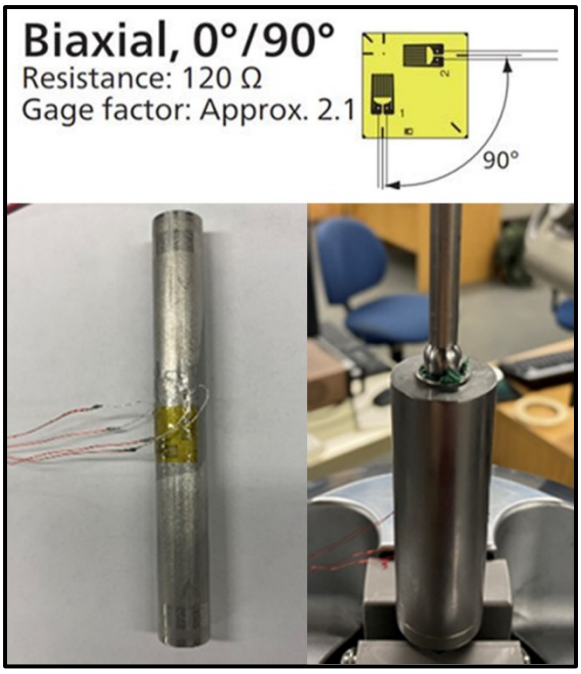

Figure 3.4 Biaxial strain-gaged tube and expansion test set-up

3.4 Experimentation

Experimental tests were performed with SS316 steel tubes. The 3/8-inch tube was expanded with the oval part of the die on a test workbench that used a hydraulic tensile/compression Material Test System (MTS) machine. The die and rod shown in Figure 3.3 were fixed to the upper grip while the tube guide was fixed to the lower grip of the MTS machine.

The instrumented strain-gaged tubes shown in Figure 3.3 were inserted within the guide. To monitor the axial and hoop strain of the tube during the expansion process, a tee rosette also shown in Figure 3.4 was bounded to the outer surface of the tube far from its edge. The strain gauge was 2-mm wide and able to measure up to 15% strain. The outer tube surface strains were monitored as the die was pushed through the tube at a speed of 2 mm/s. The push force, axial and hoop strains and time were measured and recorded at regular intervals. One end of the sample tube was flared providing support for axial tension while the other was free to expand.

3.5 Result and discussion

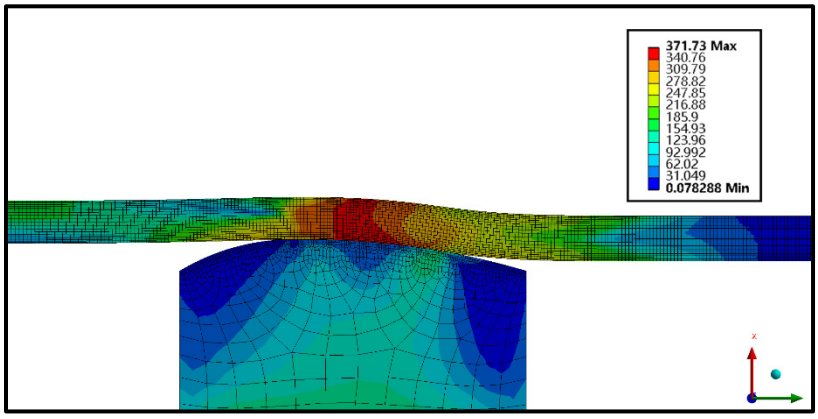

Figure 3.5 Equivalent stress distribution

Tube stress variation with die movement

Figure 3.5 shows the Von Mises equivalent stresses of the tube after the die reached a certain axial position inside the tube. As expected, the area around the contact section was the most loaded region revealing the instantaneous stress state and the deformation of the tube. Due to the axisymmetry, all the nodes that lay at the same radius underwent the same stress variation as the die moved through the tube. Therefore, all the nodes belonging to the inside and outside surface of the tube away from the end underwent the same stress state variation. Figure 3.6 and Figure 3.7 show, at the location of interest on the tube, i.e. mid-length, the stress state at the inside and outside radii as a function of the die position inside the tube. The die position refers to the movement of its center.

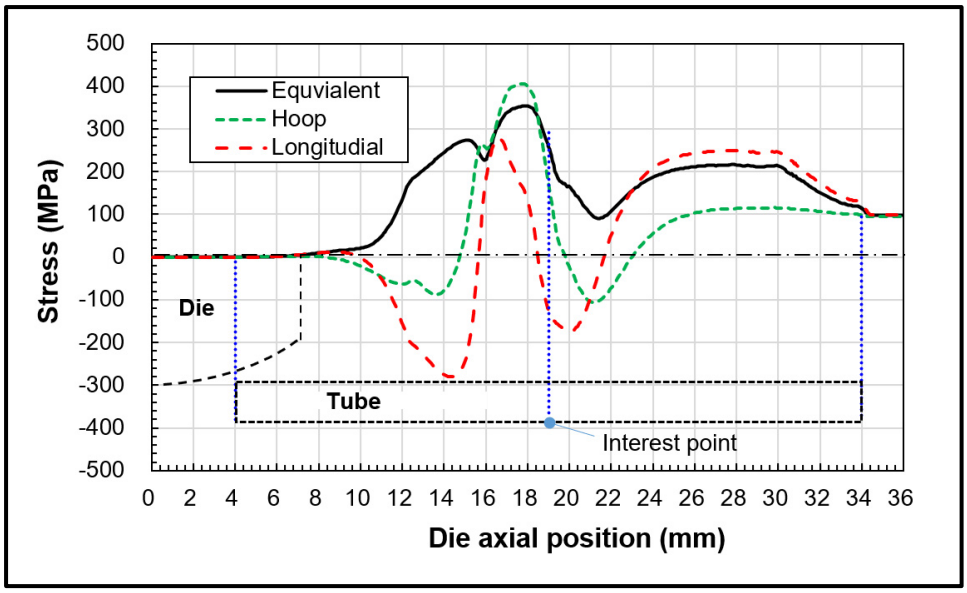

Figure 3.6 FE stress variation at outside tube surface

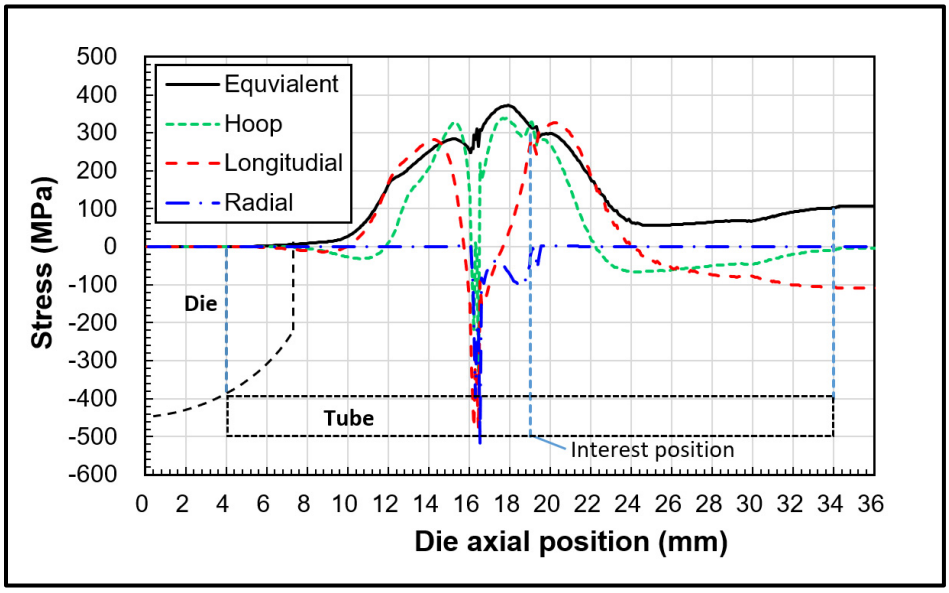

Figure 3.7 FE stress variation at inside tube surface

The mesh of this zone of interest was highly refined to obtain accurate stress results. A 1% mesh convergence criterion was adopted on the equivalent stress.

Figure 3.6 shows the stress variations at the outside radius as a function of the die position. It can be observed that the stress state was mainly dominated by the longitudinal and hoop stresses because the radial stress was zero. While the longitudinal stress was relatively higher than the hoop stress in compression at the beginning of the die movement, both stresses become positive with the hoop stress slightly higher (406 MPa) as the die get closer to the point of interest. In fact, the longitudinal stress reached a maximum value of 290 MPa before the die center reached the point of interest due to local bending produced by the die curved shape. The maximum equivalent stress was 370 MPa, which is less than the ultimate tensile strength (UTS) value. The plateau at the end of the graph indicates the residual stresses, which remained constant after the die had been extracted. The decrease in stress when the die was near the end was due to the decrease of the pull force as the contact surface tension was also reduced.

Given that the die was in contact with the tube inner surface, the inner node-stress variation was slightly different from that of the outside. As shown in , the radial stress at the inside node, which is related to the contact pressure between the die and tube, was equal to zero except when the contact was made, in which case it became very high. During the contact period, the radial stress could reach 500 MPa. It should be noted that the longitudinal stress was also high, around 480 MPa, which was very close to the contact stress and occurred before the die reached the point of interest. However, the point of interest reached a max equivalent stress when the die reached this position. At this point, the equivalent stress was dominated by the hoop stress while the longitudinal stress reached a similar value but with a small lag.

Stress distribution through tube thickness

In the previous section, the stress state at the inside and outside radii of the tube as a function of the die movement was discussed. However, there was no indication that a critical or maximum stress occurred at these surfaces. Therefore, the stress distribution within the thickness of the tube wall was investigated to locate the maximum stress location within the tube thickness. Theoretically, since the stress distribution through the thickness should be the same at all axial positions far from the ends after tube expansion, the radial position of the

maximum stress is of importance from a design standpoint. According to Figure3.6 , the maximum equivalent stress appeared to be at the tube inner surface when the die reached the point of interest. Its value was 370 MPa. Nevertheless, the outside surface was also at a similar stress level 350 MPa while the rest of the section had stress readings somewhere between these two values.

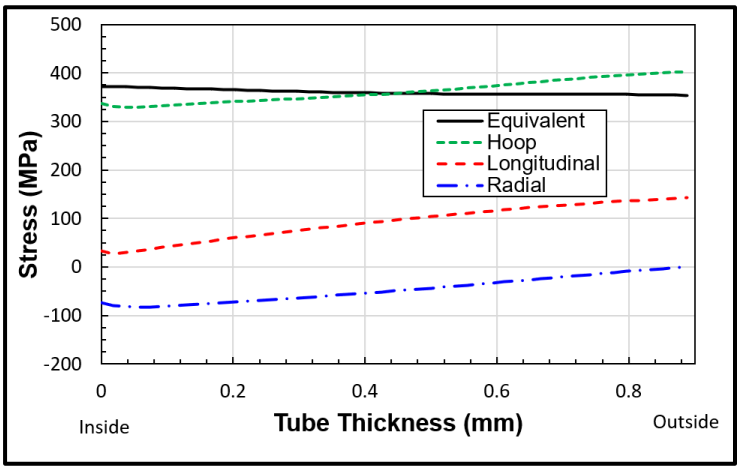

Figure 3.8 Stress distribution through thickness during expansion at the maximum equivalent stress position

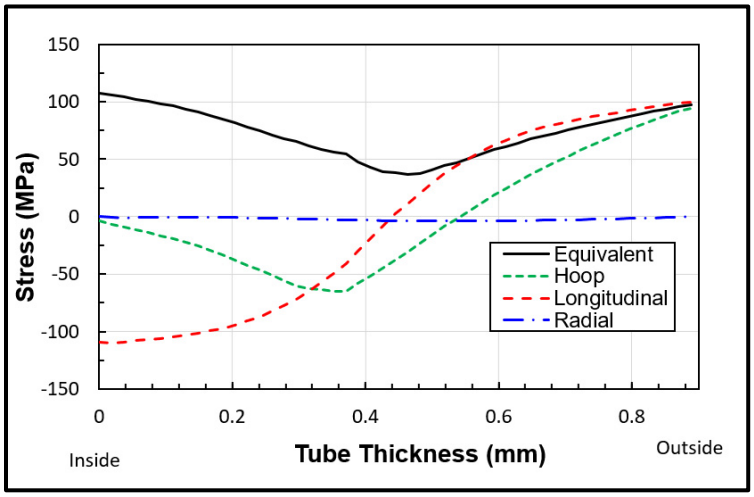

Figure 3.9 Residual stress distribution through thickness

Of importance are the residual stresses after the expansion process. Based on the results, the maximum residual stress was 105 MPa and was located on the inside of the tube as shown in Figure 3.9. The maximum stress was the longitudinal stress also located at the same position. The longitudinal and hoop stresses were in compression in the inner half of the tube diameter while they were in tension in the other half near the tube's outer diameter. The hoop and longitudinal stresses were equal and positive at the outer diameter. The net axial force should be zero as demonstrated by the distribution of the residual longitudinal stress across the thickness.

Friction effect

In practice, during the expansion process, the tube inner wall and die are lubricated with oil to reduce friction. As the main objective of the current study is to investigate the residual stresses in the tubes generated by die expansion, a suggested approximate value of the coefficient of friction of SS316L on M4 steel would suffice. Nevertheless, several values ranging from 0.25 to 0.4 were considered in the analysis to cover the range of possible variations. As expected, there was a small effect on the distribution of the residual stress across the tube thickness as illustrated in Figure 3.10. A maximum of about 10% residual stress decrease was observed at the inner diameter, where the stresses were higher.

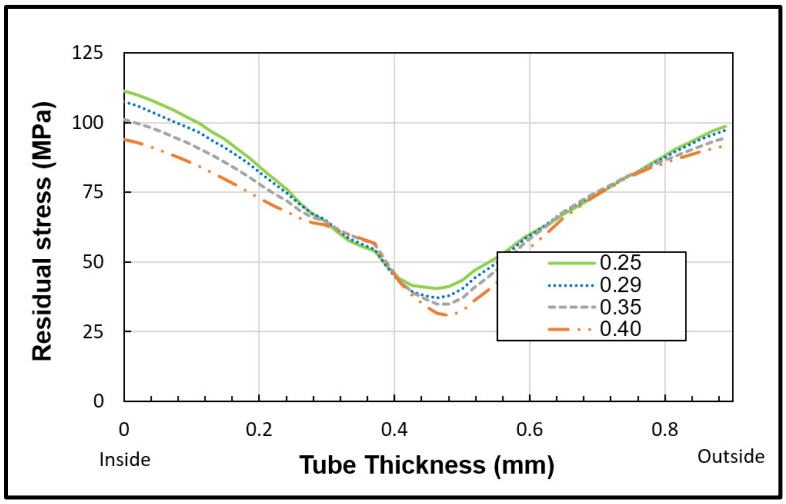

Figure 3.10 Effect of friction coefficient on residual stress

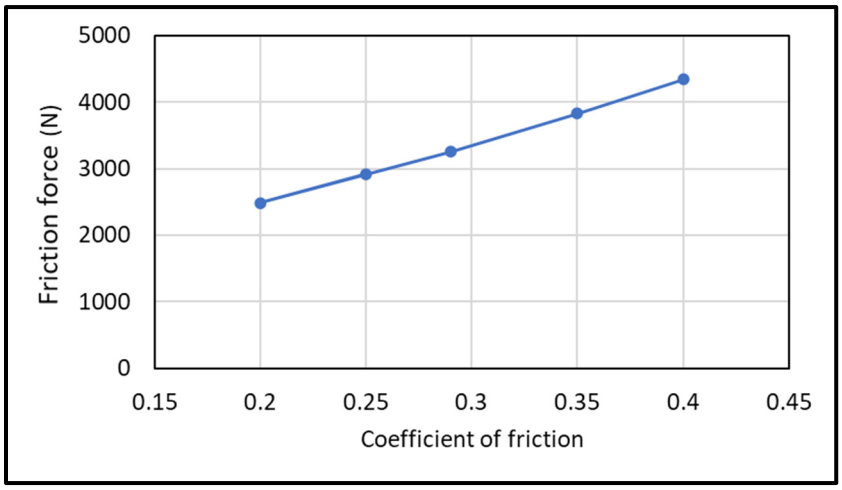

Figure 3.11 Effect of friction coefficient on the driving force

The tube expansion push force was not only affected by friction, but also the amount of energy required to expand the tube. Figure 3.11 shows, as is to be expected, a linear increase of the friction force as the coefficient of friction increased. The latter was difficult to determine by traditional friction tests in a cut circular tube and die configurations. However, using the tube expansion experimental data to calibrate this value proved simple and effective. As a result, a value of 0.29 was adopted to conduct the rest of the study.

Effect of reverse plasticity

The level and distribution of residual stress were highly affected by the plastic behavior of the tube material. In the previous section, the residual stress distribution was obtained by considering a kinematic hardening behavior. While the general trend with the isotropic hardening material modeling behavior was similar to the kinematic hardening behavior, the residual stress levels and distributions are much higher, as depicted in Figure 3.12. The maximum residual stress is around 400 MPa with isotropic hardening compared to 105 MPa with kinematic hardening.

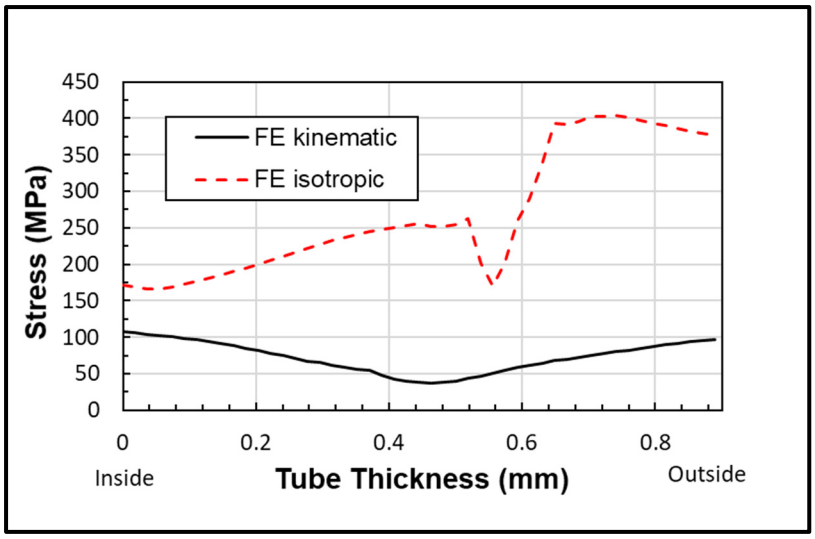

Figure 3.12 Residual stresses through tube thickness with kinematic and isotropic hardening

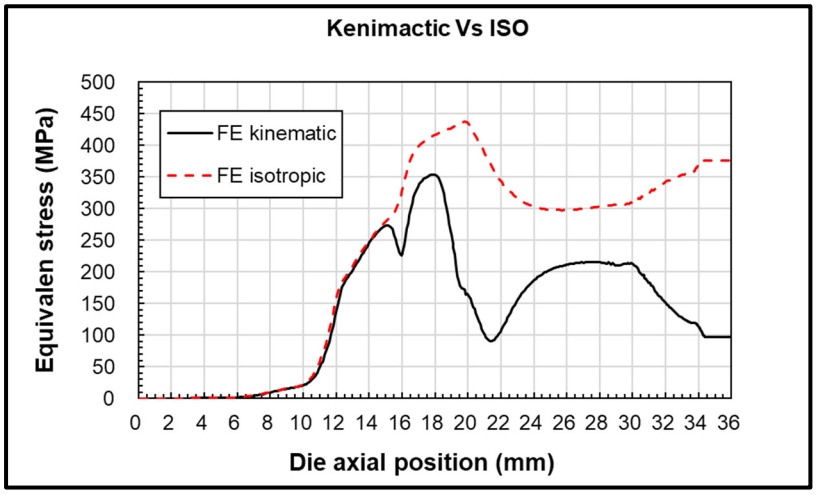

Figure 3.13 Equivalent stress change at the outside surface

Figure 3.13 shows the equivalent stress at the outside surface of the point of interest with both isotropic and kinematic behaviors. While the stresses were similar before the die reached the point of interest, which can be considered as a loading phase, the difference was marked when the die moved away from this point, which can be considered as the unloading phase. The resulting residual stresses were 380 and 105 MPa respectively, as shown by the end plateau.

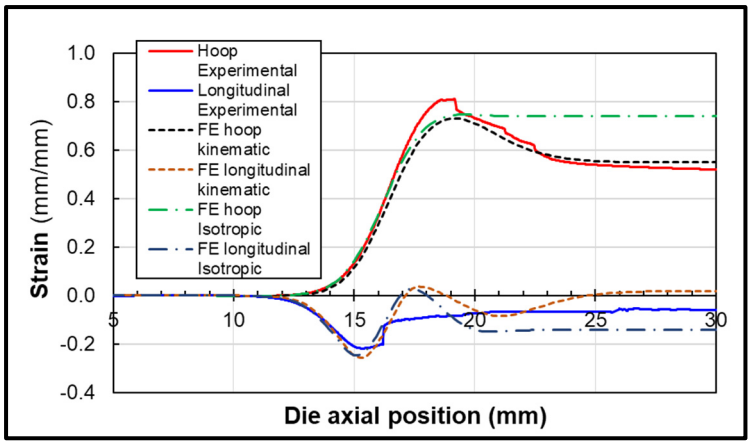

Figure 3.14 Longitudinal and hoop strain from experiment and simulation

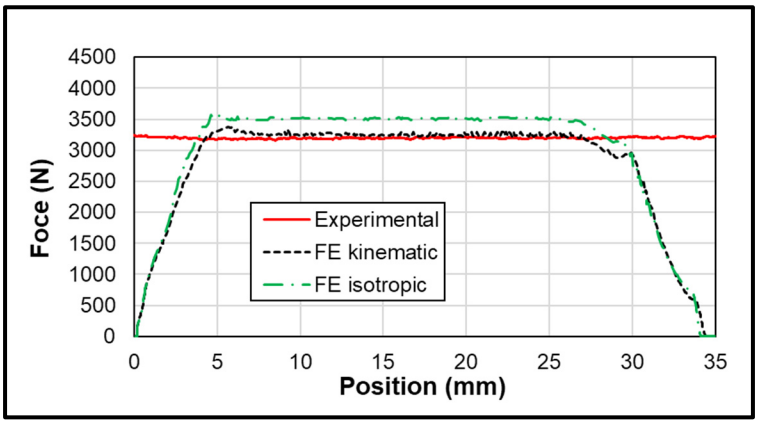

Figure 3.15 Push force applied to the die

The longitudinal and hoop strain variations caused by the die's movement at the outer surface with the two material hardening types were compared to the experimentally measured strains in Figure 3.14. Also, Figure 3.14 shows that the strains of both behaviors were superimposed during the loading phase. However, as expected the major difference between kinematic hardening and isotropic hardening was during the unloading phase or when the die passed the point of interest. The hoop and longitudinal strain differences between both materials were around 30 and 90% respectively. It is to be noted that the hoop strain of kinematic hardening matched closely the experiment indicating that the SS316L had a kinematic hardening behavior.

The push force was slightly higher for the isotropic hardening, as depicted in Figure 3.15**Erreur ! Source du renvoi introuvable.**, which plots it as a function of the die's displacement. There was a difference of just over 10% between the two behaviors and it was recorded in the simulation with a friction coefficient of 0.29. Based on the experimental results, the push force was around 3.2 kN, shown by a solid line. It should be noted that the end effects are not represented in the graph because the experimental tube is longer.

Die shape and size effect

The effect of the die shape and size on the residual stresses for the case of kinematic hardening was also investigated in this study. The oval-shaped die and the different spherical die diameters were compared in a FE simulation. Figure 3.16 shows the residual stress distribution across the tube thickness between an oval and spherical die having the same outside diameter. Based on Figure 3.16, the die shape did not change the overall residual stress distribution, but had an effect on the level of stress: a 10% increase at the inside and outside of the tube and a 25% decrease at the mid-thickness are depicted in the graphs between the oval and spherical shapes. The residual stress distribution across the thickness was less pronounced with the spherical dies and will be discussed in the following paragraph.

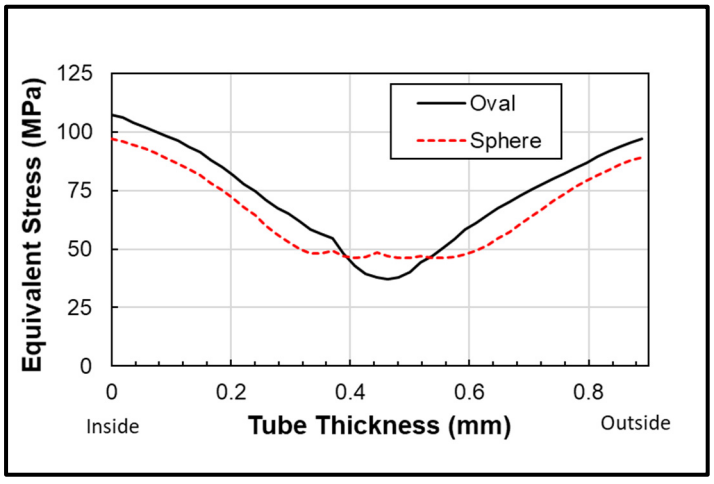

Figure 3.16 Residual stress with different die shapes

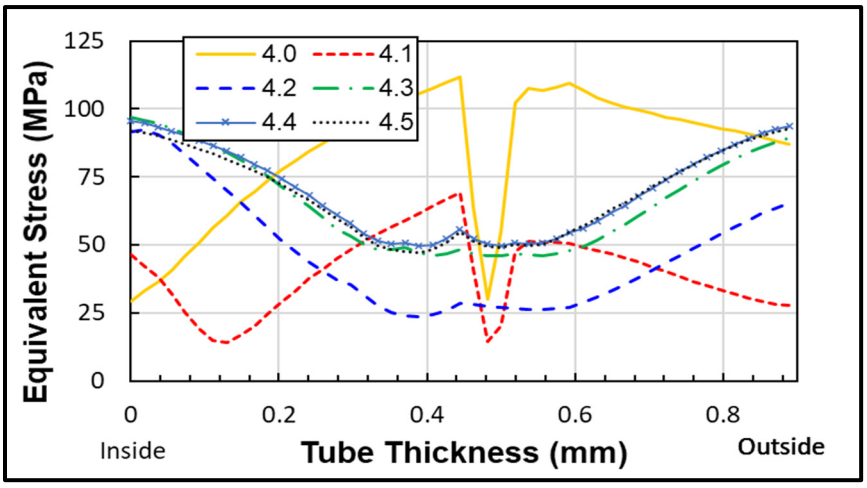

Figure 3.17 Residual stress distributions with different die radius

The residual stress distributions obtained when increasing the die diameters are shown in Figure 3.17. In general, the level of residual stress increased as the die-size diameter increased. While the higher die size was preferable to achieve a better fin to tube adhesion to increase heat transfer, the maximum stress levels may reach critical values during the expansion process or the residual stress after expansion when combined with those generated by pressure and temperature loading during operation. A compromise is required to find a balance between stresses and heat transfer.

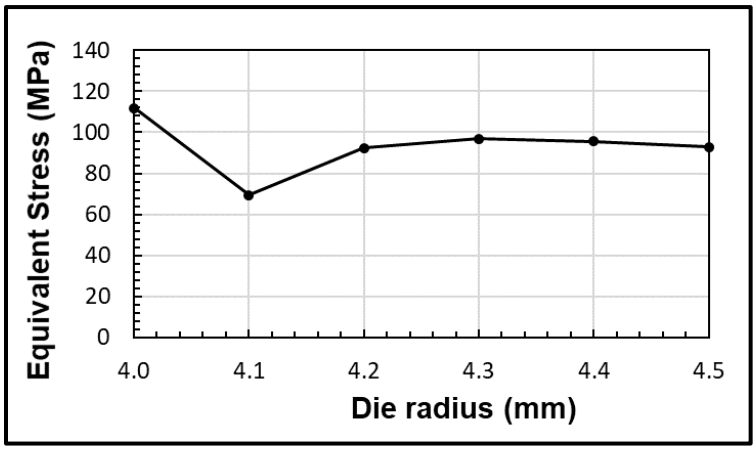

Figure 3.18 Maximum residual stress vs die radius

Figure 3.17 shows the residual stress distribution through the thickness and the maximum stress variation with all five die size diameters. The maximum residual stress was located at the mid-thickness location but moved away to the inner and outer surfaces of the tube as the die size increased. As shown in Figure 3.18, the maximum residual stress decreased and then increased as the die radius increased before stabilizing at about 100 MPa after a radius of 4.3 mm. Currently, work is underway to analyze the contact conditions between the tube and fin to improve adhesion and heat transfer performance. Optimum die size and clearance between the fin and tube are very important design parameters.

3.6 Conclusion

The stresses generated in the process of die expansion of SS316L tubes used in gas coolers were analyzed. The maximum stress during expansion combined the radial and longitudinal stresses at the inner surface of the tube with the equivalent stress not surpassing the UTS in all cases. However, at the outer surface, the hoop stress was the greatest. These findings were obtained at the die and tube contact location. The effect of the material reverse yielding behavior was highlighted. Under the isotropic hardening rule, the predicted residual stresses were much higher with the push force being about 10% higher compared to the kinematic hardening behavior. A comparison of the experimental data with the FE simulation suggested that SS316L had more of a kinematic hardening behavior. The strains and push force were in good agreement in this case.

Finally, the die size effect on the residual stresses was acknowledged. Under the kinematic hardening behavior, the residual stresses were shown to slightly fluctuate before stabilizing with the increase of the die radius. The stresses generated during the process and the residual stresses that remained after the expansion depended on the die size, and in general, the maximum stress was at the outer surface.

CHAPTER 4

A METHOD OF EVALUATING THE DRIVING FORCE AND STRESSES DURING TUBE DIE EXPANSION

Zijian Zhao [a], Abdel-Hakim Bouzid [b], Linbo Zhu [c]

[a] Ph. D. student, Mechanical Engineering Department, École de technologie supérieure, 1100 Notre-Dame St. West, Montreal, Quebec, H3C 1K3

[b] ASME Fellow, Professor, Mechanical Engineering Department, École de technologie supérieure, 1100 Notre-Dame St. West, Montreal, Quebec, H3C 1K3

[c] Professor, School of Chemical Engineering and Technology, Xi'an Jiaotong University, Xi'an 710049, PR China

Paper published in the Journal of Pressure Vessel Technology, January 2023.
(145(2):021304-9, DOI: 10.1115/1.4053877)

4.1 Abstract

In this study, an analytical approach based on the energy method is used to estimate the force required to expand tubes with different die shapes. The proposed method calculates the driving force using the energy of deformation and the energy produced by friction. The new approach greatly reduces the difficulty of the analysis and simplifies the calculation. The stress distribution in the transition zone is also estimated using an analytical approach based on a self-adaption of the stress strain curve.

The approach is validated using four different numerical axisymmetric finite element models with different size, materials and die shapes subjected to push and pull die expansion. Additionally, stainless steel and copper 3/8 in. tubes have been expanded with a prolate spheroid (oval) die in an experimental test bench under the two conditions of push and pull. The tangential and longitudinal strains and driving force are monitored and recorded during

the expansion process. Finally, the results from the three approaches show a very good agreement.

NOMENCLATURE

ε	Strain
ε_θ	Hoop strain
ε_y	yield strain
θ	Tube rotation angle, °
μ	Friction coefficient
ν	Poisson ratio
σ	Equivalent stress, MPa
σ_l	Longitudinal stress, MPa
σ_θ	Hoop stress, MPa
A	Section area of tube, mm²
$A_{\beta x}, B_{\beta x}, C_{\beta x}, D_{\beta x}$	Attenuation factors
E	Young's modulus, MPa
F	Driving force, N
K	Strain-hardening constant
ℓ	Length of tube, mm
M	Moment, Nmm/mm
m, n, q	Dimensionless parameters
n_o	strain-hardening exponent
N	Hoop membrane force, N/mm
Q	Edge load, N/mm
P	Shear force, N/mm
R	Radius of die, mm
R_C	Radius of die contact surface, mm
r	Inside radius of tube, mm
S_y	Yield stress, MPa

t Thickness of tube, mm

U Energy, J/mm³

V Volume , mm³

x Axial position, mm

y The radial displacement, mm

Subscripts

i refers to sub zone

c refers to contact position

4.2 Introduction

Tube forming is a mechanical process that involves plastic deformation of tubes. Expansion, reduction, die forming, bending and hydroforming are work hardening processes that generate residual stresses. Expansion tubular technology is widely used in the production of joint assemblies for heat exchangers, steam generators, boilers and other pressure vessels. The manufacturing of tube-to-tubesheet and tube-to-fin assemblies involves processes the control of which is often obtained by trial and error (Bouzid & Pourreza, 2019).

Die expansion of tubes creates not only high stresses when combined with operating stresses but also micro-cracks during expansions when the process is not well controlled. Studies on the elastic-plastic behavior and the developed stresses of tubes subjected to die expansion are rare and difficult to conduct experimentally because the measurement of stresses is not an easy task to achieve with current technologies. The stresses and deformations of expanded joint assemblies are often analyzed numerically using the finite element method and seldom analytically because of the complexity to model plastic deformation. In addition, the expansion-contraction process involves reverse yielding in most cases which makes the analysis cumbersome.

The general die expansion process is conducted with the diameter of the die larger than the inner diameter of the tube, and a considerable force is required to push the die inside the tube causing plastic deformation while generating residual stresses. The die referred to as a mandrel in some applications is made of harder material. Tube expansion forming is a traditional process and the research in this field has inspired the pressure vessel world decades ago. In 1960 Sawczuk and Hodge (1960) conducted a study to compare the yield conditions for circular cylindrical shells subjected to axially symmetric loading. Since then, several analytical, numerical and experimental studies were specifically conducted on tube expansion (Pearson, 2005; Pettersen et al., 1998; Ding Tang et al., 2009).

The affected portion of the tube during the expansion process is divided into three zones: the expansion, transition, and unexpanded zones. In the first two zones, the stresses exceed the yield stress of tube and therefore these zones should be paid more attention. Bouzid et al. (2016) propose a new analytical methodology which consists of dividing the expansion process into the loading phase and the unloading phase while considering the three zones. Different from the previous theoretical studies, Liu et al.(2016) developed a tube expansion theoretical model based on the energy dissipation theory.

Tube materials such as copper and nickel alloys are widely used in gas coolers, however, their capacity for high-pressure applications is limited. In fact, more rigid tubes made of stainless steel are considered as replacements because of the switch to the lower pollutant refrigerant like CO_2 requires higher pressure. In fact, due to global warming potential gases, the air conditioning refrigeration industry is focussing on the use of high strength steel to fabricate expanded finned tubes. Although die expansion process of steel tubes is similar to copper tubes, the related studies on the former only begin recently.

A study on tube thickness reduction in expansion forming with different die shapes are evaluated by Almeida et al. (2006) in 2005. Later in 2006, Alves et al. (2006) studied tube expansion numerically using 2D and 3D finite element models with aluminum alloys. Related tests were also conducted to support and validate the overall investigation. In the same way,

die expansion is also a forming process applied to plastic tubing. PVC tube expansion using a die was investigated by Alves et al.(2016). An analytical model based on the Hoop stress reaching yield to predict the push force applied to the expansion of a tube with a die using a rigid-linearly hardening model is provided in (Avalle et al., 2018).

An analytical model for estimating the stress change in an expanded tube-to-tubesheet joint based on a power law strain hardening is proposed by Bouzid et al. (2015). The effect of tube expansion on the residual stress distribution of SS316L tubing is also investigated numerically using FEM in our previous study (Zhao & Bouzid, 2020). In several studies, tube expansion with a conical die was investigated due to its simple geometry. The related parameters such as contact pressure, cone angle, and friction are considered in the developed models. However, the modeling of die expansion is complex when the die shape is curved. The contact pressure and contact area are difficult to estimate analytically and even with similar die shapes, these parameters change with the tube size and materials.

The simplified elastic-perfectly plastic and linear hardening behaviors were considered in most studies. The developed models based on these material behaviors led to deviations when compared to practical cases where true stress-strain behavior prevails. A self-adaption methodology is utilized in this study to determine the stresses and deformations in the tube transition zone. The driving expansion force is estimated based on the determination of the radial expansion force, the friction state, and the deformation energy.

4.3 Analytical approach

The expanded region of the tube is divided into three zones; the transition zone, the contact zone, and the residual stress zone as shown in

Figure 4.1. In the model, the position of beginning of the contact of the tube with the die and the radial expansion force are parameters required to estimate the stresses and the driving force. The analytical method uses a self-adaptive approach to assess the stress distribution of the tube in the transition zone.

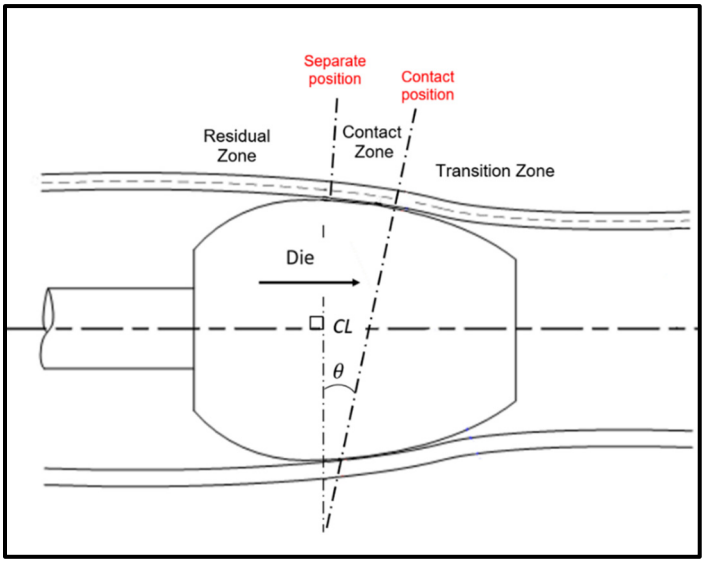

Figure 4.1 Different zones of the expanded tube

4.4 Stress distribution analysis

The limits between the three zones are as follows; the limit between the first two zones is the position of the beginning of the contact of the die and tube while the limit between contact and residual stress zones is the location of the beginning of the separation of the tube from the die. The developed analysis deals with the driving force and the stresses in the transition zone while the contact and residual zones will not be addressed in the following.

4.4.1 Contact zone

The die shapes such as spherical and ogive can be described in a cartesian coordinate system. The limit between the transition and the contact zones, shown in Figure 4.1, is the beginning of the contact, where the tube is considered tangent to the die surface. This location will be considered as the limit between the contact zone and the transition zone, therefore, the parameters considered for separation consist of the tube rotation angle (θ_c) and tube radial displacement (y_c) shown in Figure 4.2. These parameters are obtained for the different die shapes; Eq.(1a) for conical shape, Eq.(1b) for spherical die and Eq.(1c) for oval die.

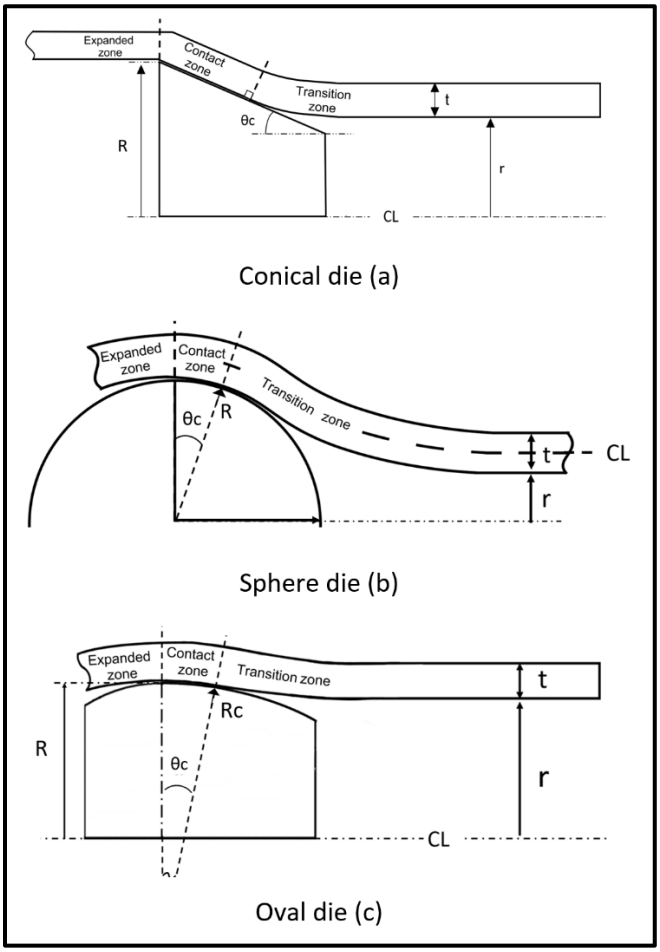

Figure 4.2 Different die shapes,
a) Conical die, b) Spherical and c) Oval

For a conical die, the contact zone is defined by the generator line and therefore only the cone apex angle is needed in Eq.(4.1a); at the contact position, the contact surface angle of the tube is equal to the apex angle and this angle is constant in the contact zone.

$$\theta_c = \alpha_c \tag{4.1a}$$

$$\mathrm{y_c} = R\cos\theta_c - r \tag{4.1b}$$

$$\mathrm{y_c} = R_c(\cos\theta_c - 1) - r + R \tag{4.1c}$$

Where y_c is the radial displacement of the tube and can also be obtained using beam on elastic foundation theory.

4.4.2 Analysis of the transition zone

From the previous study (Bouzid & Laghzale, 2016), it was revealed that the equivalent stress in the tube will reach and even surpass yield with a very small radial expansion causing strain harden of the tube to a certain extent before making contact with the die. Since the material may experience hardening during the process of expansion, its behavior can be approximated using the secant modulus during the loading process. Likewise, the self adaptive method is utilized to estimate the stresses. The transition zone is, therefore, divided into multiple unequal length sections each characterized by a radial displacement and a rotation angle as shown in Figure 4.3.

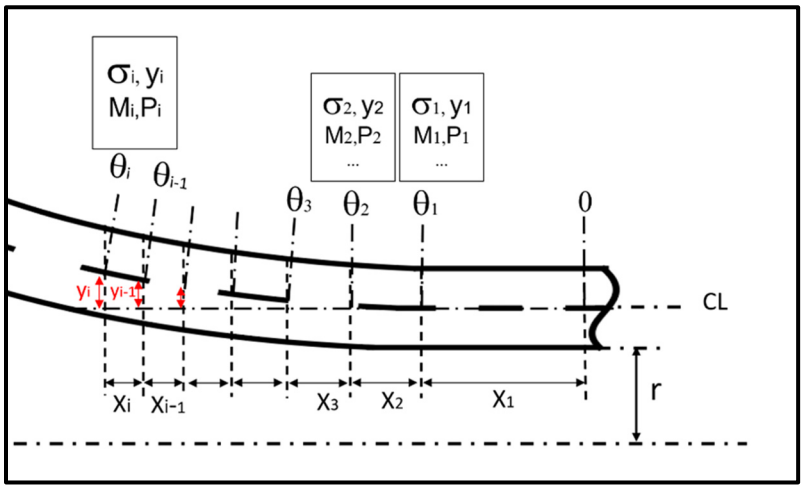

Figure 4.3 Subsections of the tube transition zone

While the tube rotation angle θ_c at the contact is tangent to the die surface and is equal to the apex angle α of the conical die, it is not known initially for the spherical and oval dies. Let the section rotation be incremented by $\Delta\theta$ and therefore:

$$\theta_i = \theta_{i-1} + \Delta\theta \tag{4.2}$$

The stress σ_i and the relevant secant modulus E_i of each section are obtained from the stress strain curve. An iterative process is used to obtain convergence for the rotation and displacement. This process is referred to as the self adaptive process and is used to estimate the stresses. The Von Misses effective stress and a power law strain hardening behavior are used; the material data of stainless steel and copper are generated based on the ASTM standards and the true curve is fitted with the non-linear hardening equation as follows:

$$\begin{aligned} \sigma &= E\,\varepsilon && for\ (\varepsilon \le \varepsilon_y) \\ \sigma &= \sigma_y + K\,(\varepsilon - \varepsilon_y)^{n_o} && for\ (\varepsilon > \varepsilon_y) \end{aligned} \tag{4.3}$$

where ε_y is the yield strain, K and n_o are the stain hardening constants of the Ludwik power law.

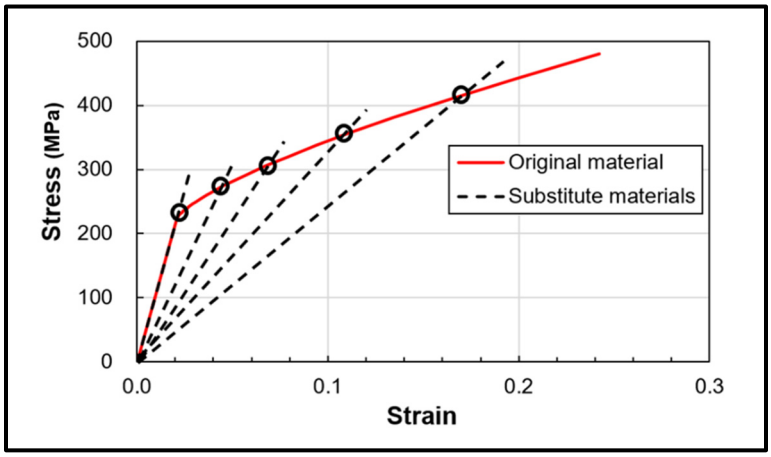

Figure 4.4 Simplified material behaviour

The stress condition for each section of the tube is that the equivalent stress is equal to the current stress σ_i. The secant modulus of the transition zone shown in Figure 4.4 is defined by Eq. (4.4).

$$\begin{aligned} E_i &= E && for\ (\varepsilon \le \varepsilon_y) \\ E_i &= \frac{\sigma_i}{\sqrt[n_o]{\frac{\sigma_i - S_y}{K}} + \varepsilon_y} && for\ (\varepsilon > \varepsilon_y) \end{aligned} \tag{4.4}$$

The beam on elastic foundation theory applied to cylinder is used to obtain the four following parameters; radial displacement, rotation, moment, and shear force (Grant & Bullock, 2005):

$$y_i = \frac{2\,P_i\beta_i}{k_i}\,D_{\beta x} + \frac{2\,M_i\beta_i^2}{k_i}\,C_{\beta x} \tag{4.5}$$

$$\theta_i = \frac{2P_i\beta_i^2}{k_i}\,A_{\beta x} + \frac{4M_i\beta_i^3}{k_i}\,D_{\beta x} \tag{4.6}$$

$$M_i = \frac{P_i}{\beta_i}\,B_{\beta x} + M_i\,A_{\beta x} \tag{4.7}$$

$$P_i = P_i\,C_{\beta x} + 2\beta_i M_i\,A_{\beta x} \tag{4.8}$$

Where

$$\beta_i = \frac{\sqrt[4]{3(1-\nu^2)}}{\sqrt{rt}}, \qquad k_i = \frac{E_i t}{r^2} \tag{4.9}$$

And the influence coefficients are given by

$$\begin{aligned} A_{\beta x} &= e^{-\beta x}(\cos\beta x + \sin\beta x) \\ B_{\beta x} &= e^{-\beta x}\sin\beta x \\ C_{\beta x} &= e^{-\beta x}(\cos\beta x - \sin\beta x) \\ D_{\beta x} &= e^{-\beta x}\cos\beta x \end{aligned} \tag{4.10}$$

The longitudinal and tangential stresses can then be evaluated based on the edge loads P_i and M_i on each section such that:

$$\sigma_{li} = \pm\frac{6\,M_i}{t^2} \tag{4.11}$$

$$\sigma_{\theta i} = \frac{6\,\nu\,M_i}{t^2} + \frac{E_i y}{r} \tag{4.12}$$

$$\sigma_i = \sqrt{{\sigma_{li}}^2 + {\sigma_{\theta i}}^2 - \sigma_{li}\sigma_{\theta i}} \tag{4.13}$$

In the case of thin tubes, to simplify the analysis the stresses are averaged through the thickness. In each section, the beam on elastic foundation theory is used in two steps; in the first step it is utilized to calculate the stresses in section i with its conditions at the end and then in the following step with the information obtained from the previous step with the condition from the previous zone to calculate the size of this zone x_i as shown in Figure 4.3. The process is shown in the diagram of Figure 4.5. Therefore, this simple approach provides an estimate of the stress distribution in the transition zone.

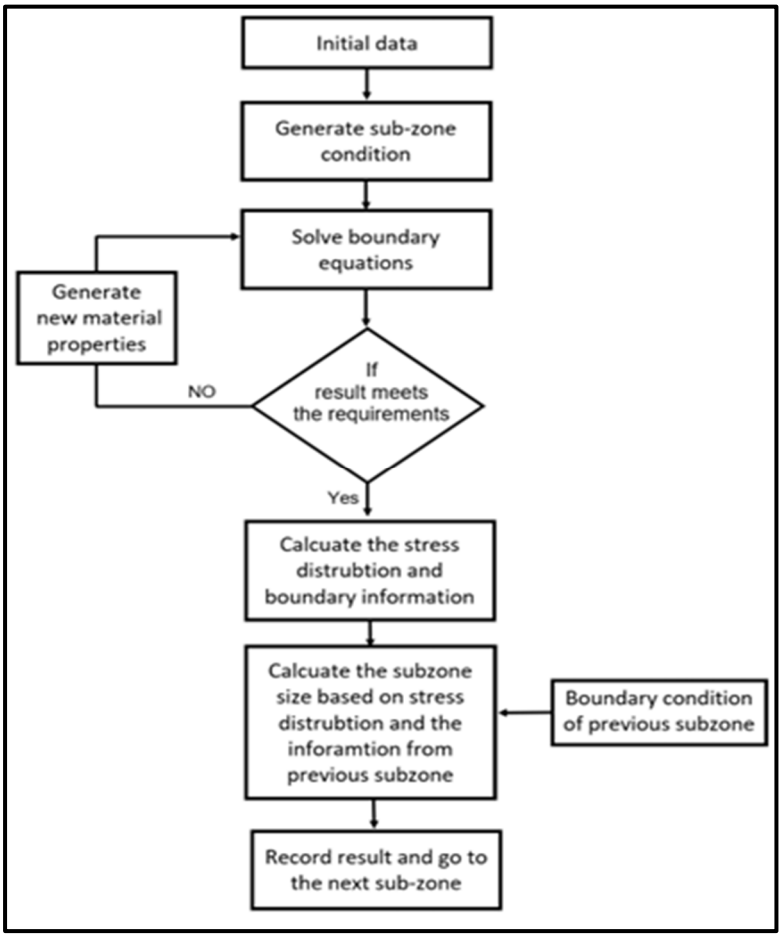

Figure 4.5 Flowchart to evaluate stresses in transition zone

4.5 Driving force prediction

The driving force prediction can be obtained from the strain energy and friction concepts. The total energy (U_t) required to expand a tube is considered of two parts. The first part is the strain

energy (U_d) required to plastically deform the tube to reach a radial displacement y. The second part is the friction energy (U_f) which is generated by the friction force at the interface between the die and tube and dissipates as heat. Therefore,

$$U_t = U_m + U_f \tag{4.15}$$

In the tube expansion process, the die moving speed is relatively low and the contact surfaces are lubricated. The die speed is 2mm/s in the numerical simulation and experiments, and the temperature change is relatively small.

4.5.1 Strain energy U_m

The strain energy required to expand a tube of length ℓ and surface A to plastically deform by a strain ε_a and expand to a radial displacement y is given by,

$$U_m = A\ell \int_0^{\varepsilon_a} \sigma \, d\varepsilon \tag{4.16}$$

Considering the elastic and plastic regions gives

$$U_m = A\ell \int_0^{\varepsilon_y} E\varepsilon \, d\varepsilon + A\ell \int_{\varepsilon_y}^{\varepsilon_a} \left(S_y + K\left(\varepsilon - \varepsilon_y\right)^{n_o}\right) d\varepsilon \tag{4.17}$$

Where ε_y is the yield strain and is given by σ_y/E; the total strain energy is therefore

$$U_m = A\ell \left[\frac{1}{2}\frac{{S_y}^2}{E} + S_y\left(\varepsilon_a - \frac{S_y}{E}\right) + \frac{K}{(n_o+1)}\left(\varepsilon_a - \frac{S_y}{E}\right)^{n_o+1}\right] \tag{4.18}$$

The Hoop strain is obtained by considering the maximum radial displacement y_m given by:

$$\varepsilon_\theta = \frac{y_m}{r} = \frac{R-r}{r} = \frac{R}{r} - 1 \tag{4.19}$$

Considering there is no volume change during the plastic deformation $\varepsilon_\theta + \varepsilon_r + \varepsilon_l = 0$ and assuming the radial strain equal to the longitudinal strain

$$\varepsilon_r = \varepsilon_l = -\frac{\varepsilon_\theta}{2} = \frac{1}{2} - \frac{R}{2r} \tag{4.20}$$

Where R is the maximum radius of the die whether conical, oval or spherical and r the tube radius. The total equivalent strain ε_a is therefore given by:

$$\varepsilon_a = \frac{\sqrt{2}}{3}\sqrt{(\varepsilon_\theta - \varepsilon_r)^2 + (\varepsilon_\theta - \varepsilon_l)^2 + (\varepsilon_l - \varepsilon_r)^2} \tag{4.21}$$

Substituting for the strains of Eqs. (4.19) and (4.20) into Eq. (4.21) gives the equivalent strain ε_a:

$$\varepsilon_a = \varepsilon_\theta = \frac{R}{r} - 1 \tag{4.22}$$

4.5.2 friction energy U_f

In order to determine the friction energy, the normal force per unit circumference to expand the tube using a die till reaching plasticity needs to be found. The simplified model suggests with the yield condition for a cylindrical shell subjected to axially symmetric loading proposed by Sawczuk and Hodge (1960) is adopted. The tube shell is assumed to be homogeneous having a rigid perfectly plastic behavior. Figure 4.6 shows the loading within a tube of infinite length. The pressure is assumed to act as a ring load or a force per unit circumference. Once the tube is expanded under the applied force, a region delimited by x_1 from each side of the force is assumed to be fully plastic.

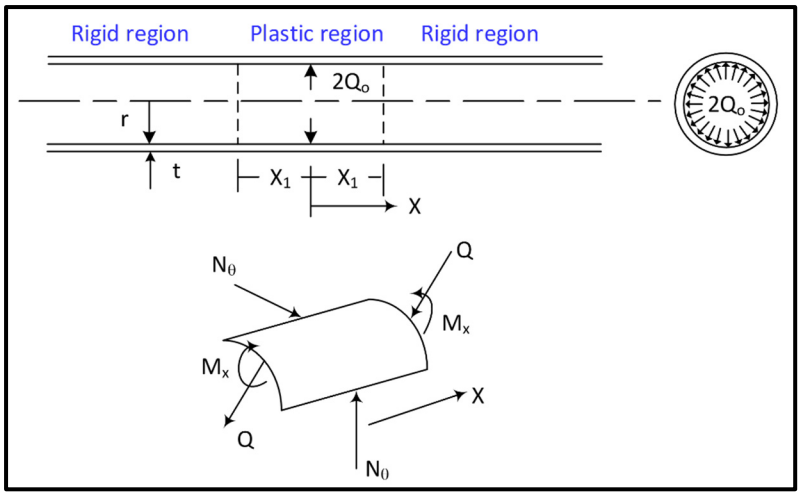

Figure 4.6 Tube element with forces and moments

The problem is introduced by various parameters, which are well known as the basic equations in plastic analysis of cylindrical shells. The definitions of these parameters are in dimensionless form as follows:

$$n = \frac{N_\theta}{N_0} \tag{4.23}$$

$$m = \frac{M_x}{M_0} \tag{4.24}$$

$$q = \sqrt{\frac{r}{2M_0N_0}}Q_0 \tag{4.25}$$

$$x = \sqrt{\frac{2N_0}{rM_0}}X \tag{4.26}$$

$$N_o = tS_y \tag{4.27}$$

$$M_o = \frac{t^2S_y}{4} \tag{4.28}$$

Where M_o and Q_o are the edge loads at the junction between the expansion and transition zones of the tube and N_θ, M_x and X are the hoop membrane force, longitudinal moment, and axial position, S_y is the tube yield stress and R and t are the radius and thickness of the tube.

In the above equations, zero indexes stand for the limit between the expansion zone and the transition zone. The assumed rigid perfectly plastic tube shell behavior is defined by two equilibrium equations and an interactive curve based on the flow rule (Sawczuk & Hodge Jr, 1960). In case of no existence of distributed surface loads, the equilibrium equations are given as following:

$$q' + n = 0 \tag{4.29}$$

$$m = q \tag{4.30}$$

Where the dash is the derivative with respect to the distance x. The plastic boundary conditions are $q = q_0$ and $m' = 0$ at $x = 0$ and $m' = 0$ and $w = 0$ at $x = x_1$

Assuming the plastic flow takes place according to the plastic potential flow law, and the effect of radial and shear stresses in plastic yielding is negligible, the description of the plastic behavior of the tube is defined in terms of m and n' for a Von Mises uniform shell. Therefore, one can derive the corresponding interaction curve in terms of n and m by introducing a new parameter p so that $0 \leq p \leq \pi$ and $dm'/dp \geq 0$:

$$n = \pm \tan p \ \log \tan\left(\frac{p}{2}\right) \tag{4.31}$$

$$m = \pm\left(\frac{2}{\sqrt{3}}\right)\left[\tan^2 p \log \tan\left(\frac{p}{2}\right) + \sec p\right] \tag{4.32}$$

Substituting equations (4.32) and (4.33) into Eqs. (4.29) and (4.30) leads to:

$$q^2 = q_0^2 - 2\int_{p_0}^{p} n(dm/dp)dp \tag{4.33}$$

Once the radial expansion force $Q_0$is obtained according to Eqs. (4.25) and (4.33) replacing yield by the maximum equivalent stress obtained with ε_a to correct for strain hardening, the friction force is given by:

$$F_f = 4\,\mu\pi r Q_0 \tag{4.34}$$

The energy produced by friction over a length of the tube ℓ is given by

$$U_f = F_f\,\ell \tag{4.35}$$

The driving expansion force F is given by considering the energy balance over the distance d such that the energy balance is respected:

$$F\,\ell = U_m + U_f \tag{4.36}$$

Substituting for U_f, U_m and F_f from Eqs. (4.18), (4.34) and (4.35) into Eq. (4.36) gives the driving force as:

$$F = 4\,\mu\pi r Q_0 + A\ell\left[\frac{1}{2}\frac{S_y}{E}^2 + S_y\left(\varepsilon_a - \frac{S_y}{E}\right) + \frac{K}{(n_o+1)}\left(\varepsilon_a - \frac{S_y}{E}\right)^{n_o+1}\right] \tag{4.37}$$

4.6 Numerical model

In this study, the finite element analysis is conducted on Ansys workbench 2019R1. Three types of dies and four tubes with different sizes and materials were analyzed to validate the analytical approach. The three die shapes are conical, spherical, and oval and are shown as in Figure 4.2. Their dimensions and those of the tubes are given in Table 4.1 and their materials are given in Table 4.2. Three types of materials are used: normal copper, copper C122 (050), and stainless steel (SS 316L). The copper tubes are extensively used in the manufacture of low-pressure gas cooled exchangers, and the stainless steel is to accommodate the use of the preferred refrigerant CO_2 that requires high pressure.

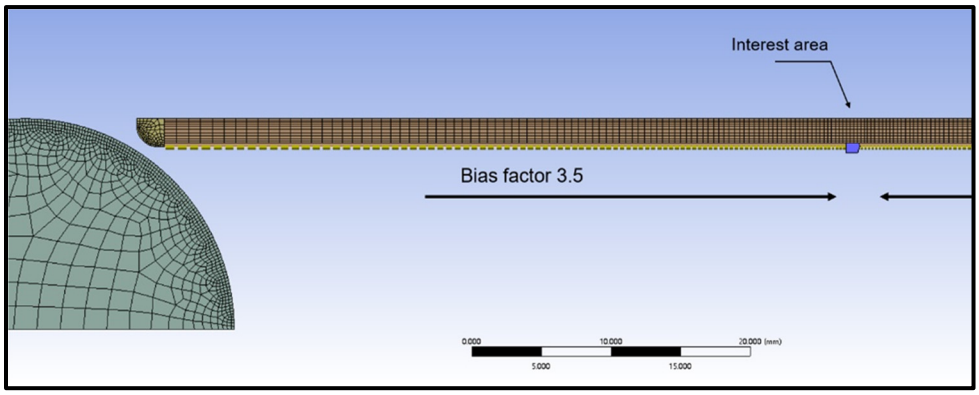

Figure 4.7 Finite element mode

Table 4.1 Dimensions of tubes and dies

Dies (M4)			
	Conical	Sphere	Oval
R (mm)	12	15	4.32
α_c (deg.)	20	-	-
Rc (mm)	-	-	15
Tubes			
Material	Copper Nickel (BFe10-1-1)	Copper Nickel (BFe10-1-1)	Copper (C122) & Steel (316L)
Ri (mm)	10	13	3.8735
t (mm)	0.9	2	0.889

The fitted stress-strain curves follow the Ludwick material plastic behavior, the hardening constants of which are given in Table 4.2 (Zhao & Bouzid, 2021; Zhao, Bouzid, & Laghzale, 2022). The multilinear kinematic strain hardening behavior option is used in the simulations. Since the tube expansion process is an axisymmetric problem where the geometry and loading do not vary with the angle, the 2D axisymmetric method is utilized for the analysis. This reduces the calculation consumption. The tube mid-length position throughout the whole thickness is selected for observation. The tube is sufficiently long so that there is no end effect on this position and in particular when the die travels half of the tube length. The tube lengths

of 70 mm, 100 mm, and 35 mm namely for the 21.8 mm, 30 mm and 3/8 in. tubes respectively were found to be sufficient. As shown in Figure 4.7, the tube and the area around the die in contact with the tube are refined to obtain accurate stress results. There are 9468, 8967, and 6893 PLANE183 elements used in the three types of die cases separately. Similar models have been used successfully in previous studies (Zhao & Bouzid, 2021; Zhao et al., 2022).

Table 4.2 Material properties

	Tube 21.8 x 0.9 mm & Tube 30 x 2 mm	Tube 3/8 x 0.035 in		Die
Property	Copper Nickel (BFe10-1-1)	Copper (C122)	S. Steel 316L	Steel M4
E (GPa)	140	112	206	214
ν	0.3	0.3	0.25	0.29
S_y (MPa)	123	69	175	800
K (MPa)	772	455	800	-
n	0.73	0.68	0.575	-
μ (friction)	0.2	0.28	0.29	

In practice, during the expansion process, the tube inside wall and die are lubricated with oil to reduce the friction force. Friction coefficients of 0.2 to 0.29 between the tube and die were adopted in the analysis. The die travels inside the tube from one end to the other. With all tubes, the pull and push cases were simulated. The dies are made to move with a constant speed of 2 mm/s which is reasonable according to the literature (M. Alves et al., 2006). This speed is also used in the experiment.

4.7 Experimental testing

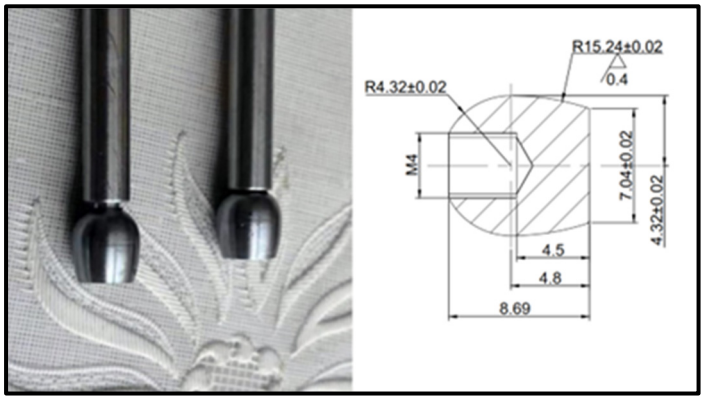

Figure 4.8 Oval dies used in the experiment

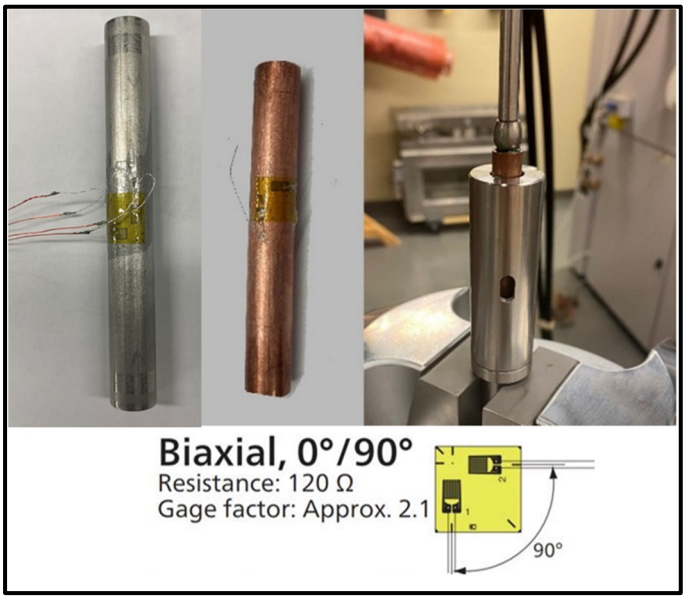

Figure 4.9 Expansion test workbench with SS316L
and C122 3/8 in. tube samples and biaxial strain gage

As a mean of validation, experimental tests are also conducted on the 3/8 in. SS316 and copper C122 tubes. The tubes are expanded with the oval die on a test workbench that uses a hydraulic tensile/compression MTS machine. The die with the rod shown in Figure 4.8 is fixed to the upper grip while the tube guide is fixed to the lower grip of the MTS machine. The tube guide

shown in Figure 4.9 is specially designed for the expansion of 3/8 in. tubes. The tube is restrained by the guide at either the top or the bottom depending on the push or pull case. The instrumented strain gaged tubes shown in the same figure are inserted inside the guide to be expanded. To monitor the axial and Hoop strain of the tube during the expansion process, a tee rosette is bounded to the tube external surface. This specific strain gage of 2 mm width allows up to 15% strain. The longitudinal and Hoop strains are continuously monitored through a quarter bridge configuration as the die moves inside the tube. The driving force, axial and Hoop strains, and time are monitored and recorded at regular intervals.

4.8 Result and discussion

This study proposes an analytical method to evaluate the driving force of the die during the tube expansion process and the stress distribution in the transition zone. To validate its performance, the analytical results are compared with those obtained from the numerical FE models and experimentation. The four expanded tubes are 21.8 mm 30 mm and 3/8 in used respectively with conical, spherical, and oval die shapes. Figure 4.10 illustrates the simulations with the three dies. The maximum equivalent stresses found in these cases are 356 MPa, 294 MPa, and 378 MPa and are way beyond the yield stress. More details will be given for each case separately.

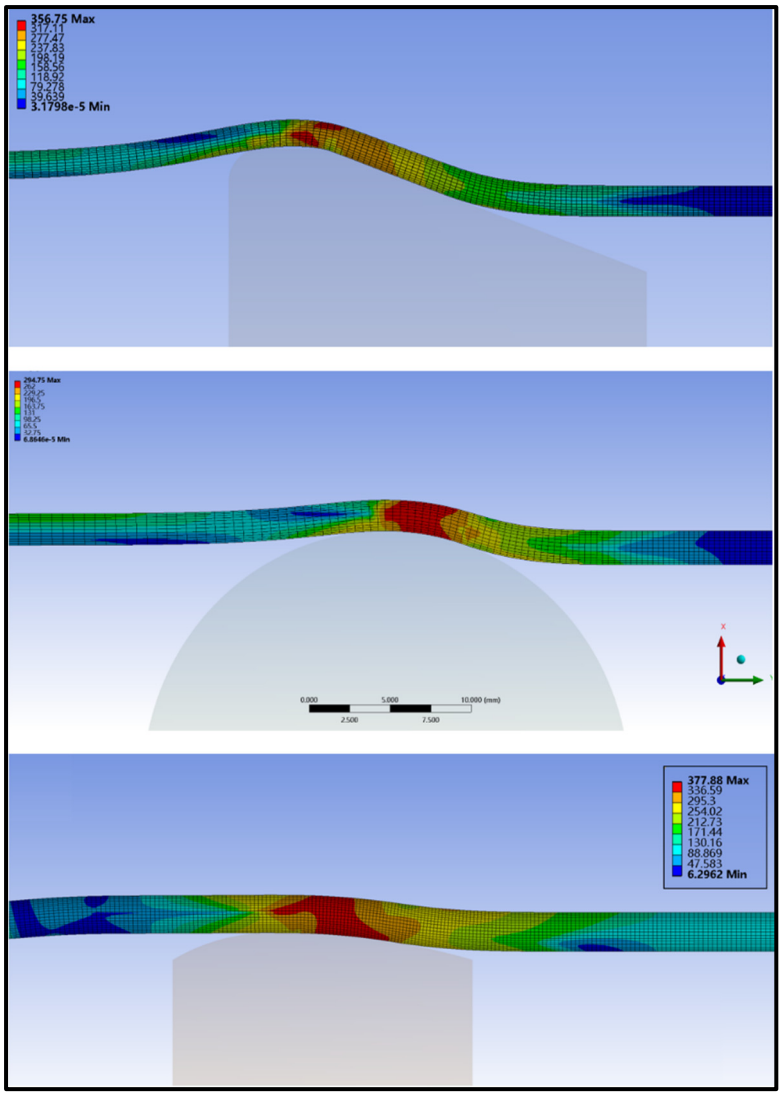

Figure 4.10 FE simulations with different dies showing the equivalent stress in the tubes

4.8.1 Case 1: 21.8 mm Copper Nickel Tube with Conical Die

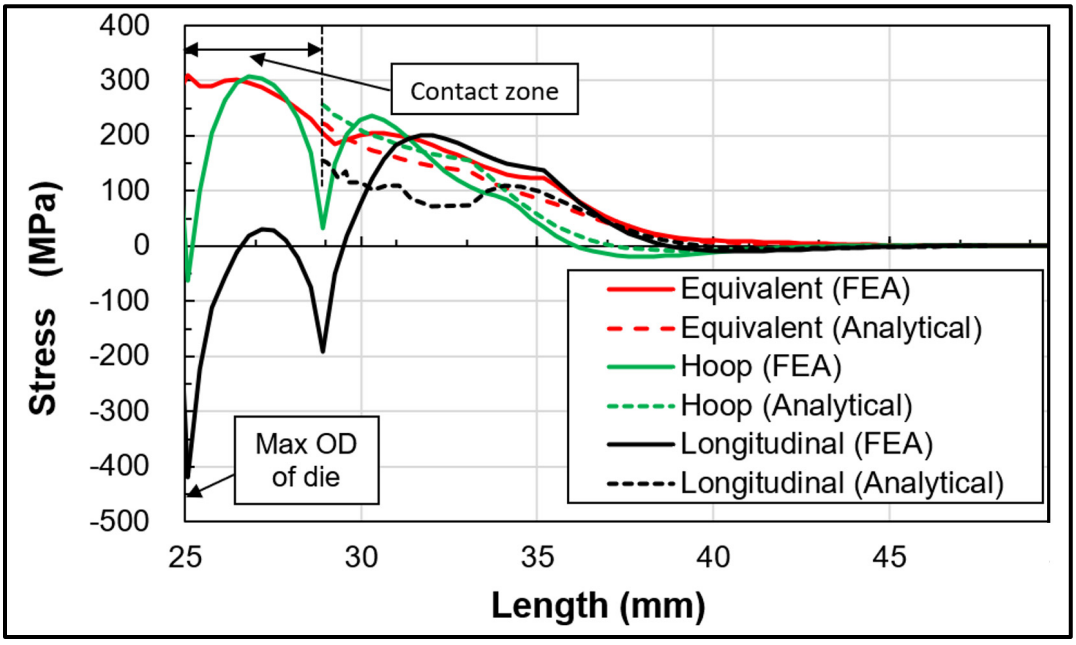

Figure 4.11 Stress distribution at ID of 21.8 mm copper nickel tube with conical die

Figure 4.11 shows the stresses of the numerical and analytical models during the expansion process. Both methods are in good agreement in predicting the contact position and to a lesser extent the stress distributions. From the numerical results, the contact surface can be easily identified and is limited between the sudden change in the stress distribution curves due to the contact pressure. The start of the yield position and the beginning of the contract are accurately estimated by the model. The equivalent stress distributions in the transition zone of the analytical approach agree relatively well with the numerical method in comparison with other stresses. While the radial, longitudinal and equivalent stresses are rather high at the point of maximum deformation the hoop stress is rather low as observed with FEM. The driving force with different support conditions is compared in Table 4.3. The result shows a good agreement in the case of the push force.

4.8.2 Case 2: 30mm Copper Nickel Tube with Spherical Die

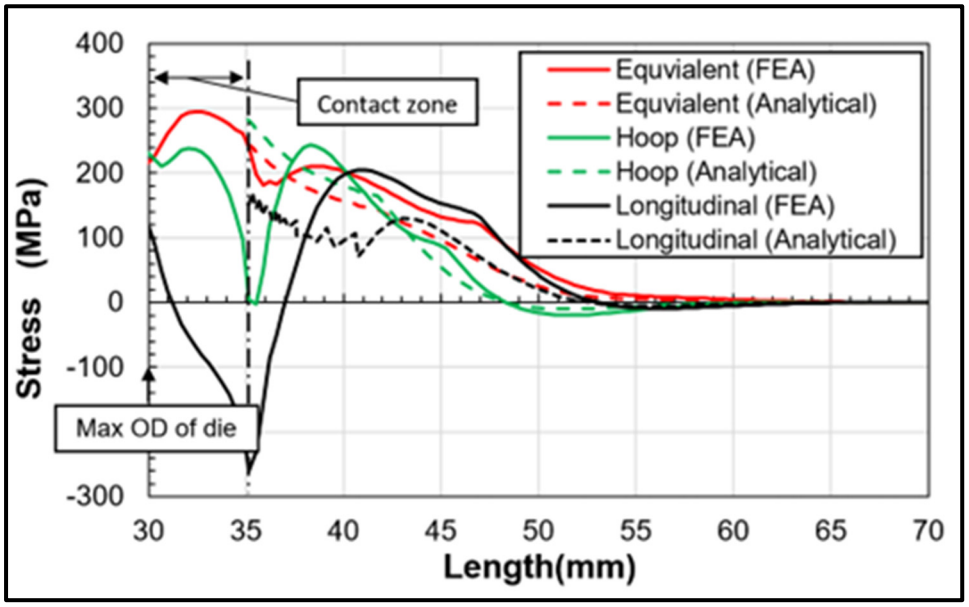

Figure 4.12 Inner stress distribution of 30 mm copper nickel tube with spherical die

The results of the spherical die with 30 mm tube expansion are shown in Figure 4.12. Again, the analytical model gives a good estimate of the limiting boundary of the transition zone. The stress distributions at the inner surface from analytical and numerical results are shown for comparison in the same figure. There is an important stress sign change at the end of the transition zone and the beginning of the contact zone. Nevertheless, it is clear from the FE results that the position of maximum stress is just before the maximum outer diameter of the spherical die. The estimated results of the driving forces shown in Table 4.3 shows once again that the analytical model gives a value close to the FEM under the push condition.

4.8.3 Case 3: 3/8 in. Stainless Steel Tube with Oval Die

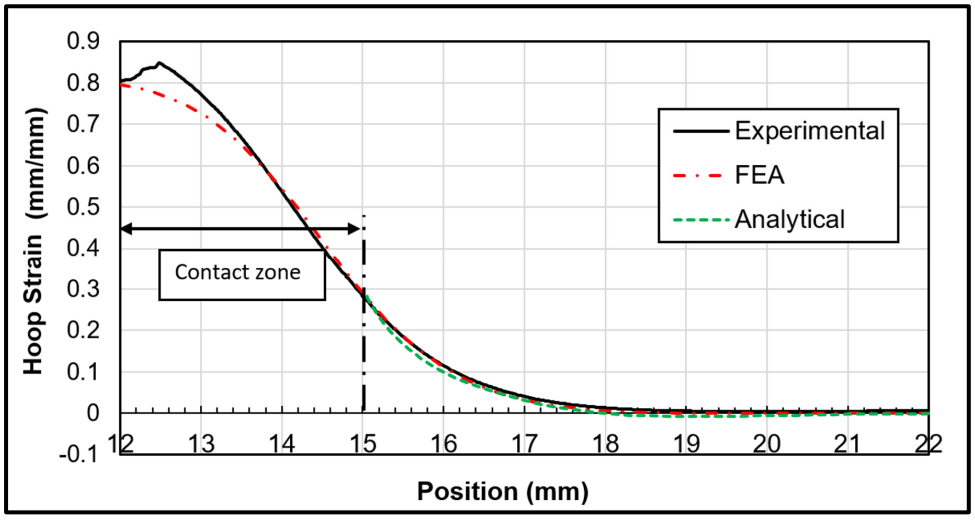

Figure 4.13 Hoop strain at OD. of 3/8 in. SS316L tube with oval die

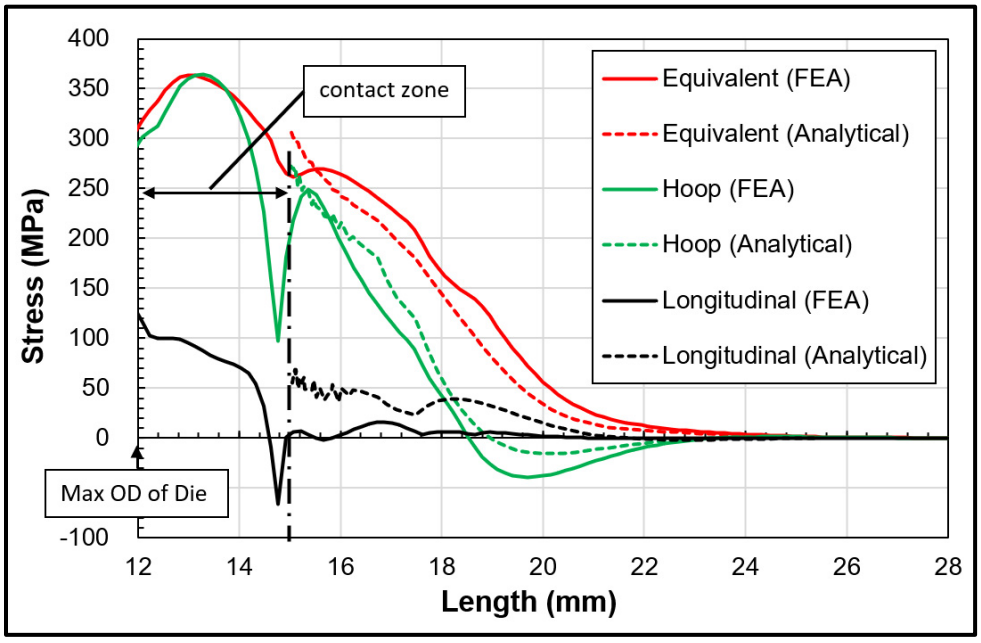

Figure 4.14 Average stress distributions across thickness of 3/8 in. SS316L tube with oval die

Although the 3/8 in. gage 20 tube is widely used in small cooling systems, the thin shell theory is less appropriate to use because of the high radius to thickness ratio of 4.35. However, the analytical approach still gives a fairly good estimate of the transition zone and the equivalent stresses. Figure 4.15 shows the radial displacement results from the experiment, numerical and analytical methods. The analytical and FEM predictions are in good agreement with the test results. Figure 4.14 shows that the contact position found with the analytical approach is close to that predicted by FE analysis. The analytical and numerical stress distributions are averaged across the thickness. It would appear that, due to the impact of the high radius to thickness ratio, the analytical stress distributions are slightly different than their FEM counterparts. The stress variations across the thickness of the thick tube becomes important and averaging the stresses through the thickness of the tube does not give a good estimate and, in particular, the longitudinal stresses.

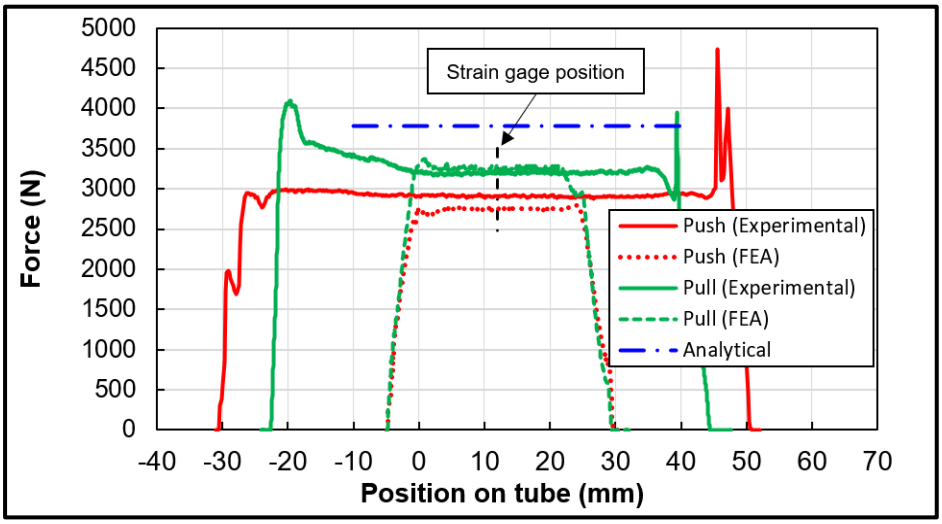

Figure 4.15 Die driving force as a function of traveling distance inside SS316L tube

Figure 4.15 shows the die driving force as a function of the die movement inside the tube. The push force is shown to be higher for both the experimental and numerical methods. The force increases as the die starts entering the tube and then stabilizes to a certain value. The peak values are due to the edge effects. In general, the results of the FE method are in a good

agreement with the experimental approach. The analytical results agree better with the push condition. Table 4.3 show the results for all cases and are given at the strain gage position.

4.8.4 Case 4: 3/8 in. Copper C122 Tube with Oval Die

The Copper Nickel 3/8 in. gage 20 tube is also expanded by the oval die of the same size for comparison with SS316L. Figure 4.16 compares the equivalent stress of the analytical method to that of the FE numerical one. While the results are comparable, the general trend of the curve is similar to that of SS316L and all other cases in general which gives confidence in the methodology.

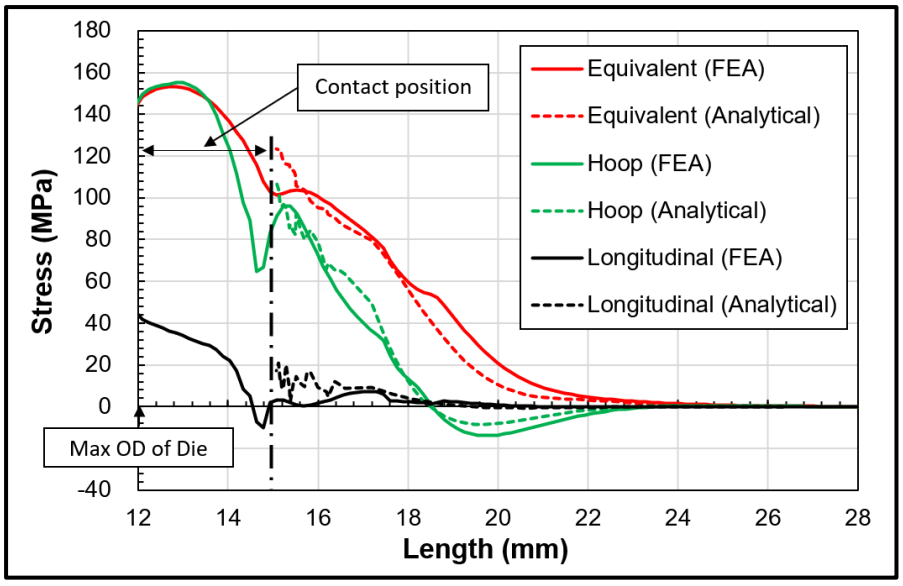

Figure 4.16 Average stress distributions across thickness of 3/8 in. C122 tube with oval die

In the push test, the copper tube experiences a slight bending during the expansion process. It is suspected that the axis of the die was not in line with that of the tube. The bending makes the driving force decrease because its magnitude decreases as the die advances inside the tube. However, the force level becomes stable as the die approaches the tube middle position where the strain gage is bounded. Table 4.3 shows the results obtained from three different

approaches. Once again, the results between all methods compare well with each other with the analytical method giving a slightly higher value due to the thin shell hypothesis.

Finally, based on the results from the four treated cases, it can be deduced that this analytical method offers a good alternative to FEM to estimate the stresses in the transition zone and the driving force in tube die expansion. The method is applicable to cases with different die shapes and tube materials while it does not differentiate between the push and pull conditions for the estimation of the die friction force. The accurate determination of the radial expansion force is a key factor in the evaluation of the driving force. While the methodology is based on a rigid perfectly plastic model, the results underestimate this force. In addition, the radial force requires to expand an axially loaded tube is smaller which results in lower friction force. Consequently, a lower driving force is required for the push condition as can be noted from. From a stress comparison perspective, it can be concluded that the developed simple model can be used to assess the integrity of tube expansion while providing a good estimate of the driving force.

Table 4.3 Die driving force (N)

Tube size	BFe10-1-1, 21.8x 0.9 mm		BFe10-1-1 30 x 2 mm		SS316L 3/8 x 1/16 inch		C122 3/8 x 1/16 inch	
Die shape	Conical		spherical		Oval		Oval	
	Pull	Push	Pull	Push	Pull	Push	Pull	Push
Analytical	5198		13377		3787		1585	
FEA	6120	5490	14900	12300	3308	2748	1330	1080
Experimental	-	-	-	-	3244	2890	1248	1105

4.9 Conclusion

An analytical approach capable of estimating the stresses in the transition zone and driving force during the process tube expansion is developed. The good agreement between the results from the three different methods namely analytical, numerical and experimental indicates that the simple developed approach is reliable. It can also be concluded that the theory of beams on

elastic foundation with self-adaption material modulus can be applied in the elastoplastic transition zone.

The approach was successfully used with different materials and die shapes although it is limited to the thin tube under small to moderate plastic expansion. The driving force is obtained by considering the friction force obtained by the radial expansion force the calculation of which is based on a rigid perfectly plastic behavior which underestimated its value. Nevertheless, the simple analytical methodology can assess the integrity of expanded tube and give a good estimate of the driving force.

CHAPTER 5

STRESS ANALYSIS OF TUBES DURING DIE EXPANSION PROCESS

Zijian Zhao [a], Abdel-Hakim Bouzid [b]

[a] Ph. D. student, Mechanical Engineering Department, École de technologie supérieure, 1100 Notre-Dame St. West, Montreal, Quebec, H3C 1K3

[b] ASME Fellow, Professor, Mechanical Engineering Department, École de technologie supérieure, 1100 Notre-Dame St. West, Montreal, Quebec, H3C 1K3

Paper submitted for publication, February 2023

5.1 Abstract

In practical applications, the stress state of expanded tubes is a critical parameter to insure structural integrity and avoid stress corrosion cracking. Therefore, it is important to analyze the stresses and strains generated by tube die expansion. Unfortunately, there are only a few theoretical approaches available for estimating the stress distribution of formed tubes, especially for cases where the expansion is achieved with spherical and oval dies.

In this study, 3/8 stainless steel and copper tubes were expanded with an oval die in a designed test workbench, and the tangential and longitudinal strains were monitored during the expansion process. A new analytical approach is developed to estimate the stresses and strains in the different zones of the expanded tube during the expansion process. The model identifies three expanded zones each treated with a separate theory. An axisymmetric numerical finite element model is used to analyze the stresses and strains based on a multi-linear kinematic hardening behavior to validate the analytical model.

In addition to the stresses and strain in the expanded tube, the push force of the die is also provided by the analytical model and compared to those of the numerical and experimental methods. Finally, the results from the three approaches are in relatively good agreement.

NOMENCLATURE

ε	Strain
ε_e	Equivalent strain
ε_θ	Hoop strain
ε_y	yield strain
θ	Tube rotation angle, °
μ	Friction coefficient
ν	Poisson ratio
σ	Equivalent stress, MPa
σ_r	Radial stress, MPa
σ_l	Longitudinal stress, MPa
σ_θ	Hoop stress, MPa
σ_m	Mean stress, MPa
$A_{\beta x}, B_{\beta x}, C_{\beta x}, D_{\beta x}$	Attenuation factors
E	Young's modulus, MPa
K	Strain-hardening constant
M	Moment, Nmm/mm
n_o	strain-hardening exponent
N	Hoop membrane force, N/mm
Q	Edge load, N/mm
P	Shear force, N/mm
R	Radius of die, mm
R_C	Radius of die contact surface, mm
r	Inside radius of tube, mm
S_y	Yield stress, MPa

t Thickness of tube, mm

x Axial position, mm

y The radial displacement

Subscripts

i refers to sub zone

c refers to contact position

5.2 Introduction

Tube forming is a mechanical process that involves the plastic deformation of tubes. Expansion, reduction, die forming, bending and hydroforming are work hardening processes that generate residual stresses. Expansion tubular technology is widely used in the production of joint assemblies for heat exchangers, steam generators, boilers, and other pressure vessels. The manufacturing of tube-to-tubesheet and tube-to-fin assemblies are a few examples where joint stiffness is obtained by plastic deformation. The control of such expansion processes is often obtained by trial and error (Bouzid & Pourreza, 2019).

Tube expansion forming process is widely applied in heat exchanger productions and in particular in the assembly of tube-to-tubesheet and tube-to-fin parts (Bouzid, 2018). Mechanical rolling, hydraulic, and die expansion are the most popular expansion processes used in the manufacture of tubular heat exchangers and gas coolers. Die expansion of tubes may result in not only high residual stresses but also micro-cracks and in particular when the process is not well controlled. There are few proposed studies on the elastic-plastic behavior and the estimation of the residual stress state in tubes to fins assembly but very few of them deal with the modeling of the tube's different zones during the die expansion process.

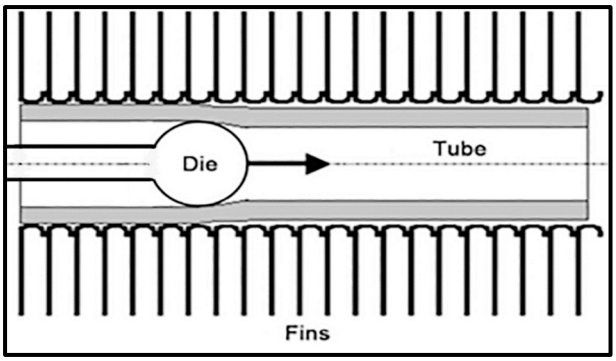

Figure 5.1 Tube expansion with a die (Mandrel)

In the literature, the stresses and deformations of the assembly are analyzed analytically, experimentally, and numerically using the finite element method(Hing et al., 2012; Kang et al., 2019; Tang et al., 2010). The expansion and contraction process is modeled considering an elastic-plastic material behavior with different strain hardening exponents. The normal die expansion process is shown in Figure 5.1; the outer diameter of the die is larger than the inner diameter of the tube, and the die can either be pushed or pulled through to expand the tube in order to close the gap between the tube and the fin hole and ensure a proper adhesion favorable for joint stiffness, structural integrity, and heat transfer (Wang & Chang, 1997). Although tube expansion forming is an old traditional process, there is limited research conducted in this field. In 1960 Sawczuck and Hodge (1960) conducted a comparative study of yield conditions for circular cylindrical shells subjected to axisymmetric radial pressure. In general, during the expansion process, the affected expansion region of the tube is divided into four zones: residual stress, contact, transition, and unexpanded zones(Laghzale & Bouzid, 2009). The first zone is the after expansion part of the tube where residual stresses are located. The next two zones are part of the tube that is work hardening and its stresses are beyond yield, therefore, these zones should be paid more attention. Bouzid et al. (2015) proposes a methodology to estimate stresses in hydraulically expanded tube-to-tubesheet joints that have similar zones produced by the expansion process by modeling the joint loading and unloading phases separately. Different from the previous theoretical method based on Cauchy momentum equations, Yuzhe Liu et al. (2016) developed a new tube expansion theoretical model based on the energy dissipation theory. Widely used tube materials such as copper and nickel alloys have less capacity to

withstand high-pressure and therefore more rigid tubes such as stainless steel are required in applications such as CO2 cooled exchangers. Unfortunately, with such applications being recent, the effect of the expansion process with a die on stainless steel tubes is less documented and consequently, there is a need for more research on the use ACR steel tubing. Although die expansion process of steel tubes is similar to that of copper tubes, the related studies may reveal their limitations and their capacity to produce efficient and optimum finned joints(Critoph, Holland, & Turner, 1996; Y. J. Kim, Cho, & Kim, 2008).

The tube thickness reduction as a result of the expansion forming with different die shapes is evaluated by Almeida et al. (2006) in 2005. Later in 2006, Alves et al. (2006) studied the same topic numerically using 2D and 3D finite element models with aluminum alloy. Related tests were also conducted to support and validate the overall investigation. Die expansion is not only applied to metallic tubes but also to plastic pipes. PVC tube expansion with dies and was investigated by Alves (2016). An analytical model based on the Hoop stress reaching yield is provided (Avalle & Scattina, 2018) to predict the push force applied to the expansion of a tube with a die using a rigid-linear strain hardening material behavior.

An analytical model to estimate the residual stresses in a hydraulically expanded tube-to-tubesheet joint is proposed by Bouzid et al. (Bouzid et al., 2015; Bouzid & Laghzale, 2016). The effect of reverse yielding is shown to have a major impact on the residual contact stresses. The kinetic versus isotropic material behaviors of die expansion of finned tube were the subject of an investigation in a previous theoretical study (Zhao & Bouzid, 2020). The stresses in the transition zone were modeled in Zhao et al. (2023) by the same authors but the hight stresses in the contact zone where the die comes into contact with the tube were not investigated.

This paper gives a methodology that can be followed to estimate the stress and strain state in finned tube expansion in the different expansion zones. The analytical model is supported by numerical finite element modeling and experimental data conducted on stainless steel 316 and copper tubes expanded with an oval die. The results show a good agreement between the three methods.

5.3 Analytical approach

The expanded region of the tube is divided into three zones; the transition zone, the contact zone, and the residual stress zone as shown in Figure 5.2. In the model, the position of the beginning of the contact of the tube with the die and the radial expansion force are parameters required to estimate the stresses and the driving force. The analytical method uses a self-adaptive approach to assess the stress distribution of the tube in the transition zone and relies on the Prandtl-Reuss flow rule of plasticity to evaluate the stresses in the contact zone.

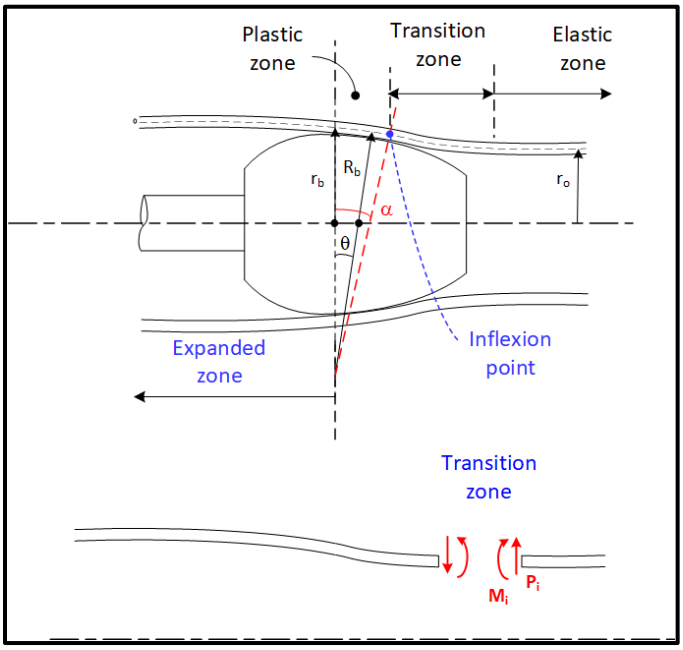

Figure 5.2 Different zones in an expanded tube

5.3.1 Stress distribution analysis

The limits between the three zones are identified by two boundaries. The transition zone extends from the unexpanded part of the tube till the position of the beginning of the contact of the die and the tube and includes the elastic, the partially plastic, and the fully plastic regions. The limit between contact and the residual stress zones is the location of the beginning of the separation of the tube and the die.

The die shapes can be spherical and ogive and are generally described in a cartesian coordinate system. The limit between the transition and the contact zones, shown in Figure 5.1, is considered tangent to the die surface. At this location between the contact zone and the transition zone the tube has a rotation angle (θ_c) and radial displacement (y_c) as shown in Fig 5.2. These parameters are related by Eq.(5.1) for a curved die shape of radius Rc.

$$y_c = R_c(\cos\theta_c - 1) - r + R \tag{5.1}$$

Where y_c is the radial displacement of the tube and can also be obtained using beam on elastic foundation theory for the transition zone.

5.3.2 Analysis of the transition zone

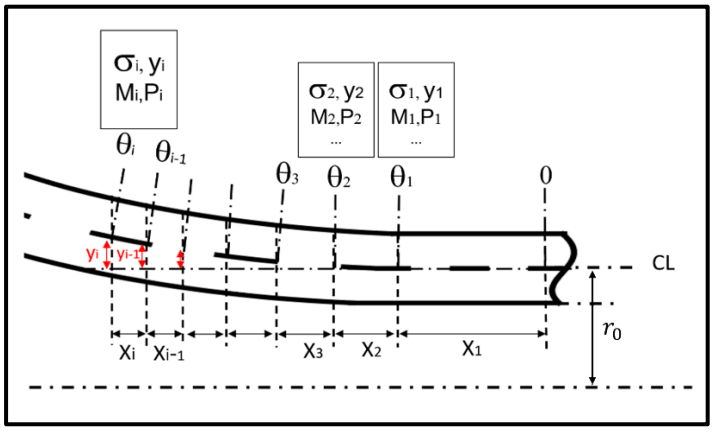

Figure 5.3 Subsections of the tube transition zone

As shown in Figure 5.2, the transition zone is simplified into two regions, the elastic region, and the plastic region. The calculation methodology of both regions of the transition zone is the same. From the previous study (A.-H. Bouzid & Laghzale, 2016), it was revealed that the equivalent stress in the tube reaches yield and or surpasses yield even with a very small radial expansion. Therefore strain hardening of the tube occurs to a certain extent before the later makes contact with the die. Because this zone is relatively small the behavior can be approximated using the secant modulus during the loading process. Likewise, the self-adaptive

method is utilized to estimate the stresses. The transition zone is, therefore, divided into multiple unequal length sections each characterized by a radial displacement and a rotation angle as shown in Figure5.3. While the tube rotation angle θ_c at the contact is tangent to the die surface and is not known initially for a curved die. Let the section rotation be incremented by $\Delta\theta$ and therefore:

$$\theta_i = \theta_{i-1} + \Delta\theta \tag{5.2}$$

The stress σ_i and the relevant secant modulus E_i of each section are obtained from the stress strain curve. An iterative process is used to obtain convergence for the rotation and displacement. This process is referred to as the self-adaptive process and is used to estimate the stresses. The Von Misses effective stress and a power law strain hardening behavior are used; the material data are generated based on the ASTM standards and the true stress-strain curve is fitted with a non-linear hardening equation such that:

$$\sigma = E\,\varepsilon \qquad for\ (\varepsilon \le \varepsilon_y) \tag{5.3a}$$

$$\sigma = A + B\,(\varepsilon - \varepsilon_y)^{n_o} \quad for\,(\varepsilon > \varepsilon_y) \tag{5.3b}$$

Where ε_y is the yield strain, K and n_o are the stain hardening constants of the Ludwik power law.

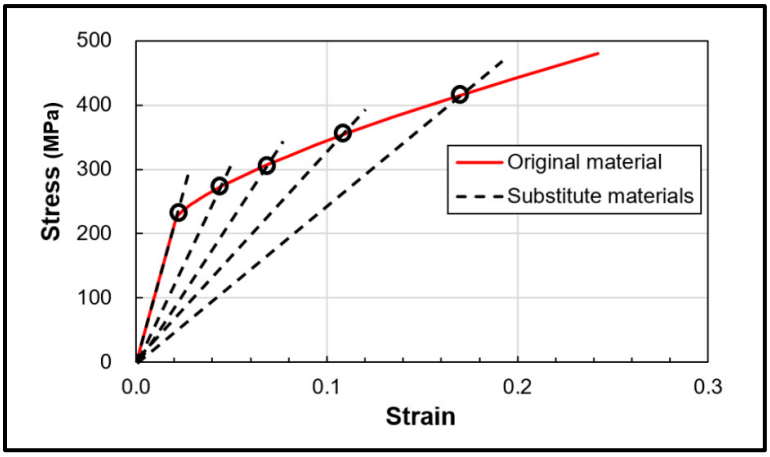

Figure 5.4 Simplified material behaviour

The stress condition for each section of the tube is that the equivalent stress is equal to the current stress σ_i. The secant modulus of the transition zone shown in Figure5.4 is defined by Eq. (5.4).

$$E_i = E \qquad for\ (\varepsilon \le \varepsilon_y)$$
$$E_i = \frac{\sigma_i}{\sqrt[n_o]{\frac{\sigma_i - S_y}{K}} + \varepsilon_y} \qquad for\ (\varepsilon > \varepsilon_y) \tag{5.4}$$

The beam on elastic foundation theory applied to a cylinder is used to obtain the four following parameters; radial displacement, rotation, moment, and shear force:

$$y_i = \frac{2\,P_i\beta_i}{k_i}\,D_{\beta x} + \frac{2\,M_i\beta_i^2}{k_i}\,C_{\beta x} \tag{5.5}$$

$$\theta_i = \frac{2P_i\beta_i^2}{k_i}\,A_{\beta x} + \frac{4M_i\beta_i^3}{k_i}\,D_{\beta x} \tag{5.6}$$

$$M_i = \frac{P_i}{\beta_i}\,B_{\beta x} + M_i\,A_{\beta x} \tag{5.7}$$

$$P_i = P_i\,C_{\beta x} + 2\beta_i M_i\,A_{\beta x} \tag{5.8}$$

where

$$\beta_i = \frac{\sqrt[4]{3(1-\nu^2)}}{\sqrt{rt}}, \qquad k_i = \frac{E_i t}{r^2} \tag{5.9}$$

And the influence coefficients are given by

$$A_{\beta x} = e^{-\beta x}(\cos \beta x + \sin \beta x)$$
$$B_{\beta x} = e^{-\beta x}\sin \beta x$$
$$C_{\beta x} = e^{-\beta x}(\cos \beta x - \sin \beta x)$$
$$D_{\beta x} = e^{-\beta x}\cos \beta x \tag{5.10}$$

The longitudinal and tangential stresses can then be evaluated based on the edge loads P_i and M_i on each section such that:

$$\sigma_{li} = \pm \frac{6\, M_i}{t^2} \tag{5.11}$$

$$\sigma_{\theta i} = \frac{6\, \nu\, M_i}{t^2} + \frac{E_i y}{r} \tag{5.12}$$

$$\sigma_i = \sqrt{{\sigma_{li}}^2 + {\sigma_{\theta i}}^2 - \sigma_{li}\sigma_{\theta i}} \tag{5.13}$$

In the case of thin tubes, to simplify the analysis the stresses are averaged through the thickness. In each section, the beam on elastic foundation theory is used in two steps; in the first step it is utilized to calculate the stresses in section i with its conditions at the end and then in the second step, the information obtained from the previous step together with the condition of section i-1 of length x_{i-1} are used to calculate the size of the current section x_i as shown in Figure5.3. The process is shown in the diagram of Figure5.5. Therefore, this simple approach provides an estimate of the stress distribution in the transition zone. The advantage of this method is to have the combination of the material hardening process and the stress theory that was only available in elastic condition. Therefore, the method provides a simplified method to estimate the stress distribution in the elastic-plastic transition zone.

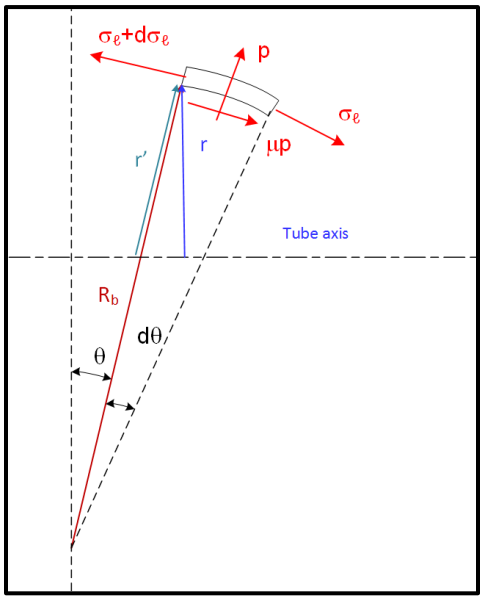

Figure 5.5 Element of tube expanded plastic zone under equilibrium

5.3.3 Contact zone analysis

The analysis of the tube plastic contact zone involves the resolution of a system of six equations with six unknowns. These equations are obtained from the axial and radial equilibrium, the plasticity Prandtl-Reuss flow rule, the volume conservation equation of plasticity and the Von Mises equivalent stress and strain relationship. Neglecting shear, the normal radial, tangential and longitudinal stresses $\sigma_r, \sigma_\theta, \sigma_\ell$ are principal stresses.

Using membrane theory

$$\frac{\sigma_\ell}{R_d} + \frac{\sigma_\theta}{r'} = \frac{p}{t} \tag{5.14}$$

With the radius *r'* given from the geometry shown in Figure 5.5

$$r' = R_d + \frac{r_d - R_d}{cos\theta} \tag{5.15}$$

The free-body diagram of the plastic region shown in Figure 5.5 gives the equilibrium equation in the x-direction as.

$$\frac{d\sigma_\ell}{d\theta} + \sigma_\ell sin\theta \frac{R_d + r'}{R_d(cos\theta - 1) + r_d} = p\frac{R_d}{t}(\mu + tan\theta) \tag{5.16}$$

The conservation of the volume due to the plastic behavior gives:

$$\varepsilon_\theta + \varepsilon_\ell + \varepsilon_r = 0 \tag{5.17}$$

The tangential strain is given by

$$\varepsilon_\theta = \log\frac{r}{r_0} = \log\frac{r'}{r_0 cos\theta} \tag{5.18}$$

The application of the Prandtl Reuss flow rule of the plastic deformation region

$$\frac{\varepsilon_\theta}{\sigma_\theta - \sigma_m} = \frac{\varepsilon_\ell}{\sigma_l - \sigma_m} = \frac{\varepsilon_r}{\sigma_r - \sigma_m} \tag{5.19}$$

The mean stress is given by

$$\sigma_m = \frac{1}{3}(\sigma_l + \sigma_\theta + \sigma_r) \tag{5.20}$$

The radial stress is assumed to be the average normal stress between the inside and outside surfaces.

$$\sigma_r = -\frac{p}{2} \tag{5.21}$$

Using the Von Misses effective stress and a power law strain hardening behavior

$$\sigma_e = A + B\varepsilon_e^{n_o} \tag{5.22}$$

with

$$\sigma_e = \sqrt{\frac{1}{2}[(\sigma_\theta - \sigma_\ell)^2 + (\sigma_\ell - \sigma_r)^2 + (\sigma_r - \sigma_\theta)^2]} \tag{5.23}$$

And the equivalent strain is given by

$$\varepsilon_e = \sqrt{\frac{2}{3}[(\varepsilon_\theta - \varepsilon_\ell)^2 + (\varepsilon_\ell - \varepsilon_r)^2 + (\varepsilon_r - \varepsilon_\theta)^2]} \tag{5.24}$$

Substituting Eqs. 5.23 and 5.24 into Eq. 5.22 and 5.21 into 5.14 and 5.16 and using Eqs. 5.14, 5.16, 5.17, 5.18, and 5.19 a system of six non-linear equations with six unknowns $\varepsilon_r, \varepsilon_\theta, \varepsilon_\ell, \sigma_r, \sigma_\theta, \sigma_\ell$ is obtained. The Matlab ODE solver with initial conditions is used to solve the non-linear system. By changing the radius r and resolving the system, the stress distribution in the contact zone is obtained. The axial pull or push force is obtained by integrating the friction force over the expanded plastic contact area with the die such that:

$$F = 2\pi R_d \int_0^{\theta_c} p(R_d(cos\theta - 1) + r_d)(\mu cos\theta + sin\theta)d\theta \tag{5.25}$$

5.4 Numerical FE model

The finite element method is used to validate the analytical approach with two types of 3/8 outside diameter by 0.035 inch thick tubes one made of copper C122 and the other one made of stainless steel SS316L. The first material is extensively used in the manufacture of low pressure gas cooler exchangers while the second material is under investigation for high pressure applications and in particular with exchangers that use CO_2 as a less pollutant refrigerant.

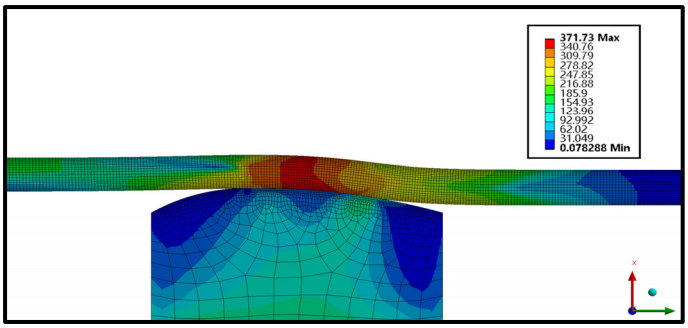

Figure 5.6 FEM simulation of oval die expansion showing the equivalent stresses

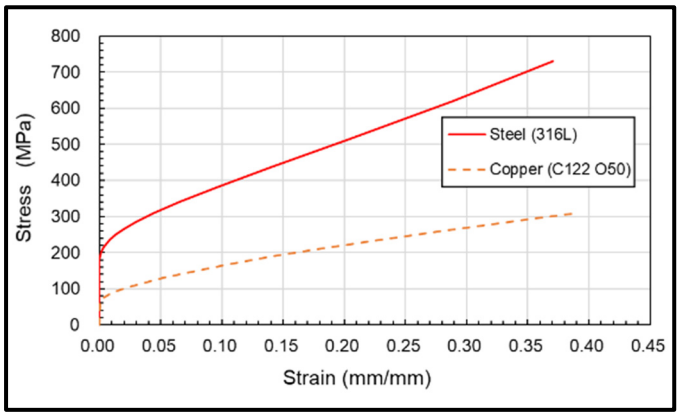

Figure 5.7 Stress-strain curve of the tube materials

The finite element refined mesh shown in Figure 5.6 is used to model the 3/8 inch tubes and the die with the dimension and materials shown in Tables 5.1 & 5.2. The stress-strain fitted data curves shown in Figure 5.7 follow Ludwick material plastic behavior the hardening constants of which are also given in Table 5.2. The multilinear kinematic strain hardening behavior option is used. A friction coefficient of 0.29 is considered during the expansion process.

Table 5.1 Dimensions of the tube and die

Dies (M4)	
	Oval
R (mm)	4.32
Rc (mm)	15
Tubes	
Material	Copper (C122) & Steel (316L)
Ri (mm)	3.8735
t (mm)	0.889

Table 5.2 Material properties

	Tube 3/8 in x 0.035 in		Die
Property	Copper C122	Stainless Steel 316L	Steel M4
E (GPa)	112	206	214
ν	0.34	0.25	0.29
S_y (MPa)	69	175	800
B (MPa)	455	800	-
n	0.68	0.575	-
μ (friction)	0.28	0.29	

The tube is constrained from axial movement at its end where the expansion starts and is free to expand in the radial direction and retract at its other end in the axial direction. The die moves from one end to the other with a speed 3 mm/s as suggested by a local manufacturer and also used in the experiment.

5.5 Experimental procedure

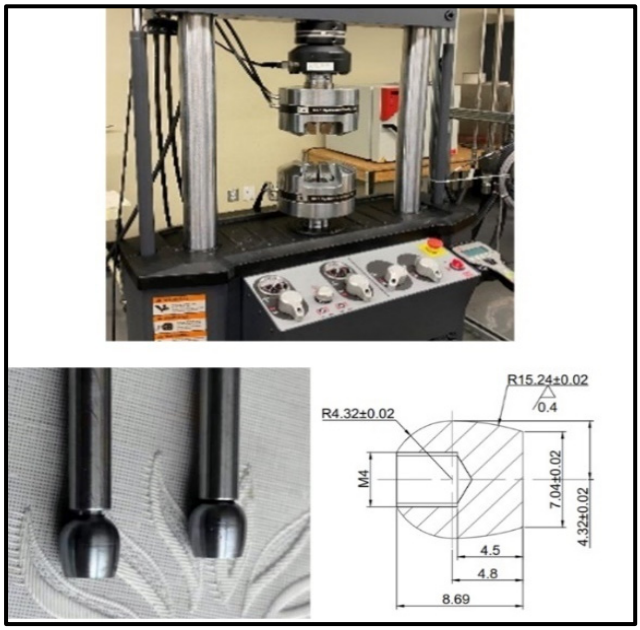

Figure 5.8 Hydraulic tensile compression machine used for the die expansion tests and die details

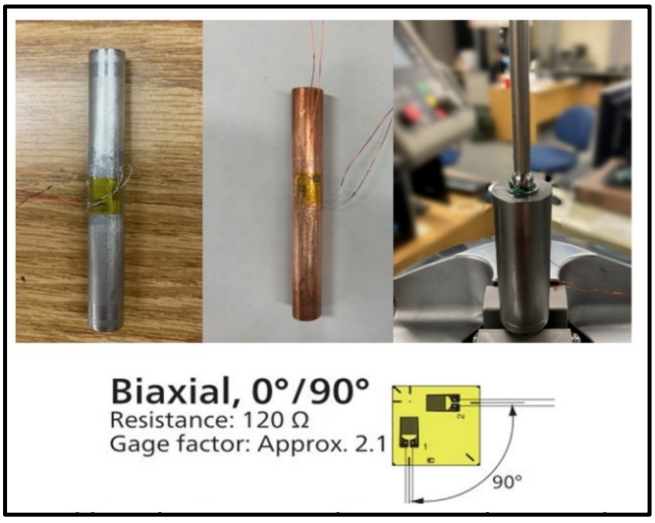

Figure 5.9 Expansion test workbench Copper and SS316L tube samples and biaxial strain gage

As a mean of validation, experimental tests are also conducted on the 3/8 in. SS316 and copper C122 tubes. The tubes are expanded with the oval die on a test workbench that uses a hydraulic tensile/compression test machine. The die with the rod shown in Figure 5.8 is fixed to the upper grip while the tube guide is fixed to the lower grip of the test machine. The tube guide shown in Figure 5.9 is specially designed for the expansion of 3/8 in. tubes. The tube is restrained by the guide at either the top or the bottom depending on the push or pull case. The instrumented strain gaged tubes shown in the same Figure are inserted inside the guide to be expanded. To monitor the axial and Hoop strain of the tube during the expansion process, a tee rosette is bounded to the tube's external surface. This specific strain gage of 2 mm width allows up to 15% strain measurement. The longitudinal and Hoop strains are continuously monitored through a quarter bridge configuration as the die moves inside the tube. The driving force, axial and Hoop strains, and time are monitored and recorded at regular intervals.

5.6 Results and discussion

This study proposes an analytical method to evaluate the stress and strain distributions in the transition and contact zones. To validate its performance, the analytical results are compared with those obtained from the numerical FE models and experimentation.

5.6.1 Copper C122 tube expansion

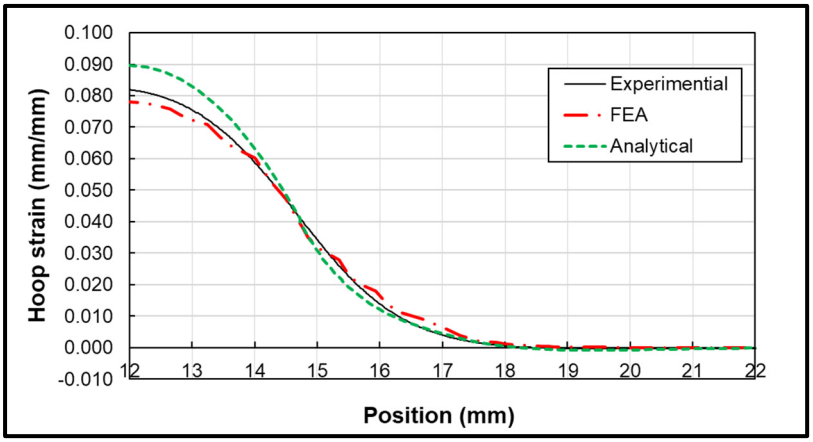

Figure 5.10 Hoop strain results for outside copper tube

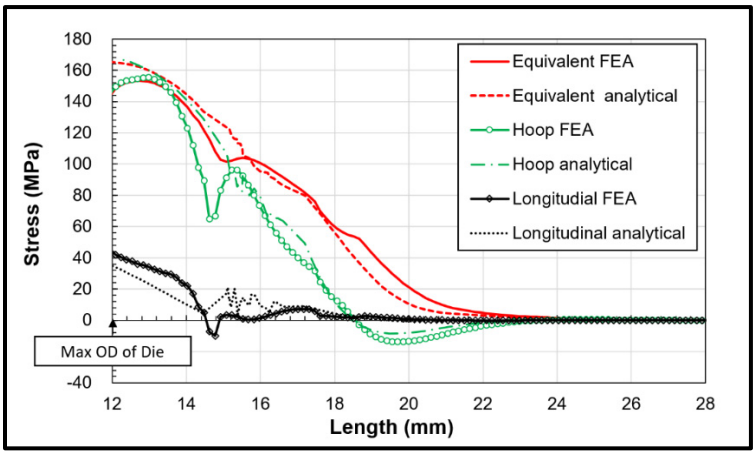

Figure 5.11 Stress distribution of copper tube

The 3/8 in. gage 20 copper tube is expanded using the oval die. This material is widely used in small low pressure cooling systems. Although the thin shell theory is less appropriate to use because of the high radius to thickness ratio of 4.35, the analytical approach still gives a fairly good estimate of the stresses and strains of contact and transition zones. Figure 5.10 shows the hoop strain results from the experiment, numerical and analytical methods. The analytical and FEM predictions are in good agreement with the test data. The maximum hoop strain during expansion is located at the maximum die radius and is about 8% as measured experimentally. The maximum difference between the analytical and the experiment values is at this location and is about 10%. This difference is due to the fact that the calculated strain uses the average radius while the measured strain is at the outside surface.

Figure 5.11 shows the stress distribution along the tube length including the transition and contact zones obtained with the analytical model and compared to that obtained by FE analysis. It is to be noted that the analytical and numerical stress distributions are averaged across the thickness. It would appear that, even with the radius to thickness ratio well below 10, the analytical stress distributions are comparable to their FEM counterparts. The longitudinal, hoop, and equivalent stresses of both methods are shown to match well, however, there are noticeable differences at the limit between the contact and transition zones. It is suspected that the bending stresses due to the change of curvature between the two zones are not well taken care of by the analytical model. A similar remark can be drawn at the maximum die radius

position, where the difference is also caused by the effect of tube bending as the result of the change of the tube curvature where the contact with the die ends and contraction begin and stresses are released.

5.6.2 Stainless Steel 316L tube expansion

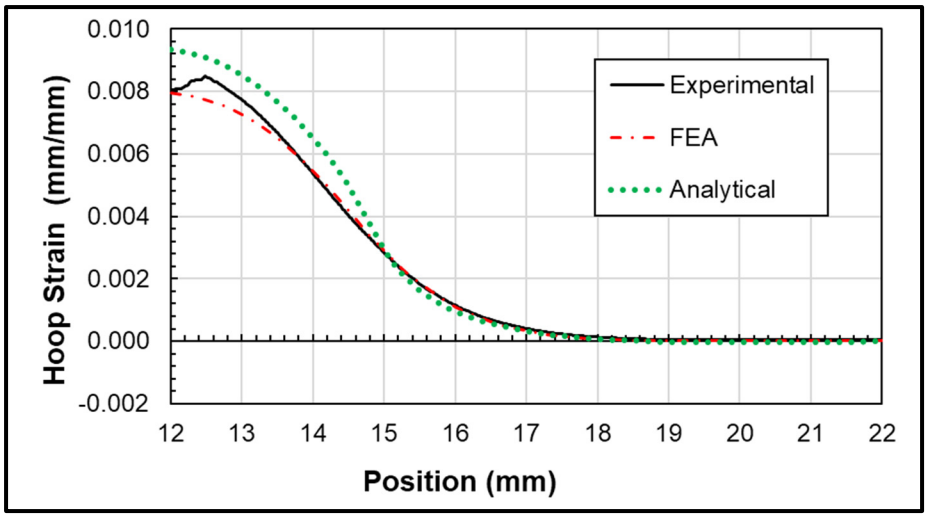

Figure 5.12 Hoop strain results for outside steel tube

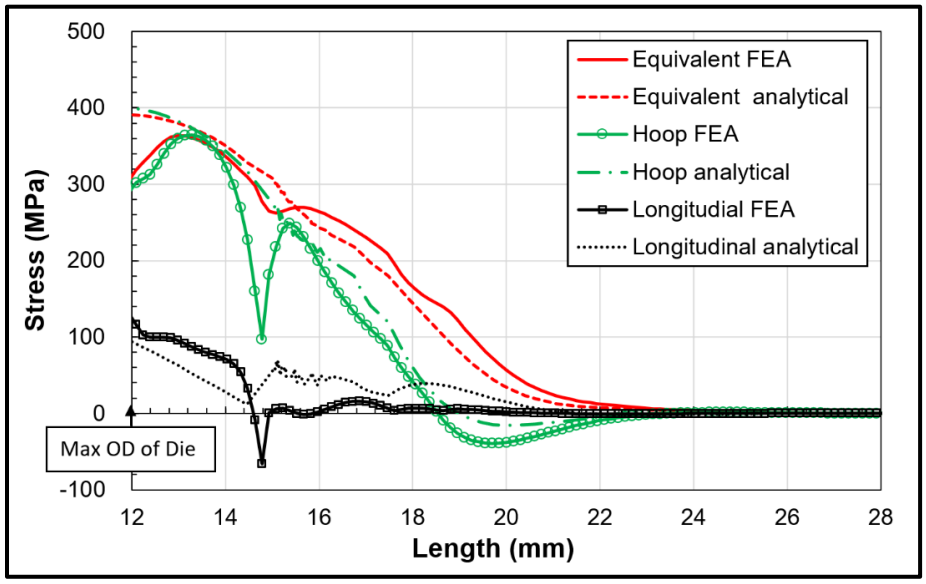

Figure 5.13 Stress distribution on outside surface of steel

The stainless steel 316L tube is also expanded by the oval die of the same size for comparison purposes. The hoop strain is shown in Figure 5.12. Again the maximum hoop strain is obtained at the die maximum diameter and the deformation curve is similar to that of the cooper tube shown in Figure 5.10. The maximum strain is also conditioned by the die maximum radius and the measured value is about 8.6% while the analytical model gives 9.3%. The general trend of the hoop strain of analytical and FE results agrees with the experimental data with the maximum difference observed at the maximum die diameter. Again around an 8% difference exists at this location. The experimental data show a sudden reduction at the maximum strain position. This is believed to be the result of a loss of adhesion between the tube and the strain gage carrier caused by the high deformation of the tube. Special adhesive for high strain may reduce this effect.

Figure 5.13 shows the longitudinal, tangential, and equivalent stress distributions during the process of expansion in the contact and transition zones of the stainless tube 316L. The stresses from both the analytical and numerical FE models are compared together in these expanded zones. The stress recovery passed the contact zone or at part of the tube that has already been subjected to die expansion is not treated by the theory and is not represented in the graphs. The stresses in the transition zone show a good agreement between analytical and numerical FE models. The stresses in the contact zone correlate less at the interface between the transition zone and contact zone and the maximum OD position. This significant difference is due to the presence of the bending moment that is not taken care of by the analytical model.

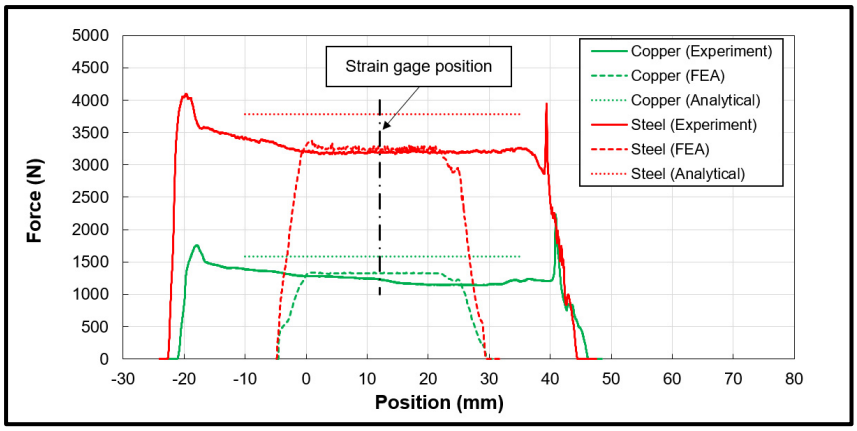

Figure 5.14 Driving force comparison

The contact zone pressure distribution is utilized to evaluate the die driving force per Eq.(5.24) and the results are presented in Figure 5.14. The measured force is higher at the start of the expansion when the die is in contact and the tube begins to expand but quickly settle to a constant lower value when all the die is inside the tube. The spicks of the copper and stainless-steel curves are due to the end effects, the presence of the sharp tube edges and the lack of proper lubrication. This is less obvious with FEM which shows similar settled values of the push force. The estimated forces are slightly higher than the measured and FEM average values. The overestimation of the radial stress or contact pressure and the lack of the model to simulate bending is believed to be the cause of the higher estimation of the die driving force.

5.7 Conclusion

An analytical model capable of estimating the stresses and strains in the transition and contact zones of a tube subjected to die expansion is developed. The good agreement between the analytical, numerical, and experimental methods indicates that the simple developed approach is quite reliable. The strains are predicted within 10% while the stresses are found to be comparable with a difference at the regions where the change of curvature is important such as at the interfaces between the transition and contact zone and between the contact and residual stress zones. It can also be concluded that the theory of beams on elastic foundation

with the self-adaption method can be applied to the low plastic region, such as the transition zone.

The approach was successfully used with different materials namely copper and stainless steel and limited to thin tubes although, in the two treated cases, the tube radius to thickness ratio is 4.35. The stresses in the contact zone reach maximum values and can be considered as the critical zone for the level of stress to be verified and ensure that necking is not reached during the expansion process.

CHAPTER 6

A STUDY ON THE CONTACT QUALITY IMPROVEMENT OF FIN TO TUBE ASSEMBLIES

Zijian Zhao [a], Abdel-Hakim Bouzid [b]

[a] Ph. D. student, Mechanical Engineering Department, École de technologie supérieure, 1100 Notre-Dame St. West, Montreal, Quebec, H3C 1K3

[b] ASME Fellow, Professor, Mechanical Engineering Department, École de technologie supérieure, 1100 Notre-Dame St. West, Montreal, Quebec, H3C 1K3

Paper submitted for publication, April 2023

6.1 Abstract

Fin to tube assembly is a common type of connection in heat exchangers, especially for smaller equipment. The tube is expanded by a die or an expander during the assembly process to close the gap between the tube and the fin collar for better heat transfer. The generated interference and the contact area depend not only on the radial expansion produced by the die and initial gap but also on the shape of the fin contact area with the tube before expansion. The die expands to close the gap and produces a small interference that allows the fin collar to adhere to the tube. However, the contact at the interface is not continuous across the width of the mating surfaces according to recent research. As a result of this poor contact quality, the heat transfer due to conduction is considerably reduced and the heat exchanger efficiency is highly compromised.

This study is aimed at establishing a relationship between the profile shape of the fin hole and the contact quality and provides guidelines for improving the quality of tube to fin contact. Tubes with different materials, dies with different sizes and fins with collar with hourglass proposed shape will be assessed using a series of expansion simulations conducted on different

FE models. Finally, the micro gaps generated during the expansion process at the tube to fin interface are utilized to evaluate the quality of the contact surface.

6.2 Introduction

Fin-to-tube expansion is a work hardening process that makes a good thermal contact between the tube and fins and generate residual stresses. Expansion tubular technology is widely used in the production of gas cooled heat exchangers made of copper and stainless-steel tubing. The latter is used for recent development of CO_2 cooled heat exchangers. The manufacturing of tube-to-fin assemblies is basically traditionally a trial-and-error process. It is only recently that analytical and numerical studies are being introduced to adjust the control of this process (Bouzid & Pourreza, 2019).

Die expansion of fin-to-tubes creates not only high stresses but also micro-gaps during expansions when the process is optimized. The studies on the elastic-plastic behavior and the developed stresses of copper and stainless-steel tubes due to die expansion are available in the literature (Bouzid, 2018; Hing et al., 2012; Kang et al., 2019).

The studies of fin design geometry and shape to improve the contact quality of the tube to fin to enhance the heat transfer performance are rare in the literature. In the past, the contact between fin to tube as a result of tube expansion was not considered to be an issue and was accepted de facto. However, a recent study using experimental tests showed that the contact between the fin and the tube is not continuous and gaps exist between them (Tang et al., 2011). Finite element simulation conducted by few researchers showed similar results(Bouzid & Kazeminia, 2016; Liu & Qiu, 2016).

Previous researchers investigated the effect of interference between the die and tube to improve the tube to fin contact (Cheng & Madhusudana, 2006; Chung et al., 2005) and reduce the thermal contact resistance (Tang et al., 2010). Critoph et al. (1996) reported that the overall thermal resistance could be increased by 10% with a gap between the fin and tube of 10 μm.

However, recent studies (Tang et al., 2010; Tang, Peng, & Li, 2009) showed that high interference can cause fin plates to bend and distort and reduce the contact quality. Nevertheless, die size is not the only factor to affect the contact quality, fin geometry, material of tube, and the expansion process are other parameters that can have considerable effects on the final result. In order to have an insight on the impact of these parameters and understand their interaction, a finite element study is worth pursuing. Such study can bring the research one step ahead by investigating the impact of die to tube interference, tube material, and initial collar profile contact surface.

In reference (Tang et al., 2011) the authors uses the contact pressure as a target parameter to assess the contact quality, however, while small contact areas may provide large contact pressure, its magnitude does not guarantee higher heat transfer. Since contact cannot easily be achieved over the hole target contact surface, the gap size between the fin collar and the tube will be used as the critical factor affecting heat transfer in general. Therefore, instead of using the contact pressure, the average gap size of the contact area of the collar and tube will be directly utilized to evaluate the contact quality in hereafter.

6.3 Finite element model

In this study, the general-purpose finite element Ansys workbench 2019R1 is used to conduct the investigation. The 3/8 inch tube is expanded with different die to tube interferences and collar contact profiles to analyze the effect of the previously cited parameters on the interface contact quality. The FEM model is constituted of three parts; the tube, the fins and the die as shown in Figure 6.1 and the geometry is defined in Table 6.1. Since the tube expansion process is an axisymmetric problem where the geometry and loading do not vary with the angle, the 2D axisymmetric method is utilized for the analysis.

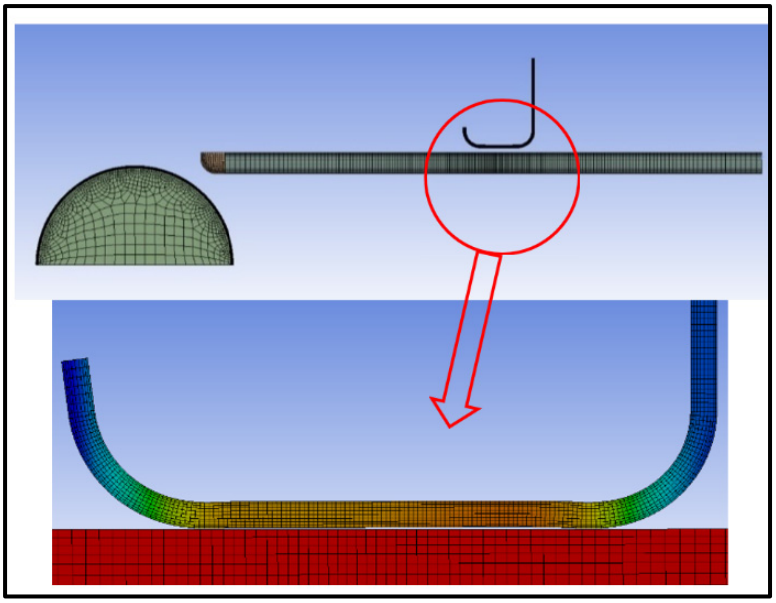

Figure 6.1 Finite element model

The mesh of the tube and sphere are refined at the matting surfaces; The criterion of the mesh refinement is based on less than 1% difference in the maximum equivalent stress on the tube. The variation in maximum equivalent stress, as depicted in Figure 6.2 , exhibits a discernible pattern with alterations in the dimensions of the computational elements. Notably, once the element size below to 0.037 mm, the scope of stress fluctuations remains confined within a negligible 1% threshold. Consequently, it can be concluded that this element size is sufficient for the qualitative analysis required for this study.

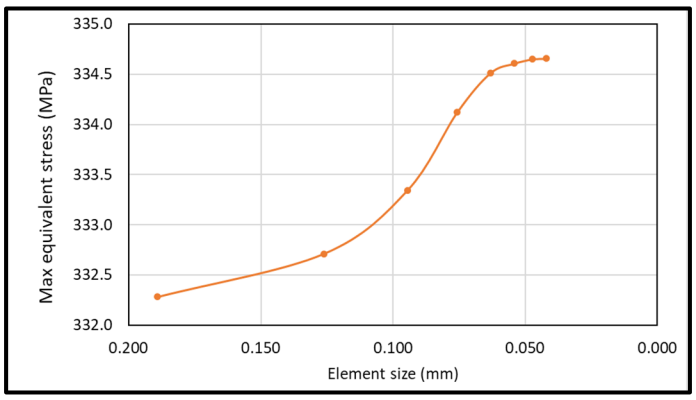

Figure 6.2 Stress change with element size

The model uses isoparametric axisymmetric 8 node-elements to model the structures and employs target and contact elements at the interface with the friction coefficient as indicated in Table 6.2. In practice, during the expansion process, the tube inside wall in contact with the die is lubricated with oil to reduce the friction force. Friction coefficients of 0.28 and 0.29 between these two surfaces are usually adopted in the analysis for copper and steel respectively. However, for the aluminum collar in contact with the coper and stainless steel a typical coefficient of friction value of 0.23.

Table 6.1 Fin-to-tube assembly geometry

Parameter	3/8 tube
Tube O.D (mm)	9.52
Tube O.D (mm)	7.45
Tube thickness (mm)	0.89
Fin collar diameter (mm)	9.91
Fin thickness (mm)	1
Radial interference (mm)	200, 230, 255, 280, 305, 390
Contact radius (mm)	4, 9, 14, 19

The tube is fixed in the axial direction at one end and the other end is flared for ease of die engagement. The spherical die is pushed inside the tube with a rate of 2 mm/s according to the recommendations of reference (M. Alves et al., 2006).

The simulations will be run with 3/8 inch gage 20 tubes made of Copper C122 (050) and stainless steel (SS 316L) and fins are made of Aluminum 3003. The copper tubes are extensively used in the manufacture of low-pressure gas cooled exchangers, and stainless steel is to accommodate the use of the pollutant refrigerant CO_2 that requires high pressure. Aluminum sheets are used for the manufacture of fins due to its high thermal conductivity. They are 1mm thick with collars of 9.91 mm. The geometrical data of these components are given in Table 6.1.

The fitted stress-strain curves of the materials used in the simulations are shown in Figure 6.3. These materials follow the Ludwick material plastic behavior, the hardening constants of which are given in Table 2. The material data are obtained from references (Desu et al., 2016; Roberts et al., 1998). The multilinear kinematic strain hardening behavior option is used in the FE simulations:

$$\begin{aligned} \sigma &= E\,\varepsilon && for\ \left(\varepsilon \le \varepsilon_y\right) \\ \sigma &= \sigma_y + K\,(\varepsilon - \varepsilon_y)^{n_o} && for\ \left(\varepsilon > \varepsilon_y\right) \end{aligned} \tag{1}$$

where ε_y is the yield strain, K and n_o are the stain hardening constants of the Ludwik power law.

Table 6.2 Material properties and geometry

	Tube 3/8 x 0.035 in		Fin	Die
Property	Copper (C122)	Steel 316L	Aluminum (3003)	Steel M4
E (GPa)	112	206	68.9	214
ν	0.3	0.25	0.33	0.29
Sy (MPa)	69	175	57	800
K (MPa)	455	800	234	-
n	0.68	0.575	0.373	-
μ (friction co.)	0.28	0.29	0.23	

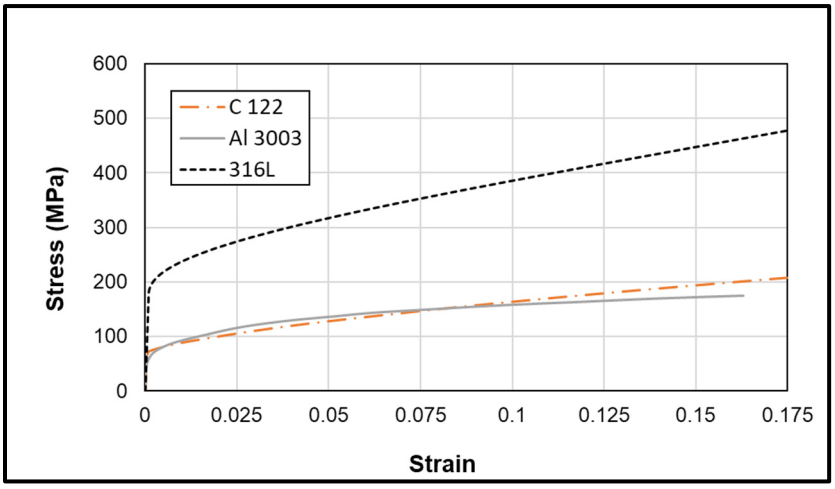

Figure 6.3 Material stress-strain curves

6.4 Proposed fin collar shape

The tubes are inserted in the fins before being expanded with a spherical die. The fin collar shown in Fig 6.4 is usually cylindrical with straight generators. After expansion one can observe that contact is not homogeneous and micro-gaps are left after the process producing a low thermal contact conductance. The thermal heat transfer resistance can be increased by eliminating the mico-gaps and increasing the contact between the fin collar and the tube. It is proposed to make the fin collar an hourglass shape to achieve this goal. Therefore, the straight cylindrical surface of the fin collar is replaced with an hourglass shape with a radius of curvature that can be optimized to minimize the micro-gaps.

The radius of curvature of the collar hourglass shape is to be varied from 4 to 19 mm in order to optimize the contact and increase the thermal contact conductance. Figure 6.4 shows the sketches of the different radii of the collar hourglass shapes before expansion. It's worth mentioning that to facilitate the insertion of the tubes inside the fins and avoid reducing the initial gap between the fins and tubes, the initial average gap is kept constant.

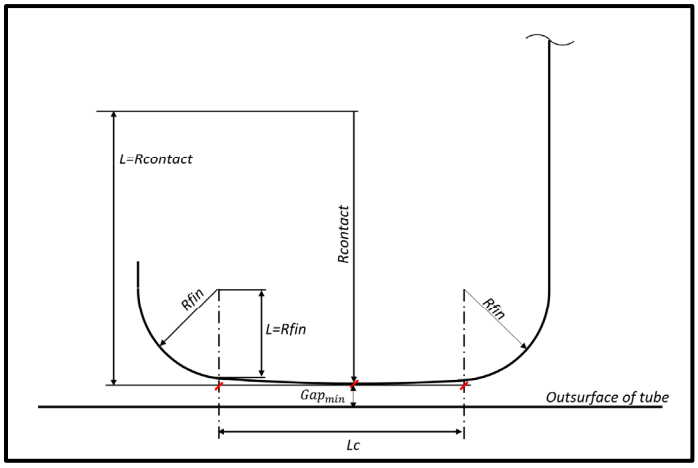

Figure 6.4 Hourglass shaped fin collar

6.5 Results and discussion

6.5.1 Effect of Die and Tube Interference

The effect of the die and tube interference was first investigated with a coper tube and an aluminum collar having a regular cylindrical shape. A series of spherical dies of different radius ranging from 0.1575 in. to 0.17 in. with 0.0025 in. interval to produce an interference of 200, 230, 255, 280, 305, 390 μm respectively was analyzed. The inner radius of the unexpanded fin hole is 0.195 in. and the outside radius of the tube is 0.1875 in. The initial gap between the fin and the tube is 7.5 mils (190 μm) before expansion. The final reduced gap between the tube and fin collar generated by expansion is shown in Figure 6.5 for the different interferences.

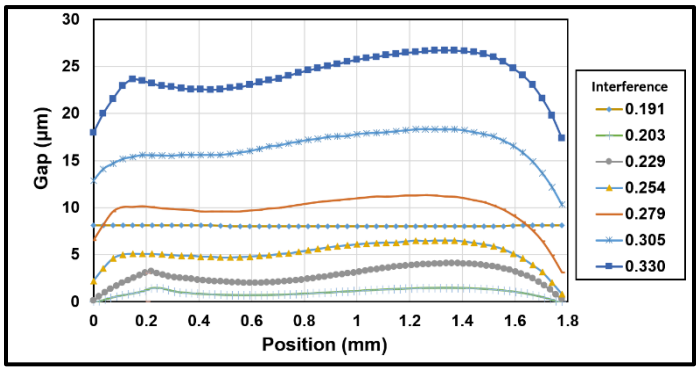

Figure 6.5 Micro-gaps at tube-to-fin interface

The average gap size as a function of the interference obtained after expansion is shown in Figure 6.6. The result shows that there is a minimum value of the average gap obtained with a certain value of the interference. In this case, it is obtained with an interference of 255 µm. The better contact between the fin collar and tube is not necessarily obtained with highest interference. Therefore, since increasing the die size does not improve the final contact quality between the tubes and the fins, it is worth conducting a interference optimization analysis. Obviously, the optimized thermal contact resistance depends not only on the interference but on the pair of material strain hardening of the tube and fin and such a methodology should be followed in the fabrication of tube-to-fin gas-cooled exchangers.

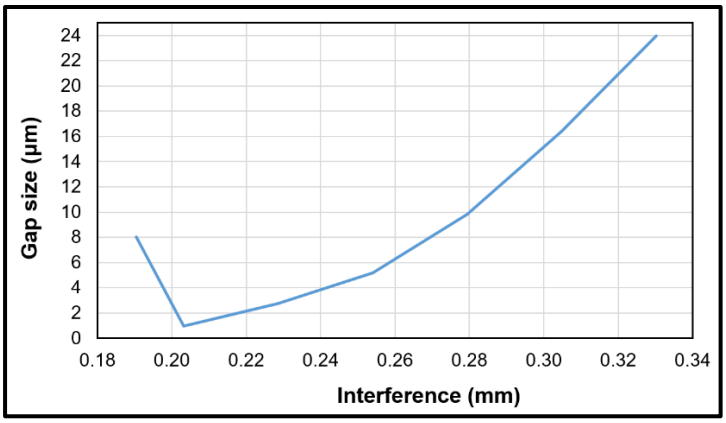

Figure 6.6 Average gap size vs interference

6.5.2 Effect of tube constraint on contact quality.

In order to be able to expand a tube with a die, the tube should be constrained in the axial direction at one of its ends. Depending on the case the unexpanded part of the tube is free from stress or undergoes a compression before being expanded. This is referred to as push and pull conditions. The results shown in Figure 6.7 with copper tube indicates that the average gap as a function of the initial gap of the two constraint types have similar trend. However, the push case provides lower gaps and better contact quality at all times. The average gap decreases by 15 times when the push condition is adopted. The push case leads to lower final gap because the unexpanded part of tube is under compression during the die expansion process. During the expansion process, this unexpended part of the tube already in compression expands and therefore decreases the initial gap between the tube and fin. In addition, the push case requires 20% less expansion force than the pull condition as reported with 3/8 in gage 20 copper and stainless-steel tubes. Nevertheless care should be taken to avoid buckling of the tube.

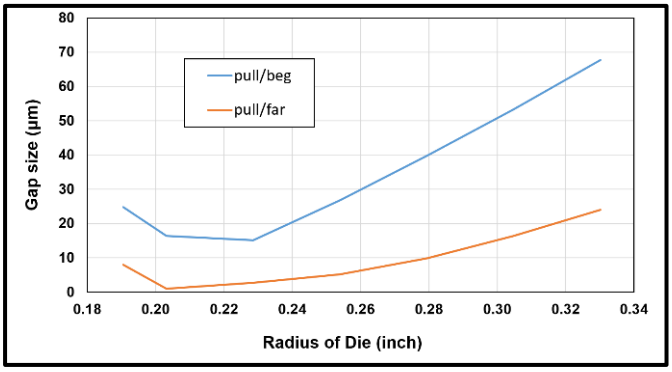

Figure 6.7 Effect of tube end conditions

6.5.3 Effect of fin collar shape on contact quality

The replacement of flat collar shape by an hourglass shape was conducted for the purpose of decreasing the micro-gaps and improving the contact quality. In effect, the comparison of the flat part of the fin collar vs the curved surface can be done by comparing the micro-gaps over the collar contact length shown in Figure 6.5 for a straight collar and Figs. 6.8 to 6.11 for

collars with different hourglass contact radii ranging from 0.15 to 0.75 in. The hourglass contact radii and initial gap were designed to have an average initial gap constant. The expansion with each hourglass contact radius was simulated multiple times to evaluate its performance under different die sizes. The outside diameter of the die was increased as before from 0.1605 in. to 0.1655 in. in the step of 0.001 in. (ie. 4, 9, 14, 19 mm).

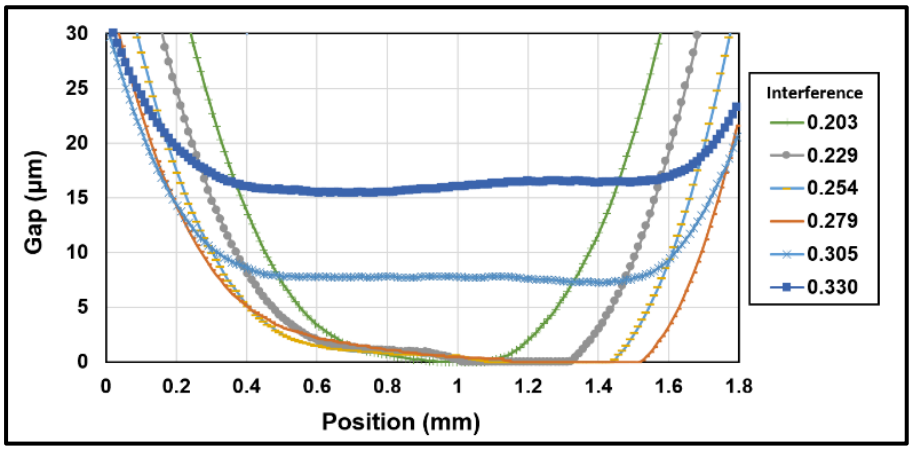

Figure 6.8 Micro-gaps at tube-to-fin interface with 0.15 in. hourglass radius

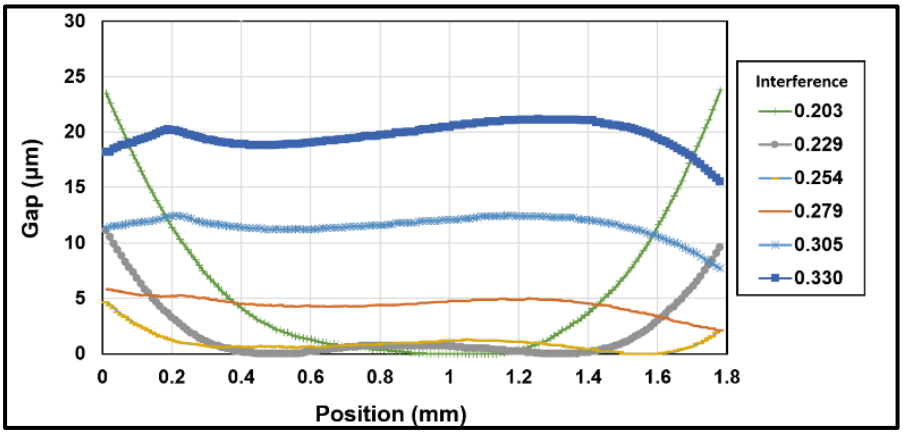

Figure 6.9 Micro-gaps at tube-to-fin interface with 0.35 in. hourglass collar radius

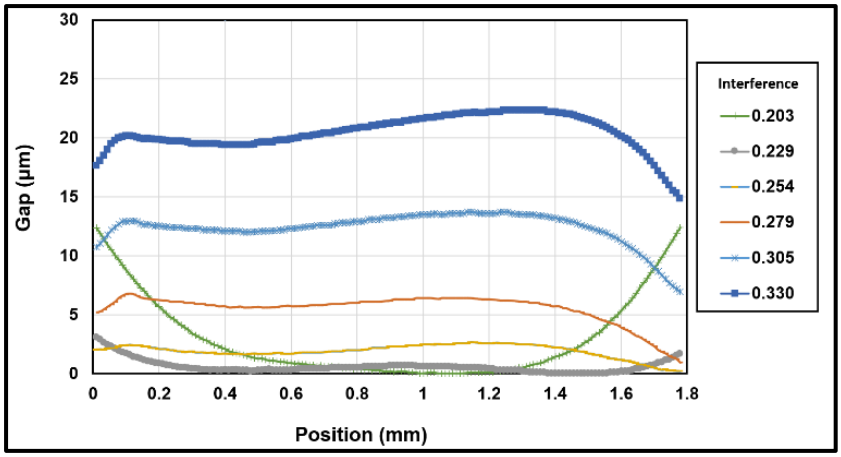

Figure 6.10 Micro-gaps at tube-to-fin interface with 0.55 in. hourglass radius

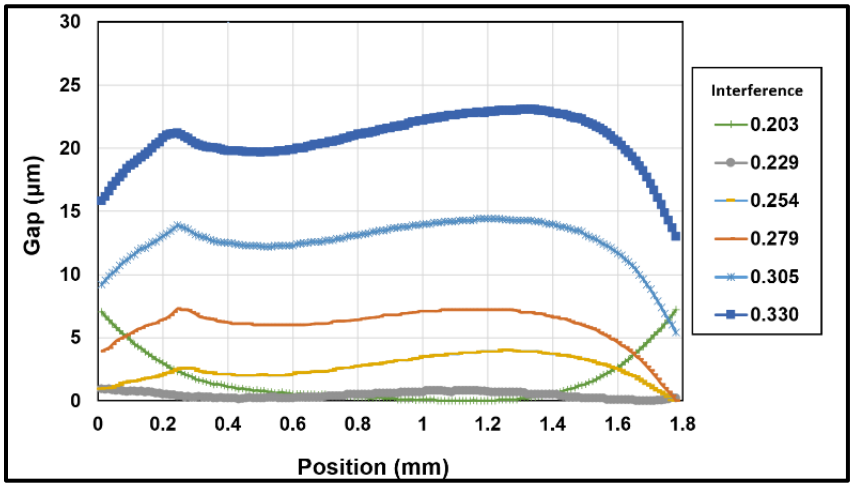

Figure 6.11 Micro-gaps at tube-to-fin interface with 0.75 in. hourglass radius

Figures 6.8 to 6.11 show in general, a significant improvement in the contact between the fin and tube over the collar length. The better contact quality is obtained with specific interferences depending on the hourglass contact radii and therefore an optimization process is worth considering.

Figure 6.12 shows the comparison of the average micro-gap for different hourglass collar contact surface radii and different tube and die interferences. Under these conditions, it can be seen that the curved collars have an advantage over the flat collar, the average gap decreases by 16 to 60 % depending on the hourglass contact radius. The average gap size of the curved fin collar is smaller than the cylindrical fin collar for the same initial interference for all hourglass radius greater than 0.15 in. or 4 mm. and the interference below 280 µm. It can be seen that the average gap reduces as the hourglass collar radius increases.

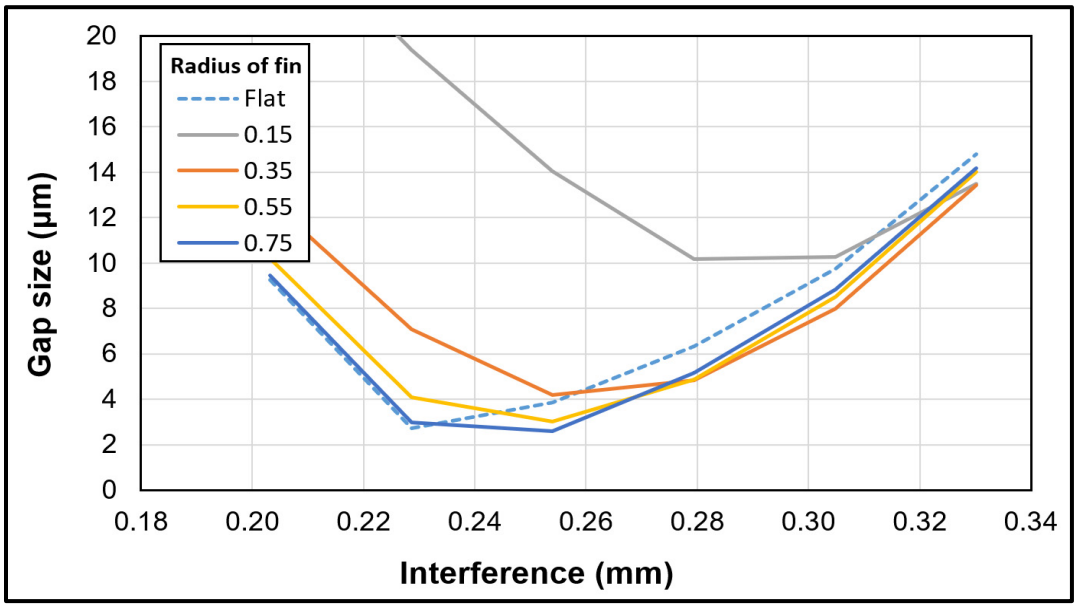

Figure 6.12 Average gap size of different hourglass collar radius with copper tube

6.5.4 Effect of tube material on contact quality

The gap comparison of different hourglass contact radius with stainless steel 316L tube under the pull condition is shown in Figure 6.13. Similar results to the copper tube are obtained where a larger hourglass collar radius gives better results. The graph clearly shows that there is an optimized interference that gives the lowest average gap. The curved fin collars give smaller gaps at higher interference that the flat collar. However, the average gap is much higher than with copper. This is because SS316L has a higher yield stress than that copper. In this case, it

is recommended to use another grade of aluminum that has higher yield stress than that of 3003 such as 6061.

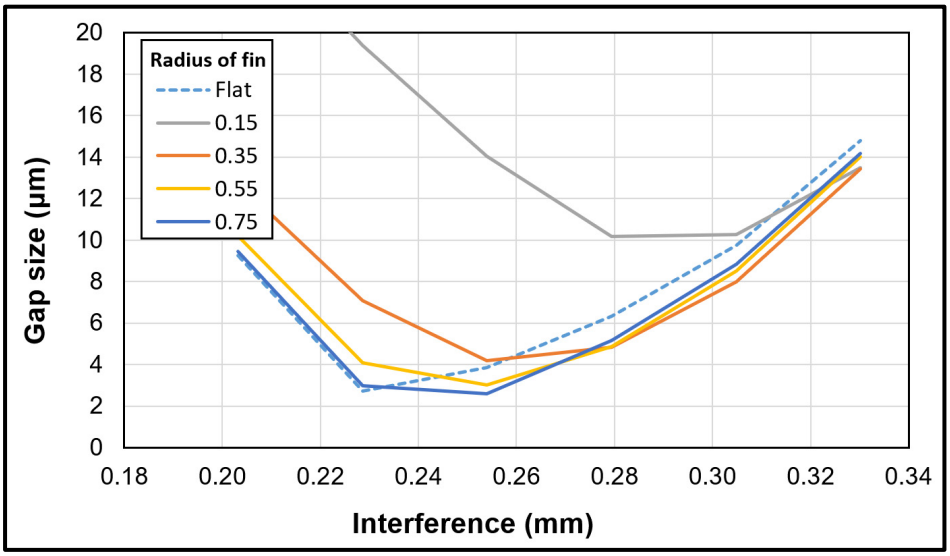

Figure 6.13 Average gap size of different hourglass collar radius with SS316L tube

6.5.5 Thermal analysis of the contact

In order to assess the performance of thermal conductive between different gaps shape. Two local transient thermal contact models are created based on the flat fin with 203 umm interference and 0.75 inch curved fin with 229 µm inferences shown in Figure 6.14. Those two cases are the size of the minimum gaps for flat and curved fins. Gap shapes have been shown in the previous figure.

Both models were only selected at the contact area to focus on the gap effect and the two models have the same size and location. The micro gap between the fin and the tube is treated as a static air domain. The standard isotropic thermal conductivity of 0.024 W/m·K is applied to this region. Subsequently, the remaining contact area between the fin and the tube is assumed to be perfect and continuous. The inside surface of the tube is applied with a constant

temperature of 75 °C , and a temperature depended metal to air convection coefficient is applied on the out surface of the fin.

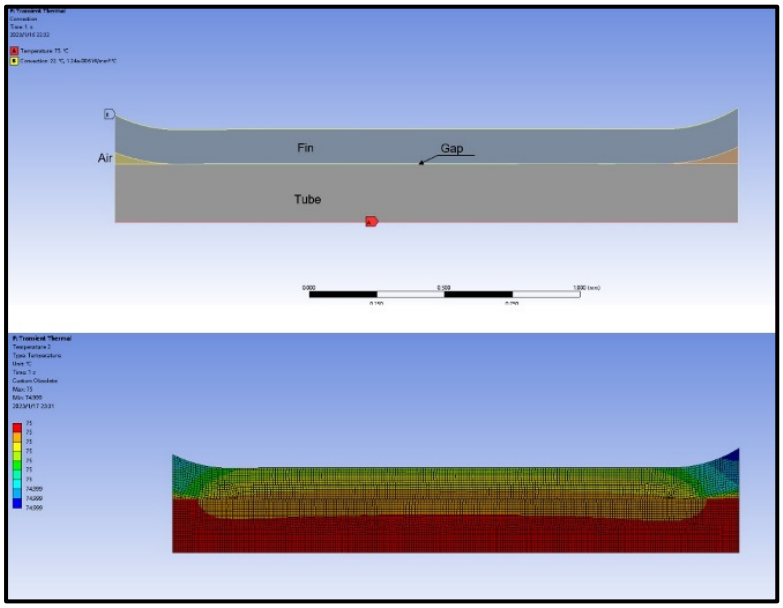

Figure 6.14 Thermal transient model

The final result shows that the heat flux of the inside tube from the curved fin model which has a small gap size is 42% more than the flat fin model with a larger gap. The difference in heat flux is close to the gap size difference between the two models.

6.6 Conclusion

The result shows that the tube to fin interface contact depends on the interference between the die and the tube. There is an optimized value that generates the lowest average gap over the collar contact length. The result shows that the fin collar with an hourglass shape improves the contact quality when the hourglass radius is optimized. The better contact quality is obtained with a combination of the hourglass contact radius and interference. Smaller hourglass contact radii are to be avoided as they require a tight tolerance on the interference.

The end tube constrain has an effect on the contact quality. Smaller micro-gaps are obtained with the push condition, which in addition requires 20% less die force. However, care should be taken to avoid buckling.

Finally, the materials have a considerable effect on the contact quality, particularly on the yield stress. The fin aluminum grade is important when tube expansion is performed on SS316L rather than on copper.

CONCLUSION

This study significantly impacts the manufacturing and fabrication of heat and gas-cooled exchangers. In particular, their finned tube -to-fin component plays a crucial role in conducting heat transfer and therefore special attention must be paid during their expansion design. Enhancing the reliability and performance of this component greatly influences industrial equipment such as coolers, heaters, steam generators, condensers, and boilers. Thus, innovative research focusing on improving tube to fin quality is of utmost importance. The objectives of this study are accomplished by:

- Examining the influence of die size on residual stresses and exploring the performance of various plastic hardening behaviors.
- Establishing a new analytical approach to estimate stresses in the expansion, transition and elastic zones and the driving force during the tube expansion process.
- Investigating the distribution of stresses and strains within the contact zone using diverse approaches.
- Enhancing tube to fin contact quality and thermal contact capacity by altering fin shape or modifying tube expansion conditions.

Initially, the investigation was centered on material reverse yielding effect on the residual stresses of finned tubes subjected to die expansion. When applying the isotropic hardening rule, the predicted residual stresses are considerably higher. With the push force they were found to be around 10% higher compared to kinematic hardening behavior. Later, the experimental data, when compared to the FE simulation, indicated that SS316L exhibits a kinematic hardening behavior. In fact, the strains and push forces of the two methods showed a good agreement. Concurrently, the effect of die size on residual stresses is recognized. Under kinematic hardening behavior, residual stresses exhibit slight fluctuations before stabilizing as the die radius increases. Stresses generated during the expansion process and the residual stresses that remained after expansion are dependent on die size and the maximum stress,

generally found on the tube outside surface. However, the position of maximum residual equivalent stress varies with the die size, potentially appearing inside, in the middle, or outside.

The second paper presents a development of an analytical approach to estimate the stresses in the transition zone and the driving force during the process of tube expansion. The agreement between the results of the three analytical, numerical, and experimental methods indicates that the developed approach is reliable and relatively accurate. It can also be concluded that the theory of beams on elastic foundation with self-adaption material modulus can be applied to the elastic to plastic region of the transition zone. The approach was successfully used with copper and SS316L materials and various die shapes. The driving force is obtained by considering the friction force, which is calculated based on a rigid perfectly plastic material model, resulting in a slightly underestimation of its value. Nevertheless, the simple analytical methodology can still assess the integrity of the expanded tube and provide a good estimate of the driving force.

The third paper broadens the scope of the study articulated in the second paper by formulating an analytical model proficient in estimating stresses and strains in the transition and contact zones of a tube subjected to die expansion. The strong concordance among the analytical, numerical, and experimental methods underscores the substantial reliability of the developed approach. The strains are predicted within 10% while the stresses are found to be comparable with a difference at the regions where the change of curvature is important such as at the interfaces between the transition and contact zone and between the contact and residual stress zones. The approach was successfully applied to different materials, namely copper and stainless steel, and not limited to thin tubes. The stresses in the contact zone reach maximum values and can be considered critical in determining the stress level that needs to be verified to ensure that necking does not occur during the expansion process.

The findings of the fourth paper reveal that the quality of contact at the tube-to-fin interface depends on the interference between the die and the tube. An optimized interference value results in the smallest average gap along the collar contact length. It was found that a fin collar

with an hourglass shape improves the contact quality and particularly when the hourglass radius is optimized. Optimal contact quality is achieved by combining the hourglass contact radius and interference. However, smaller hourglass contact radii should be avoided, as they necessitate tighter interference tolerance. Furthermore, the results indicate that the end tube constraint affects the contact quality. The push condition requires 20% less die force but yields to smaller micro-gaps. Nevertheless, caution should be exercised to avoid buckling when the push method is adopted. Lastly, material properties, particularly yield stress, play a significant role in determining contact quality. The fin aluminum grade proves especially important when tube expansion is performed on SS316L rather than copper

BIBLIOGRAPHY

Allam, M., Chaaban, A., & Bazergui, A. 1998. Estimation of residual stresses in hydraulically expanded tube-to-tubesheet joints. *Journal of Pressure Vessel Technology, 120*(2), 129-137.

Almeida, B., Alves, M., Rosa, P., Brito, A., & Martins, P. 2006. Expansion and reduction of thin-walled tubes using a die: experimental and theoretical investigation. *International Journal of Machine Tools and Manufacture, 46*(12-13), 1643-1652.

Alves, L., Silva, C., Santos, P., & Martins, P. 2016. Mechanical joining of PVC tubes by their ends. *Proceedings of the Institution of Mechanical Engineers, Part L: Journal of Materials: Design and Applications, 230*(4), 860-868.

Alves, M., Gouveia, B., Rosa, P., & Martins, P. 2006. On the analysis of the expansion and reduction of thin-walled tubes using a die. *Proceedings of the Institution of Mechanical Engineers, Part B: Journal of Engineering Manufacture, 220*(6), 823-835.

Avalle, M., Priarone, P. C., & Scattina, A. 2014. Experimental and numerical characterization of a mechanical expansion process for thin-walled tubes. *Journal of Materials Processing Technology, 214*(5), 1143-1152.

Avalle, M., & Scattina, A. 2018. Experiment based modeling of the mechanical expansion of tubes for the construction of heat exchangers. *Procedia Structural Integrity, 12*, 130-144.

Bouzid, Mourad, & El Domiaty, A. 2015. Impact of Bauschinger effect on the residual contact pressure of hydraulically expanded tube-to-tubesheet joints. *Procedia Engineering, 130*, 176-192.

Bouzid, A.-H., & Kazeminia, M. 2016. Effect of reverse yielding on the residual contact pressure in tube-to-tubesheet joints. *Journal of Pressure Vessel Technology, 138*(6).

Bouzid, A.-H., & Laghzale, N.-E. 2016. Analytical modeling of tube-to-tubesheet joints subjected to plastic deformation and creep. *Journal of Advanced Mechanical Design, Systems, and Manufacturing, 10*(4).

Bouzid, A.-H., & Pourreza, M. 2019. Analysis of residual stresses in the transition zone of tube-to-tubesheet joints. *Journal of Pressure Vessel Technology, 141*(4).

Cheng, W.-w., & Madhusudana, C. 2006. Effect of electroplating on the thermal conductance of fin–tube interface. *Applied Thermal Engineering, 26*(17-18), 2119-2131.

Chung, W. J., Kim, J. L., Jin, H. K., Hong, D. S., Kang, H. S., & Kim, D. S. 2005. Optimization of expanding velocity for a high-speed tube expander using a genetic algorithm with a neural network. *Transactions of the Korean Society of Machine Tool Engineers, 14*(2), 27-32.

Critoph, R., Holland, M., & Turner, L. 1996. Contact resistance in air-cooled plate fin-tube air-conditioning condensers. *International Journal of Refrigeration, 19*(6), 400-406.

Desu, R. K., Nitin Krishnamurthy, H., Balu, A., Gupta, A. K., & Singh, S. K. 2016. Mechanical properties of Austenitic Stainless Steel 304L and 316L at elevated temperatures. *Journal of Materials Research and Technology, 5*(1), 13-20.

Druez, J., & Bazergui, A. 1983. Through-thickness measurement of residual stresses in thin tubes. *Experimental Mechanics, 23*(2), 211-216.

Druez, J., Bazergui, A., & Pettigrew, M. 1985. Residual stresses in roller-expanded thin tubes. *Experimental Mechanics, 25*(3), 316-324.

Grant, T., & Bullock, M. (2005). The evolution of solid expandable tubular technology: lessons learned over five years. Dans *Offshore Technology Conference*. OnePetro.

H, K., & M, P. 1976. Hydraulisches Aufweiten Em Dash Ein Neues Verfahren Zur Befestigung Von Rohren. *VGB Kraftswerkstechnik, Vol. 56* (7), 456.

Hing, Y. K., Raghavan, V. R., & Meng, C. W. (2012). Investigation of contact resistance for fin-tube heat exchanger by means of tube expansion. Dans *AIP Conference Proceedings* (Vol. 1440, pp. 621-629). AIP.

Kang, S.-Y., So, S.-R., Son, Y., Park, S., Ha, M.-Y., & Park, S.-H. 2019. Three-dimensional fin-tube expansion process to achieve high heat transfer efficiency in heat exchangers. *Journal of Mechanical Science and Technology*, 1-6.

Kim, M.-H., & Shin, J.-S. 2005. Condensation heat transfer of R22 and R410A in horizontal smooth and microfin tubes. *International Journal of Refrigeration, 28*(6), 949-957.

Kim, Y. J., Cho, J. M., & Kim, M. S. 2008. Experimental study on the evaporative heat transfer and pressure drop of CO2 flowing upward in vertical smooth and micro-fin tubes with the diameter of 5mm. *International Journal of Refrigeration, 31*(5), 771-779.

Laghzale, N. E., & Bouzid, A.-H. 2009. Theoretical Analysis of Hydraulically Expanded Tube-to-Tubesheet Joints With Linear Strain Hardening Material Behavior. *Journal of Pressure Vessel Technology, 131*(6).

Liu, Y., & Qiu, X. 2016. A theoretical study of the expansion metal tubes. *International Journal of Mechanical Sciences, 114*, 157-165.

Luo, M., Yang, J., Liu, H., Lu, G., & Yu, J. 2019. Energy absorption of expansion tubes using a conical-cylindrical die: Theoretical model. *International Journal of Mechanical Sciences, 157-158*, 207-220.

Pearson, A. 2005. Carbon dioxide—new uses for an old refrigerant. *International Journal of Refrigeration, 28*(8), 1140-1148.

Pettersen, J., Hafner, A., Skaugen, G., & Rekstad, H. 1998. Development of compact heat exchangers for CO2 air-conditioning systems. *International Journal of Refrigeration, 21*(3), 180-193.

Roberts, G., Krauss, G., & Kennedy, R. 1998. Tool steels. 5.

Sawczuk, A., & Hodge Jr, P. G. 1960. Comparison of yield conditions for circular cylindrical shells. *Journal of the Franklin Institute, 269*(5), 362-374.

Scott, D., Wolgemuth, G., & Aikin, J. 1984. Hydraulically expanded tube-to-tubesheet joints.

Tang, D., Li, D., & Peng, Y. 2011. Optimization to the tube–fin contact status of the tube expansion process. *Journal of Materials Processing Technology, 211*(4), 573-577.

Tang, D., Li, D., Peng, Y., & Du, Z. 2010. A new approach in evaluation of thermal contact conductance of tube–fin heat exchanger. *Applied Thermal Engineering, 30*(14-15), 1991-1996.

Tang, D., Peng, Y., & Li, D. 2009. An experimental and numerical study of the expansion forming of a thick-walled microgroove tube. *Proceedings of the Institution of Mechanical Engineers, Part C: Journal of Mechanical Engineering Science, 223*(3), 689-697.

Tang, D., Peng, Y., & Li, D. 2009. Numerical and experimental study on expansion forming of inner grooved tube. *Journal of Materials Processing Technology, 209*(10), 4668-4674.

Toba, A. 1966. Residual Stress and Stress Corrosion Cracking in the Vicinity of the Expanded Joint of Aluminum Brass Tube Condensers. *Journal of The Japan Petroleum Institute, 9*(5), 366-370.

Updike, D., Kalnins, A., & Caldwell, S. 1992. Residual stresses in transition zones of heat exchanger tubes. *Journal of Pressure Vessel Technology, 114*(2), 149-156.

Wang, C., Fu, W., & Chang, C. 1997. Heat transfer and friction characteristics of typical wavy fin-and-tube heat exchangers. *Experimental thermal and fluid science, 14*(2), 174-186.

Wang, R., & Li, Y. 2007. Perspectives for natural working fluids in China. *International Journal of Refrigeration, 30*(4), 568-581.

Yokell, S. 1992. Expanded, and welded-and-expanded tube-to-tubesheet joints. *Journal of Pressure Vessel Technology, 114*(2), 157-165.

Zhao, Z., & Bouzid, A.-H. (2020). Stress analysis of SS316l tube die expansion for high pressure gas coolers. Dans *ASME 2020 Pressure Vessels & Piping Conference* (Vol. V002T02A007). American Society of Mechanical Engineers Digital Collection.

Zhao, Z., & Bouzid, A.-H. (2021). Stress analysis of tubes during die expansion process. Dans *Pressure Vessels and Piping Conference* (Vol. 85321, pp. V002T002A006). American Society of Mechanical Engineers.

Zhao, Z., Bouzid, A.-H., & Laghzale, N.-E. 2022. Analysis of Stresses and Strains in Stainless Steel 316 L Tubes Subjected to Die Expansion. *Journal of Pressure Vessel Technology, 144*(5), 051509.